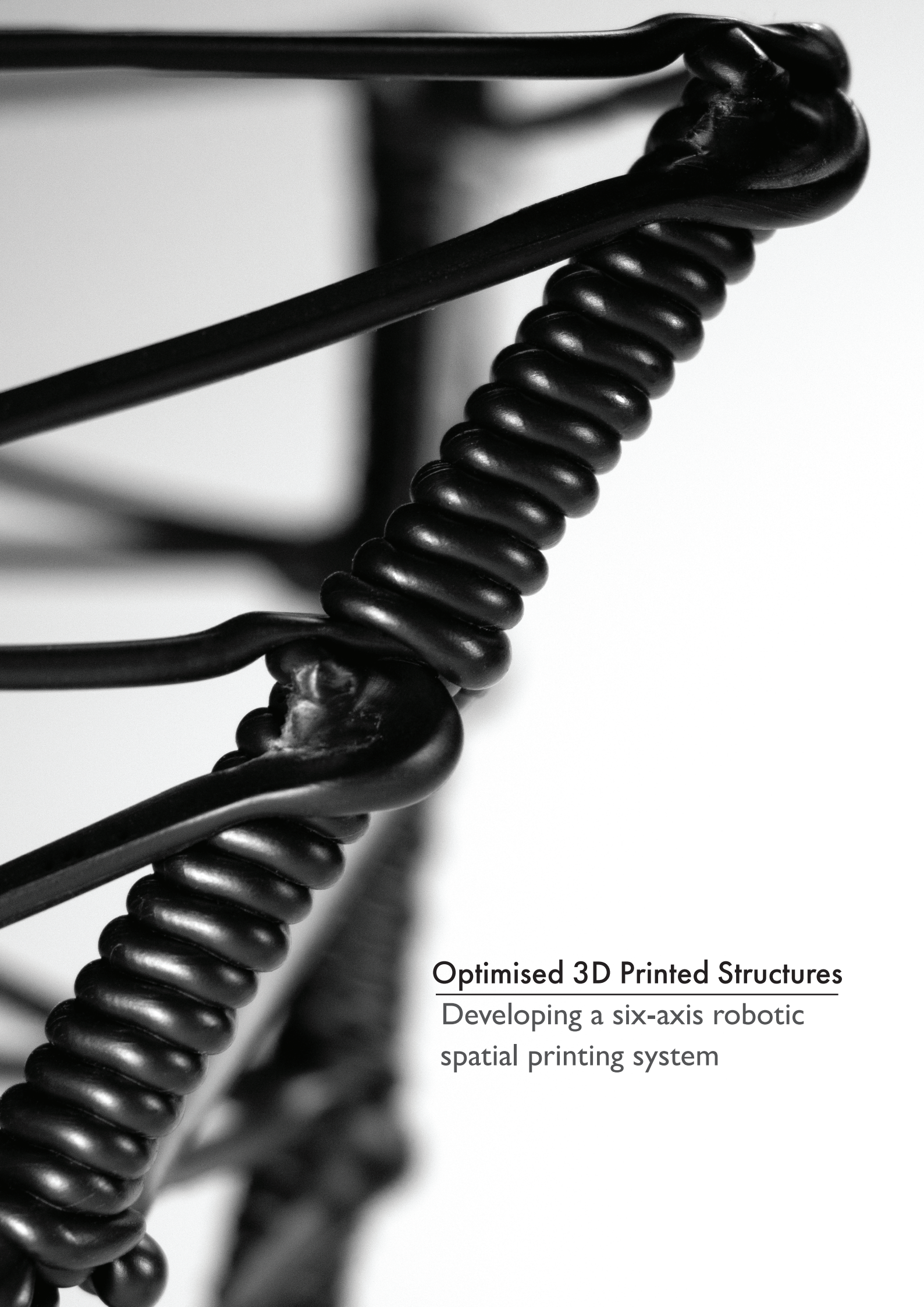

Optimised 3D Printed Structures

Developing a six-axis robotic spatial printing system

Optimised 3D Printed Structures
Developing a six-axis robotic spatial printing system

A Ninety-Point Thesis submitted in fulfilment of the requirements for the degree of Masters of Design Innovation

by

Hamish Morgan

Victoria University of Wellington
School of Design
2020

Abstract

Spatial printing is a form of additive manufacturing where material, typically thermoplastic, is extruded directly into a three-dimensional structure; unlike layer-based additive manufacturing which builds objects from two-dimensional slices. Spatial printing presents designers with a greatly improved level of control over material deposition, in comparison to layer-based FDM printing. The amount of material extruded dictates both the production time and cost of an object, encouraging designers to use materials conservatively. This also means that spatial printing has the potential to produce optimised structures.

When combined with modern digital manufacturing methods, topological optimisation can produce strong and lightweight volumetric structures. This research explores ways in which form optimisation tools can be used to generate spatially printed structures through a design science methodology.

Firstly, literature, precedents and optimisation and analysis software are reviewed, in order to identify opportunities for development. Next, Extrusion experiments are performed in order to determine the optimum temperature, print velocity and flow rate to be used throughout the thesis. Four conceptual systems are then produced which test different analysis and optimisation methods. From these concepts, one system is selected and developed through a continuous improvement process. The final version of the algorithm is applied in an application based experiment, an optimised chair design is generated from a number of theoretical loads and supports.

The systems created in *Optimised 3D Printed Structures* begin to question the role of future designers in an increasingly computationally driven world.

Acknowledgements

I dedicate this work to my fiance, *Katie*, and the rest of my family.
You have all looked after me throughout my studies, and supported me every step of the way. I could never have made it this far without all of your love.

I would also like to acknowledge

My supervisors, *Tim Miller* and *Kevin Sweet*.

My fellow workshop technicians and friends, *Graeme, Josh, Ken, Phil N, Phil J,* and *Yana*.

And the rest of my friends at the Faculty of Architecture and Design, Victoria University of Wellington.

Contents

Introduction

How can 3D topology optimisation be used to inform the design of spatially printed structures?

The development of 3D printing technology has given designers access to an unprecedented level of control over the form and structure of products. Traditional subtractive methods of manufacture prioritize the minimisation of material removal, as raw material is cheap in comparison to the time required to produce complex shapes.

"In biology material is expensive but shape is cheap
(the opposite is true in the case of technology)"
Julian Vincent, 2009, p.78

However, modern additive manufacturing methods emphasise the conservation of materials and the optimisation of shape, as the time required to produce a part and, in extension, a significant portion of its cost is determined primarily by the amount of material deposited.

There are a number of different emergent 3D printing and additive manufacturing technologies, of these technologies Fused Deposition Modelling (FDM) is the most common (Gordeev, Galushko & Ananikov, 2018). Like other 3D printing methods, FDM produces objects by depositing material in layers. FDM is one of the most suitable technologies for printing large scale objects because raw materials are cheaper than in other methods, and layer thickness can be increased to reduce manufacturing time. However, FDM is not well-suited for building objects with overhangs or thin features. To address these limitations spatial printing, an alternative form of FDM, has been developed (Oxman, Laucks, Kayser, Tsai, & Firstenberg, 2013).

In spatial printing, material is extruded directly into a 3D form, as opposed to being built up in layers. This method presents designers with the opportunity to build precise structures, without the need for support material.

With such a granular level of control over material placement, how do we design spatially printed products?

One way designers are answering this question is to use computational analysis and optimisation tools to generate designs. This research strives to use structural analysis and optimisation tools in a creative, rather than evaluative, manner to generate and inform novel spatially printed structures.

Chapter - 1

Literature & Precedent Review

Spatial Printing

In 2013, the Massachusetts Institute of Technology's (MIT) Mediated Matter group published an article detailing an experimental additive manufacturing process they referred to as "Freeform Printing" (Oxman, Laucks, Kayser, Tsai, & Firstenberg, 2013, pp.1-4). The group conducted a range of experiments using a custom-built extruder attached to a six-axis robotic arm. The experiments consisted of drawing out strands of ABS and HDPE plastic, in 3-dimensional space and generated a number of conceptual models, shown in Figure 1.

From the conceptual models, Oxman et al. (2013) concluded that spatial printing could eliminate the need for support structures, reducing waste materials, minimising fabrication and processing time and improving part quality. When building parts with overhanging or undercut features many additive manufacturing technologies, such as FDM and SLA, require the use of support structures during the printing process. "Beyond the technical challenges of support removal, these materials are wasteful – increasing fabrication and processing time while impacting quality" (Oxman et al., 2013, p.1).

Since initial experiments, conducted by Oxman et al. (2013), a number of groups have explored the prospect of spatial printing, making significant advances and identifying further benefits of the process. The precedents and literature reviewed reveal notable innovations in three major areas, material developments, generative design and optimisation, and fabrication sequence and structure.

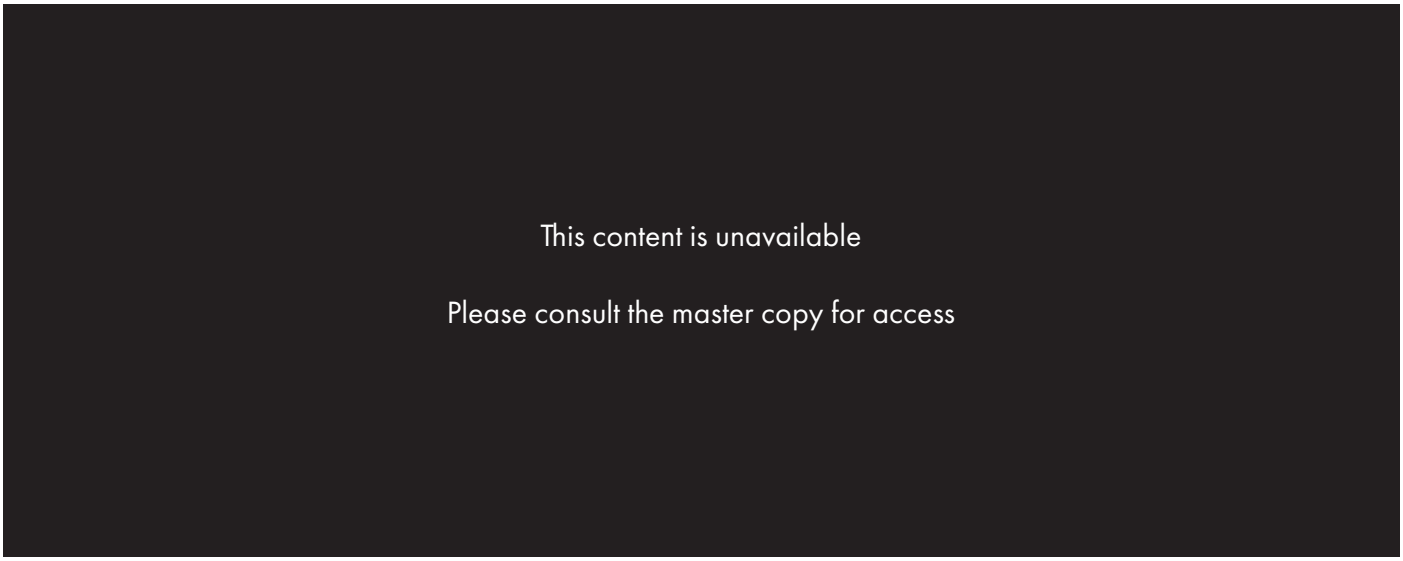

Figure 1. Early Spatial Print Models. Reprinted from Freeform 3D printing : towards a sustainable approach to additive manufacturing, by Oxman, N., Laucks, J., Kayser, M.A., Tsai, E.Y., & Firstenberg, M, 2013. Copyright [2013] by Taylor Francis.

Material Developments

For many years one of the largest factors limiting the advancement of large scale spatial printing has been the narrow range of printable, functional, materials. Materials used for spatial printing must remain flexible enough to be fed to the print head pre-extrusion, while becoming structurally self-supporting almost instantly post-extrusion, ruling out a large number of materials (Hajash, Sparrman, Guberan, Laucks & Tibbits, 2017). Ideally, spatially printable materials should also be lightweight, yet rigid, and be able to form solid joints at node connection points, to enable the construction of strong, lightweight structures (Hajash et al., 2017; Yuan, Meng, Yu & Zhang, 2016).

ABS (Acrylonitrile Butadiene Styrene) and PLA (Polylactic Acid) thermoplastic were among the first materials to be spatially printed (Oxman et al., 2013; Tam & Mueller, 2016) and continue to be used in many studies involving freeform printing (Huang et al., 2016; Retsin & García, 2016; Shelton, 2017; Yuan et al., 2016) such as the Design Miami Pavilions, pictured in Figure 2. This is likely due to the widespread use of ABS and PLA in layer-based FDM printing, where PLA is known for being a "stiff and environmentally-friendly material" while ABS is used as a "general solution for tough parts with acceptable strength" (Dawoud, Taha & Ebeid, 2016, p.39). Additionally, there is an abundance of information, resources and hardware, developed for the FDM printing of ABS and PLA, which can be readily applied to spatial printing. One such resource is the wide variety of ABS and PLA filaments that are available, including custom-blends with specialised material properties such as UV radiation resistance, conductivity, magnetism, heat resistance, and improved elasticity and toughness (Rocha et al., 2014; Rohringer, 2019; Weng, Wang, Senthil & Wu, 2016).

Despite considerable efforts to develop ABS and PLA based materials suitable for FDM printing, parts printed with these materials generally perform worse mechanically than injection moulded parts. "This is related to the nature of the injection moulding process which results in higher material compaction in addition to the enhancement of crystalline structure, thus enhancing mechanical strength" (Dawoud, Taha & Ebeid, 2016, p.45). Furthermore, ABS and PLA represent a limited range when compared to the material palette available to designers through alternative manufacturing techniques. This both "limits the applicability of parts fabricated from ME3DP [Material Extrusion 3D Printing] and inhibits the overall growth of this technology" (Rocha et al., 2014, p.1859). The need for alternative spatially printable materials has compelled research groups to investigate ulterior methods of extrusion, often resulting in new and innovative print systems.

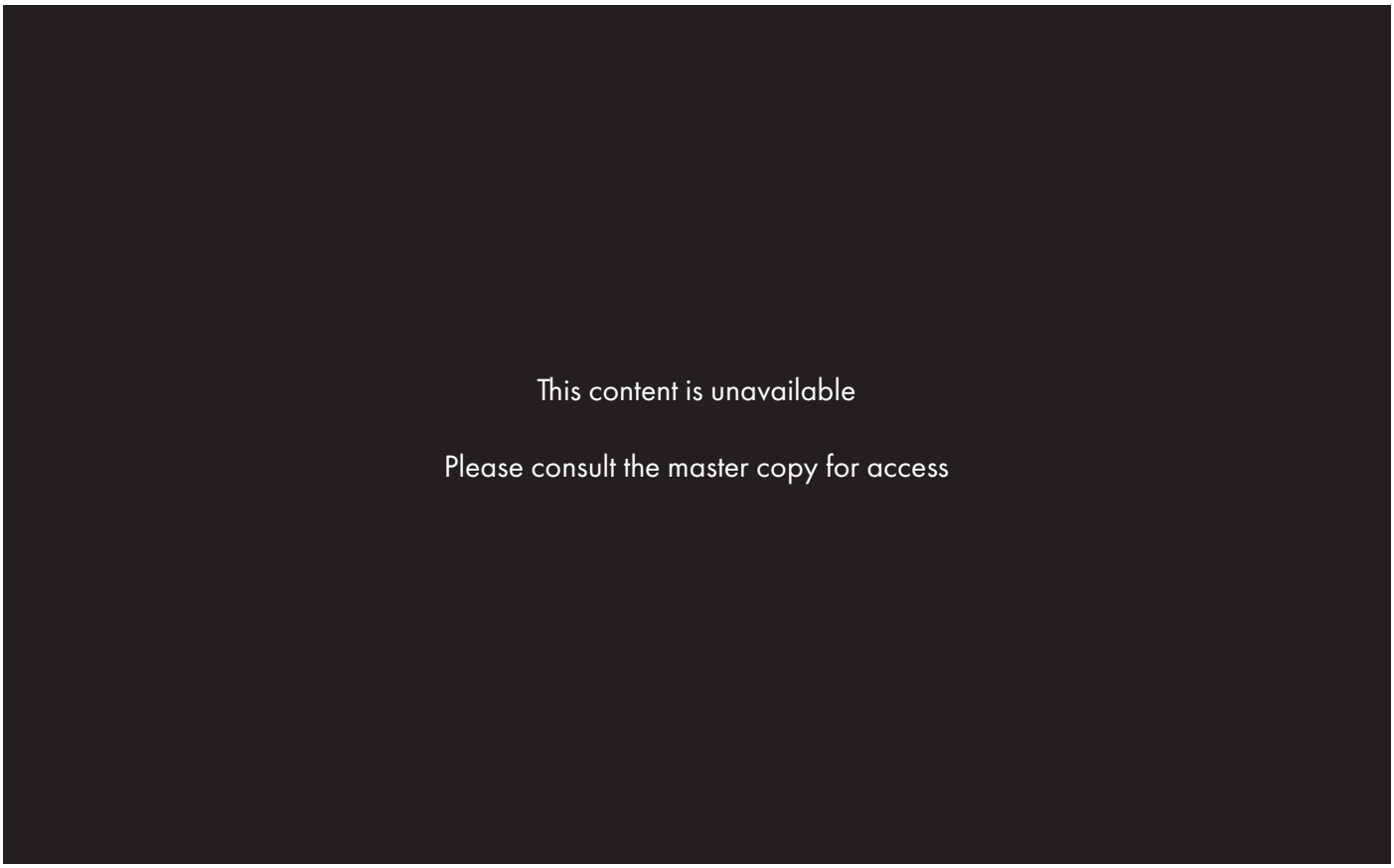

Figure 2. Design Miami Pavillions. From Branch Technology. Retrieved from https://www.branch.technology/projects-1/2017/6/9/shop. Copyright [2019] by Branch Technology.

One such research group, MX3D (2019), created the WAAM (Wire Arc Additive Manufacturing) spatial printing system, which is able to deposit a large range of metal alloys such as stainless steel, aluminium and bronze. These highly functional materials have greater rigidity and higher specific strength than PLA or ABS, enabling the production of large scale, lattice-based structures with practical applications, such as Dragon Bench seen in Figure 3. MX3D (2019) claim their system can deposit material with greater speed than competing metal printing technologies, up to 3 kg of material per hour, and that the price of the raw material is approximately ten times less than that of other metal printers, making it "clear that for large scale printed metal objects, WAAM will often be the technique of choice."(About, para. 4).

Figure 3. Dragon Bench. From Joris Laarman Lab. Retrieved from https://www.jorislaarman.com/work/mx3d-metal/. Copyright [2019] by Joris Laarman Lab.

Researchers at MIT's Self Assembly Lab have experimented with a selection of different materials, refining a technique they call RLP (Rapid Liquid Printing). By supporting printed structures in a granular gel matrix until they solidify, Hajash, Sparrman, Guberan, Laucks & Tibbits (2017) were able to spatially print a range of previously unusable liquid materials, including "urethane plastic, silicones, epoxy, concrete and liquid metals. Not only are the mechanical properties of many of these materials superior to those of ABS and PLA, but most are also chemically cured, meaning they are more heat resistant and chemically inert. The speed of previous forms of spatial printing has been limited by the speed at which materials harden post extrusion. RLP, however, allows the extrusion of the entire object, before any part begins to harden, resulting in faster print times and stronger joints at nodes (Hajash et al., 2017).

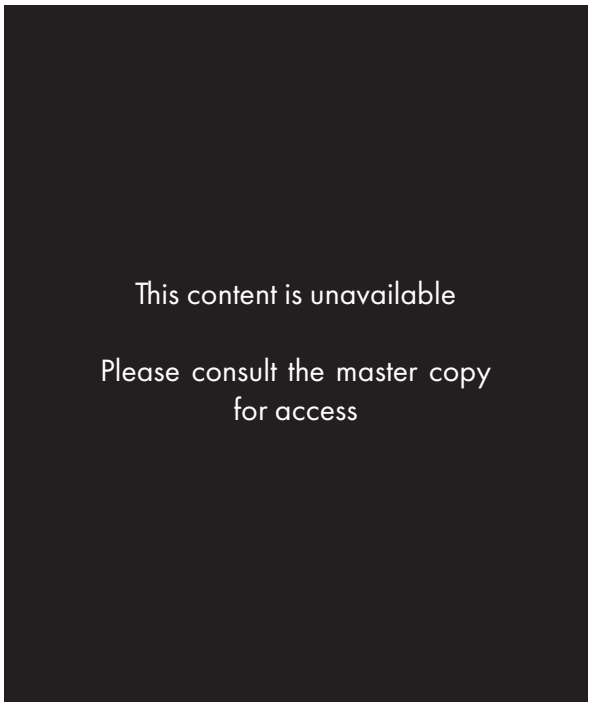

Figure 4. RLP Bag. From Dezeen. Retrieved from https://www.dezeen.com/2017/12/14/mit-self-assembly-lab-rapid-liquid-printed-bags-lamps-design-miami/. Copyright [2019] by Dezeen.

Since 2012, the University of Stuttgart's Institute for Computational Design and Construction (ICD) and Institute of Building Structures and Structural Design (ITKE) have explored two different methods of constructing large scale structures from resin-impregnated glass and carbon fibres. Typically multiple full-scale moulds would be required to create large and complex doubly-curved surfaces from composite materials. However, in the first method explored, Knippers et al. (2015) utilised a minimal steel framework to tension and support the extruded fibres, until the resin hardened, and the structure became self-supporting. The researchers were able to construct doubly-curved, rather than ruled, surfaces by exploiting the interactions between fibres laid in different directions.

The second method, devised by Doerstelmann et al. (2015), drew inspiration from the diving bell water spider which constructs its nest by first trapping a pocket of air underwater, then forming a structure by selectively laying silk filaments within the pocket. Like the spider, Doerstelmann et al. (2015) began the construction of their pavilion by fabricating a pressurised ETFE (Ethylene TetraFluoroEthylene) plastic bubble around a robotic arm. The researchers then robotically printed carbon fibres onto the inside of the inflated dome, pictured in Figure 5, employing the adhesive properties of the uncured resin to hold the fibres until the internal structure hardened. Once hardened, sections on either side of the dome were cut away, leaving the central section of ETFE as a waterproof membrane. Both the 2012 and 2015 ICD/ITKE Pavilions are extremely lightweight for their size, weighing only 320 and 260 kilograms respectively. The Pavilions demonstrate both the performance of the composite fibre materials in addition to the innovative ways Knippers et al. (2015) and Doerstelmann et al. (2015) shaped these materials, without extensive formwork or moulds.

Further notable examples of alternative material usage for spatial printing include AlOthman, Im, Jung & Bechthold's (2019) use of clay and Dritsas, Vijay, Dimopoulou, Sanadiya, & Fernandez's (2019) research involving a custom biobased composite material. In Spatial Print Trajectory, AlOthman et al. (2019) were able to "take advantage of the viscous properties of clay" (p. 168) and precisely control the shape and thickness of the clay extrusion, by performing specific actions, such as anchoring, dragging or pulling material from the nozzle. In doing so, the researchers were able to form intricate open structures with predefined material density.

In An Additive and Subtractive Process for Manufacturing with Natural Composites, Dritsas et al. (2019) utilise spatial printing techniques to produce parts made from a biobased composite material. Firstly, the researchers create a scaffolding structure, which is a porous representation of the parts final form. The scaffolding structure is designed specifically to reduce the amount of material usage, while increasing airflow, enabling parts to dry faster. Secondly, a surface layer can be spatially printed onto the scaffolding structure, once it has dried. Finally, the surface layer can be machined and/or sanded depending on the requirements of the surface finish.

Both AlOthman et al. (2019) and Dritsas et al. (2019) explored methods of 3D printing beyond the layer-based approach that is typical for clay or paste materials. By applying spatial printing methods to viscous paste materials, both teams were able to produce complex structures with definable densities.

From the examples reviewed it is clear that the use of alternative materials plays a major role in the advancement of spatial printing technology. Unique material properties exploited in each of the studies enabled the design and fabrication of novel and innovative products and structures. However, many of the examples reviewed were produced by teams, composed of designers, engineers, and material scientists. Developing spatial print systems for alternative materials requires numerous resources in the form of materials, hardware and researchers. Therefore, I believe it to be beyond the scope of this thesis.

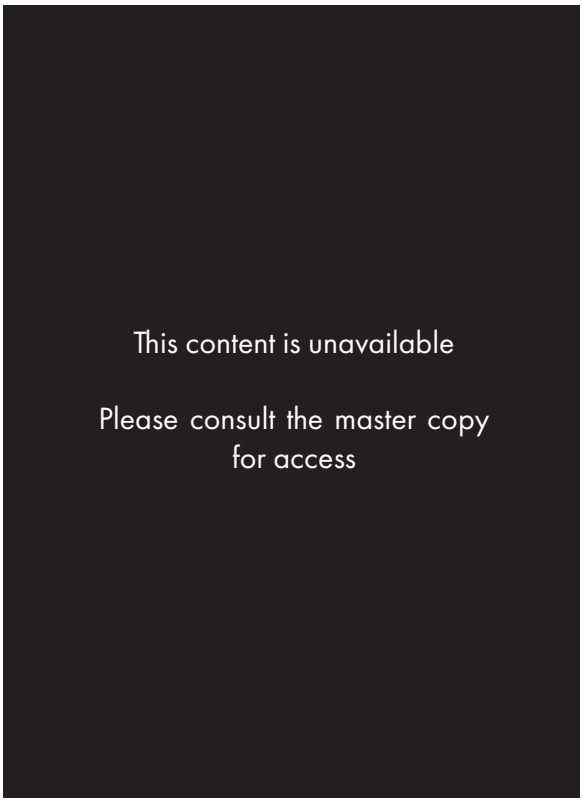

Figure 5. 2014-2015 ICD/ITKE Pavillion. From University of Stuttgart ICD. Retrieved from https://icd.uni-stuttgart.de/?p=12965. Copyright [2019] by ICD/ITKE University of Stuttgart.

Generative Design and Optimisation

The development of generative design and design optimisation techniques has altered the way in which CAD tools are used. In the past, the conceptual stages of the design process involved producing design ideas primarily through sketching and the making of physical mock-ups, while CAD programs were utilised in later stages, like development (Khan & Awan, 2018). However, generative design and analysis tools have begun to alter this workflow, allowing designers to quickly produce advanced iterations, with geometry which is optimised depending on the use of the object.

The generative design process begins with the translation of design criteria into a set of input parameters. These parameters can then be fed into a commercially available generative design system or a custom-built algorithm. The system then returns a number of designs, which are optimised based on the criteria set by the designer, typically to maximise strength-to-weight or minimise deflection or stress. At this point, designs can be evaluated, and chosen for development, based on a number of factors such as performance or appearance.

An early example of generative design and structural optimisation being used for product design was Joris Laarman Lab's Bone Chair, Figure 6. Design of the Bone Chair began in 1998, when German automobile manufacturers, Adam Opel GmbH finished development of a new simulation and optimisation software. Laarman and his team re-purposed the optimisation software, originally intended to be used to design engines, to design a collection of chairs. The software functions "by creating a virtual three-dimensional model and simulating the application of stress to specific points on the design. Then the algorithm takes away all of the material that isn't necessarily needed, without weakening the part" (Joris Laarman Lab, 2019, Bone Chair, para. 3). Since Bone Chair a number of design optimisation programs and plug-ins have become commercially available for example, Autodesk Fusion 360, Autodesk Dreamweaver, Altair, Monolith, and Rhino Plug-ins Millipede and Karamba. Many of these programs function in a similar way to the early software used by Laarman and his team.

Figure 6. Bone Chair. From Joris Laarman Lab. Retrieved from https://www.jorislaarman.com/work/bone-chair/. Copyright [2019] by Joris Laarman Lab.

Line

In the article Robotic multi-dimensional printing based on structural performance, Yuan, Meng, Yu, & Zhang (2016) discuss the development of a method for employing optimisation and simulation software to inform spatial printing. Instead of optimising the design of a structure, as a whole, Yuan et al. (2016) focused on the optimisation of an individual structural element. Taking inspiration from the spindle-knot geometry found in strands of spider silk, the researchers constructed a print head capable of extruding four strands of ABS plastic simultaneously. The structural elements produced by the extruder consisted of a central core, surrounded by three auxiliary strands which diverged from, then rejoined the centre strand at regular intervals, as seen in Figure 7. The distance between, and length of, each knot could be digitally altered, depending on optimisations informed by simulations and physical testing. By tuning the cross-sectional widths of each element, Yuan et al. (2016) were able to produce longer, self-supporting curvilinear members with less deflection than the single strand alternative.

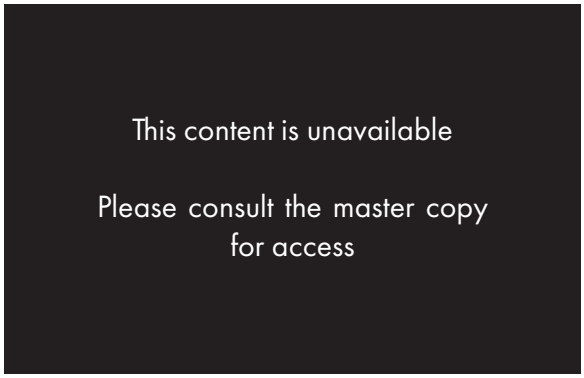

Figure 7. Multi-nozzle extruder. Reprinted from "Robotic multi-dimensional printing based on structural performance," by P. F. Yuan, H. Meng, L. Yu, & L. Zhang, 2016. In Robotic Fabrication in Architecture, Art and Design 2016, p. 101. Copyright [2016] by Springer International Publishing.

Surface

One of the first examples of optimisation software being used to define spatially printed structures was the research conducted in Stress Line Additive Manufacturing (SLAM) for 2.5-D shells. In this paper, Tam & Mueller (2016) leveraged the form-finding optimisation tool Kangaroo, to generate a shell structure. Finite element analysis tools were then used to conduct a stress line analysis, from which the researchers were able to determine areas where material continuity was most important. Tam & Mueller (2016) claim that when compared to the standard layer-based method of material deposition, common to FDM printing, SLAM produced prints of the same strength, with considerably less material consumption.

Recently Battaglia, Miller & Zivkovic (2019) used a method, similar to Tam & Mueller's (2016) SLAM method, to define robotically printed concrete structures. Battaglia et al. (2019) state that "principal stress lines were used to generate toolpaths, creating lightweight lattice double curvature shells"(p. 249). While the method of designing the concrete structure was similar to Tam & Mueller's (2016), the materiality and scale of the outputs produced by Battaglia et al. (2019) were considerably different. The research conducted by Battaglia et al. (2019) proves that the SLAM method, tested and refined at a small scale by Tam & Mueller (2016), is suitable for producing real-world concrete structures, at an architectural scale, as seen in Figure 8.

Figure 8. Concrete structure. Reprinted from "Sub-Additive 3D Printing of Optimized Double *Figure 9.* Curved Concrete Lattice Structures," by C. A. Battaglia, M. F. Miller, & S. Zivkovic, 2018, Robotic Fabrication in Architecture, Art and Design, 2019, p. 252. Copyright [2019] by the Springer Nature Switzerland AG.

Volume

The last spatial printing optimisation method I will discuss is the grid/voxel-based method used by García, Retsin, Kwon, Kaleel & Li (2015) and Huang, Carstensen & Mueller (2018). This method is the 3D equivalent to Tam & Mueller's (2016) 2.5D SLAM method. Where the SLAM method is based on the stress line analysis of thin shell structures, the grid/voxel method generates optimised 3D lattices within a predefined volumetric form.

In CurVoxels, García et al. (2015) used Verner Panton's iconic Panton chair design as the starting point for generating an optimised, spatially printed structure. The volumetric form of the chair, along with the major forces which would be imparted during use, were fed into the structural analysis software. The software then returned a 3D map of any stresses resulting from the input forces. García et al. (2015) used the stress map to inform material deposition by first breaking the form of the Panton chair down into a three-dimensional grid. Secondly, the amount of stress present within each grid space was assessed. Lastly, depending on the amount of stress present, each grid space was filled with a voxel structure, with the specific density and strength required, resulting in the optimised chair structure pictured in Figure 10.

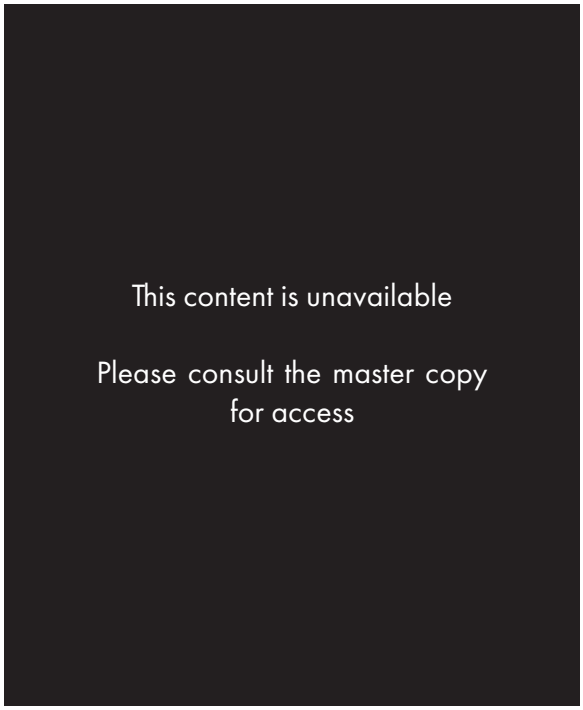

Figure 10. Voxel Panton chair. Reprinted from "CurVoxels," by M. J. García et al., 2015.

In 3D truss topology optimization for automated robotic spatial extrusion, Huang et al. (2018) also produce a method for generating an optimised 3D structure. However, where Jiménez et al. (2015) begun with a predefined form, Huang et al. (2018) began with a cuboid-shaped grided lattice. The optimisation system then removed line segments deemed unnecessary, based upon the input forces and support points set by the researchers, leaving behind the optimised structure, as seen in Figure 11.

As spatially printed structures grow in scale and complexity, they become impractical to design with traditional methods, such as sketching and modelling. All of the examples discussed in this section leverage the power of structural optimisation tools to generate spatially printable designs. However, many use just a single form of optimisation, be that stress line analysis, form optimisation, or structural analysis. Furthermore, in most of the examples, the aesthetic qualities of the output do not seem to be considered, with researchers placing optimisation at the forefront of the design process and failing to iterate upon the initial outputs of the optimisation algorithm.

Figure 11. Volumetric Optimisation. Reprinted from "3D truss topology optimization for automated robotic spatial extrusion," by Y. Huang, J. V. Carstensen, & C. T. Mueller, 2018, Proceedings of the IASS Symposium 2018, p. 6. Copyright [2018] by Yijiang Huang, Josephine V. Carstensen, Caitlin T. Mueller.

Fabrication Sequence and Structure

The last category of innovations are those related to generating structures which are printable and have viable fabrication sequences. In traditional lineated 3D printing, objects are built up in thin layers. Because layers are printed consecutively, the difference in height between printed geometry and areas which need to be built upon is typically less than 1mm, the thickness of a single layer. For this reason, print order is generally not a factor which needs to be considered when 3D printing.

However, when spatially printing, there are two issues which are associated with the order in which structures are printed. Firstly, parts of the object which have been printed must be self-supporting and remain in the correct location until the print is complete. If a section of the print moves, before completion, it is likely that the resulting structure will be disjointed and faulty (Huang et al., 2016).

Secondly, collisions between the extruder and parts of the model which have been printed must be avoided. Huang et al. (2016) emphasize the difficulty of addressing this problem, "collision detection between the moving part of the robotic system and the printed part is dynamically sequence dependent, which makes it highly computationally complicated" (p. 2).

Because of the physical size of the extruder and manoeuvrability limitations, it is possible to design spatial structures which do not have any viable print sequence, as collisions are certain. The method with which designers choose to define the fabrication sequence has a large influence on the appearance, overall strength and most importantly, the feasibility of fabricating a structure. Throughout the literature and precedents reviewed, it is evident that three unique approaches to solving this problem exist.

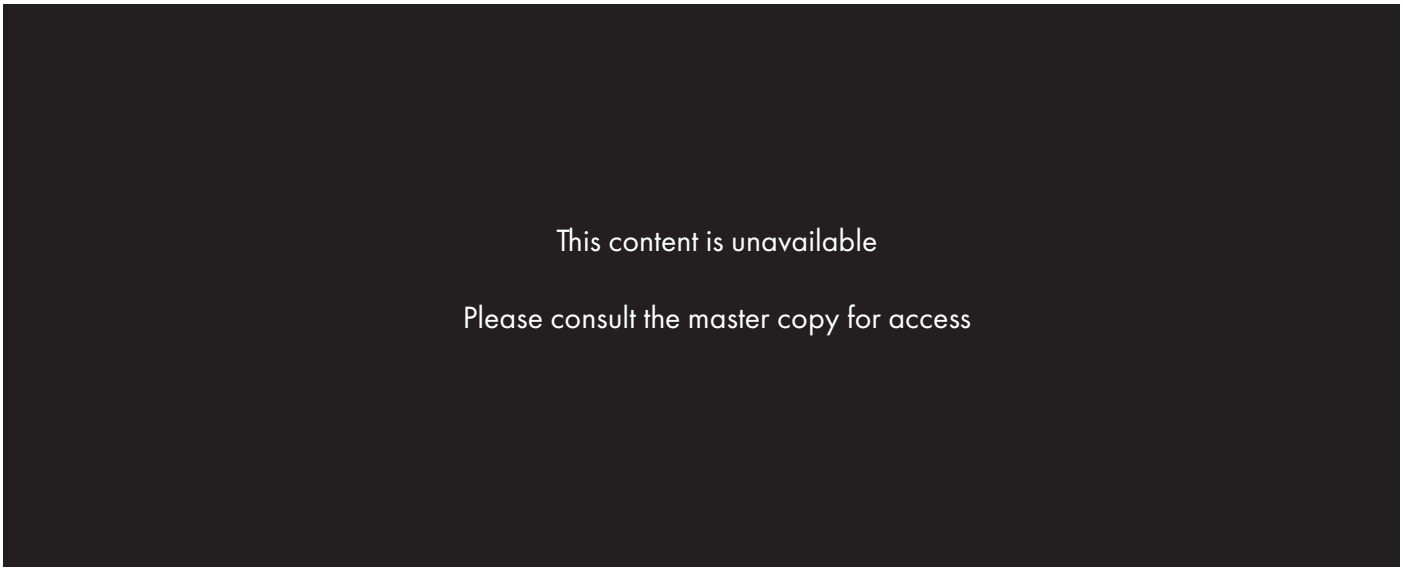

Figure 12. Spatial print with generated fabriction sequence. Reprinted from "FrameFab: Robotic fabrication of frame shapes," by Y. Huang et al., 2016, ACM Transactions on Graphics (TOG), 35(6), p. 8. Copyright [2019] by ACM, Inc.

The method detailed in Designed Deposition (Molloy, 2018) is based upon enhancing aesthetic qualities of spatially printed artefacts. It requires the designer to carefully consider and check the print order for every unique structure to be printed. Each printer movement must be simulated and the designer must visually check for collisions. If a collision is found, either the fabrication sequence must be manually reordered, or the geometry must be altered. While this method of bespoke toolpath creation can produce customised and unique small scale products, such as shown in Figure 13, as the scale of a structure grows, it becomes impractical and uneconomical to employ this method, as there are too many individual movements to check.

The second method common amongst precedents is that of breaking a form into bands which are built, one-by-one, from the ground up. Each band is made up of a gridded structure, formed from rectangular cells. To produce a specific form, the number of cells on a layer and the dimensions of individual cells is altered (Hack, Lauer, Gramazio & Kohler, 2014; Mueller et al., 2014). In CurVoxels, García et al. (2015) took this principle a step further. Instead of repeating a single cell throughout the entire structure, García et al. (2015) created multiple voxels of differing density and complexity. Each voxel was designed to be arranged and printed in any order, and in this way, printable structures with more complexity could be created by stringing unique combinations of voxels together. Building structures in this way, by repeating elements with a predetermined fabrication sequence, is computationally inexpensive and guarantees the structure is printable. However, structures produced with this method lack visual variation, due to their repetitive nature as shown in Figure 14. Additionally, they are often less form responsive than those produced with alternative methods.

The last method for calculating a viable fabrication sequence is to use a custom algorithm. Huang et al. (2016) created an algorithm which functioned by breaking down a structure into its constituent elements, then determining the order in which the elements should be printed, based upon the stability of the structure during the print, limitations in maneuverability, and the detection of collisions between the extruder and the existing structure. As a result, Huang et al. (2016) were able to produce complex prints, with non-repeating geometry, as can be seen in Figure 12. While this method offers the greatest design flexibility, developing such an advanced algorithm requires expertise in computer science, and using it would be computationally intensive, especially as structures grow in scale and complexity. For these reasons, this method of generating print sequences may be beyond the scope of this thesis.

Figure 13. Whisk, Seive and Measuring Cup. Reprinted from "Designed Deposition," by I. Molloy, 2017.

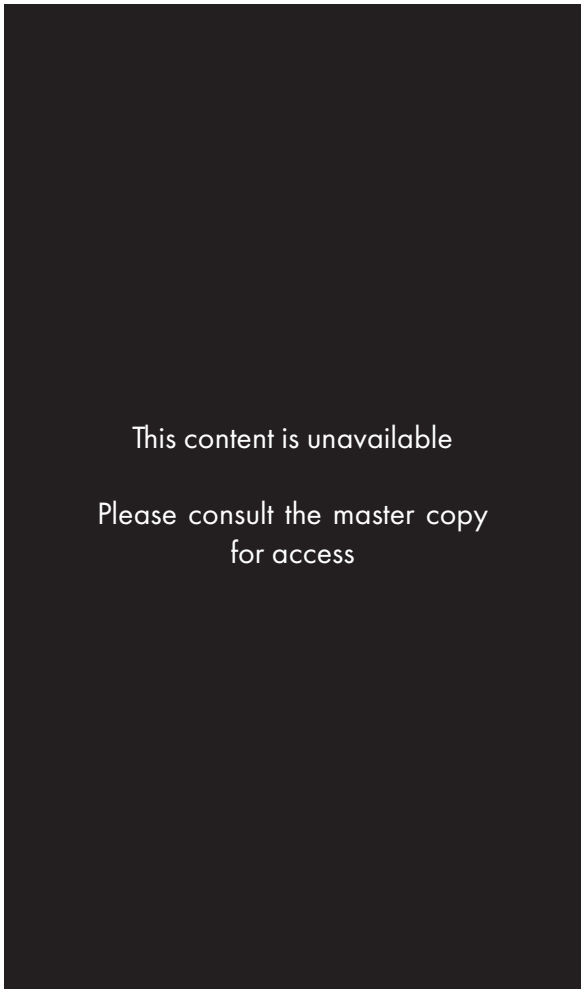

Figure 14. Mesh Mould. Reprinted from "Mesh-Mould: Robotically Fabricated Spatial Meshes as Reinforced Concrete Formwork," by N. Hack, W. Lauer, F. Gramazio, & M. Kohler, (2014), Architectural Design, 84(3), p. 53. Copyright [2014] by Gramazio & Kohler, Architecture and Digital Fabrication, ETH Zurich.

Chapter - 2

Software Review

Software Overview

The software used throughout this research will play a major role in determining the type of analyses that can be performed and the kind of structures that are able to be generated. Two types of software will be integrated into an optimised spatial printing system. Firstly, structural analysis software will be required, to generate optimised geometry based on the parameters set by the designer.

Secondly, Computer Aided Design and Manufacturing (CAD, CAM) software, will be used to transform the analysis and optimisation data into a structure which is printable. The information from this structure is then converted into instructions which are readable by the print system.

Analysis and Optimisation Software

Structural analysis is a type of Finite Element Analysis Involving simulating the effects of loads on a structure in order to determine the resulting deformation, internal forces, stresses, points of failure and stability. This form of simulation is used in many fields including Engineering, product design, architectural design and building science (Tedeschi, 2014).

Topology optimisation is the technique of utilising structural analysis tools to generate functional designs. The different types of analysis and optimisation a piece of software can perform are a defining factor in which program will be chosen for this research. Analysis software is available in both stand-alone programs, and as plug-ins for other software. If a standalone program is chosen then the ease of transferring data and geometry to another program is also an important factor to consider. Further factors which will be considered include, how well the program is documented and supported, prior knowledge of the program, how much the software costs, and how accessible it is to designers.

CAD/CAM Software

Most CAD (Computer Aided Design) software is built upon one of two geometry systems, polygon-based or NURBS (Non-Uniform Rational Basis Spline) based. Polygon-based systems are used extensively in the VFX industry, whereas NURBS based systems are used more dominantly in product design and CAM (Computer Aided Manufacturing). This is because NURBS based modelling programs represent curved geometry more accurately, while polygon-based programs simplify curved geometry into a network of flat faces (Péter Máté, 2019).

However there are exceptions, for instance, all finite element analysis systems convert models into polygon-based geometry, representing true curves as a collection of finite elements, in order to simplify calculations. Additionally, the majority of 3D printing slicers will only accept polygon file types, such as .STL and .OBJ. This is the opposite of traditional CAM technologies, where NURBS models were a requirement, due to limitations in computing power and memory of early CNC (Computer Numerically Controlled) machines (Peter Zelinski, 1999; Additive Blog, 2017).

CAD software which is able to generate, manipulate, import and export both polygon and NURBS based geometry is preferable, as this type of software offers the most flexibility and greatest number of possibilities in terms of compatibility with other software. Because we will be working with large amounts of data, importing from analysis programs and exporting to the print system, the Integrated Development Environment (IDE) and the type of scripting languages which are supported are also very important. The functionality and number of commands available in different scripting languages vary considerably, this too will have an impact on the development of the print system. Further factors to consider are documentation and support, familiarity with the program, cost, and accessibility.

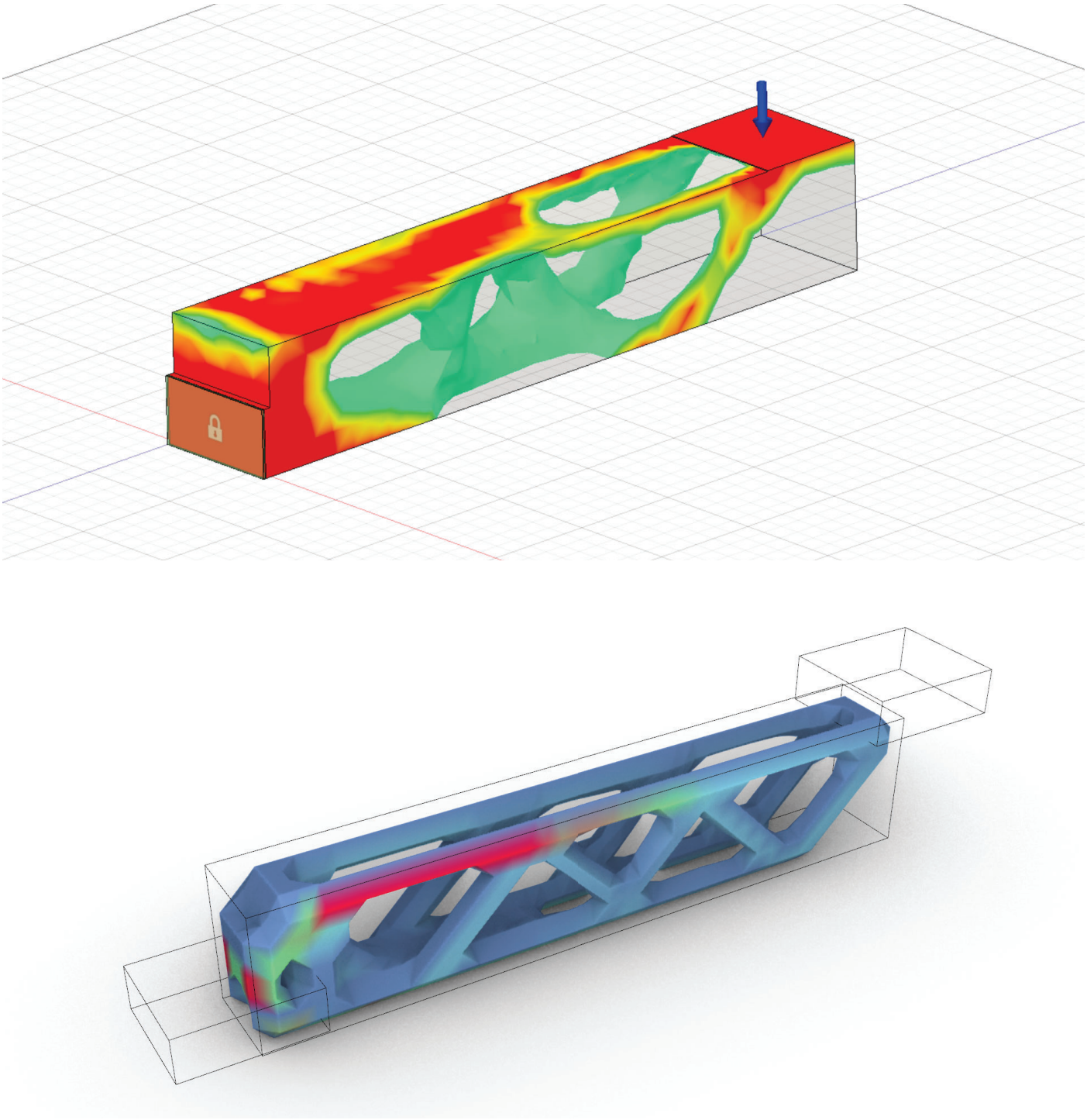

Figure 15. Examples of topology optimisaion software, Fusion 360 (top) & Millipede (bottom).

	Plug-ins		Components		Stand-Alone	
Program	Solidworks Simulation	Fusion 360	Karamba 3D	Millipede	Monolith	Altair Hyperworks
Description	Solidworks plug-in which enables topology optimisation for weight, strength, factor of safety, and frequency response.	Autodesk Fusion 360 offers cloud based computing of structural analysis and optimisation for product design and engineering.	Grasshopper component with a range of structural analysis tools. Often used in conjunction with an optimisation component such as Octopus.	Grasshopper component which offers a range of 2D and 3D structural analysis and optimisation tools.	Availaible as both a stand alone program and Grasshopper component. Monolith allows the generation and analysis of voxel based models.	Is a complete modelling, analysis and optimisation package for designers, engineers and architects.
Frame Element Analysis	No	No	Yes	Yes	No	No
Shell Element Analysis	No	No	Yes	Yes	No	Yes
Nonlinear Static Stress	Yes	Yes	No	No	No	Yes
2D Plate Optimisation	No	No	No	Yes	No	No
3D Topology Optimisation	Yes	Yes	No	Yes	Yes	Yes
Support & Documentation	Poor	Good	Good	Poor	Poor	Good
Pros & Cons	Well recognised in industry.	Offers cloud-based computing.	N/A	Millimeters are not supported as units.	Limited number of analyses.	Well recognised in industry.
Paid	Yes	Free for educational Purposes	Yes	Free for educational Purposes	No	Yes

Table 1. Analysis and optimisation software comparison.

	Nurbs Based		Nurbs & Polygon Based			Other
Program	Solidworks	Fusion 360	Rhinocerous 3D	Grasshopper for Rhino	Maya	Houdini
Description	Solidworks is a NURBS based 3D modelling software capable of manipulating curves, surfaces and solids.	Autodesk Fusion 360 offers cloud based computing of structural analysis and optimisation for product design and engineering.	Is a 3D modelling software capable of manipulating NURBS curves, surfaces, and solids and polygon meshes.	Grasshopper is a node based scripting plug-in for Rhino which offers a large range of open source components and plug-ins.	Maya is a 3D modelling, simulation and animation environment created for the VFX and Game design industries.	Houdini is a fully procedural node based scripting environment, created for the VFX and Game design industries.
Prior Knowledge	Good	Poor	Good	Good	Poor	None
Support & Documentation	OK	Good	Good	Good	Good	Good
Supports FEA/Design Optimisation	With Plug-in	Yes	With Plug-in	With Plug-in	No	Yes
Scripting Language	C#, VBA, VB.Net, VSTA	C++, Python	Rhinoscript	C#, Python, Rhinoscript, VB.net	Maya Embedded Language, Python	C++, Python, VOPs, Hscript, VEX, OpenCL, Wrangles
Pros & Cons	N/A	N/A	Import and export large number of file types	Many open source plug-ins and components.	N/A	N/A
Paid	Yes	Free for educational Purposes	Yes	Free with Rhino	Free for educational Purposes	Yes

Table 2. CAD/CAM programs comparison.

Software Evaluation

Analysis and Optimisation Software

Weights have been assigned to attributes of a program according to the relevance they hold to the research in this thesis. Firstly, programs received three points for each of the types of analysis they are able to perform. Those which are able to perform a wider variety of analyses and optimisations enable greater exploration of these methods, and so are more valuable to this study.

The next most important factor is the documentation and support which is available for each of the programs. Programs received a rating of zero, one or two, depending on the quality of documentation available, and the level of support present on forums. These ratings were then multiplied by two, the weight which has been assigned to this attribute.

Lastly, programs received one positive or negative point for each of the pros or cons identified and one negative point if a piece of software was paid. Prior knowledge is also an important factor, however, it has not been included as I have no previous experience with any of the analysis/optimisation programs listed. The total points each program scored are shown in the weighted matrix opposite, Table 3. Millipede was selected for use throughout the thesis due to the large variety of analysis and optimisations it could perform, its interconnectivity with the Grasshopper CAD program, its excellent documentation, and its accessibility for researchers looking to expand on this study.

CAD/CAM Software

A weighted matrix has also been completed for CAD/CAM software, Table 4. Prior knowledge was assigned the highest weight as learning new CAD/CAM software, in addition to analysis and optimisation software, can require a substantial amount of time. Support and documentation were allocated the next highest weight. Thirdly, programs were rated zero, one or two depending on whether they supported analysis and optimisation natively, with plug-ins, or not at all. Lastly, programs scored two points per supported scripting language and received the same scores for pros and cons, and being paid as the analysis software.

A combination of Rhinocerous 3D and Grasshopper have been selected to act as the CAD and CAM software used throughout this thesis. Firstly, Rhinocerous 3D and Grasshopper are able to work seamlessly with Millipede, creating an uninterrupted flow of data from analysis and optimisation, to structural generation and finally to robotic fabrication. This is all done without the need for exporting or importing data, which lengthens iteration time and hinders development. Secondly, Grasshopper offers an exceptional range of downloadable open source components which provide a large degree of utility and flexibility. Lastly, both programs are well documented and have active online forums, they are also used widely at Victoria University, providing access to further means of support.

	Weight	Plug-ins		Components		Stand-Alone	
Program		Solidworks Simulation	Fusion 360	Karamba 3D	Millipede	Monolith	Altair
Frame Element Analysis	3	0 (0)	0 (0)	1 (3)	1 (3)	0 (0)	0 (0)
Shell Element Analysis	3	0 (0)	0 (0)	1 (3)	1 (3)	0 (0)	1 (3)
Nonlinear Static Stress	3	1 (3)	1 (3)	0 (0)	0 (0)	0 (0)	1 (3)
2D Plate Optimisation	3	0 (0)	0 (0)	0 (0)	1 (3)	0 (0)	0 (0)
3D Topology Optimisation	3	1 (3)	1 (3)	0 (0)	1 (3)	1 (3)	1 (3)
Support & Documentation	2	1 (2)	2 (4)	2 (4)	1 (2)	1 (2)	2 (4)
Pros & Cons	1	1 (1)	1 (1)	0 (0)	-1 (-1)	-1 (-1)	1 (1)
Paid	-1	1 (-1)	0 (0)	-1 (-1)	0 (0)	0 (0)	-1 (-1)
Total		8	11	9	13	4	13

	Weight	Nurbs Based		Nurbs & Polygon Based			Other
Program		Solidworks	Fusion 360	Rhinocerous 3D	Grasshopper for Rhino	Maya	Houdini
Prior Knowledge	4	2 (8)	1 (4)	2 (8)	2 (8)	1 (4)	0 (0)
Support & Documentation	3	1 (3)	2 (6)	2 (6)	2 (6)	2 (6)	2 (6)
Supports FEA/Design Optimisation	2	1 (2)	2 (4)	1 (2)	1 (2)	0 (0)	2 (4)
Scripting Language	2	4 (8)	2 (4)	1 (2)	4 (8)	2 (4)	7 (14)
Pros & Cons	1	0 (0)	0 (0)	1 (1)	1 (1)	0 (0)	0 (0)
Paid	-1	1 (-1)	0 (0)	1 (-1)	0 (0)	0 (0)	1 (-1)
Total		20	18	18	25	14	23

Table 3. Analysis and optimisation software weighted matrix (above).
Table 4. CAD/CAM programs weighted matrix (below).

Millipede Analysis and Optimisation Methods

Frame Element Analysis

Allows structures built from elements, such as beams and columns, to be analysed. Points and curves, which represent the elements, cross-section shape, supports and loads are set as input data, from which Millipede is able to perform a structural analysis and determine maximum deflection, visualisation of principal stresses and the overall weight of the structure.

This method could be used to analyse spatial structures before printing, to verify their fitness for purpose. Yuan et al. (2016) utilised this method to analyse the performance of different configurations of spindle knot geometry before moving to physical testing. If coupled with a generational evolutionary algorithm, such as Goat or Octopus, it may also be used to generate spatially printable structures optimised for minimum deflection, through a process of iteration and analysis.

Shell Element Analysis

Enables the analysis of 2.5 Dimensional shell structures, as was demonstrated by Tam & Mueller (2016) and Battaglia, Miller & Zivkovic (2019). This type of analysis can be used in conjunction with frame element analysis to build more complex structural systems. A NURBS surface or mesh is set as input geometry, in addition to loads, support regions and whether stresses are to be calculated for the bottom or top surface of the shell. Millipede returns data and visualisations of the first and second principal stresses, estimated VonMises stress and displacement of the shell.

Research has already been produced on the use of this analysis method for generating spatially printed structures. However, these studies only investigated the use of principal stress lines to inform material deposition. Further research could investigate the use of data produced by this analysis method in alternative ways, such as altering the size of spatially printed elements based on the amount of stress present.

2D Plate Optimisation

Through repeated analysis and refinement, Millipede is able to calculate 2D plate optimisations. Curves representing plate boundaries, load and support regions, and the number of iterations to perform are set as input data. Millipede returns the principal stress lines, optimised contours, deflection, and a colourised mesh depicting optimum material distribution.

This method offers many of the same opportunities as shell element analysis, however, it is more restricted in its application, due to its 2-dimensional nature.

3D Topology Optimisation

Similar to the 2D optimisation, Millipede performs repeated analysis and refinement of a 3D mesh, in order to calculate the optimised form for a given load case. Bounding volumes representing build area, load regions and support regions are set as input geometry, in conjunction with the number of iterations to complete. Millipede returns an optimised colourised mesh, depicting principal and Von Mises stresses, and deflection.

Millipedes 3D topological optimisation system is able to produce complex organic forms which are optimised for specific loads. The data produced using this method was later used in this study to define the form, density or the size of the elements in a spatially printed structure.

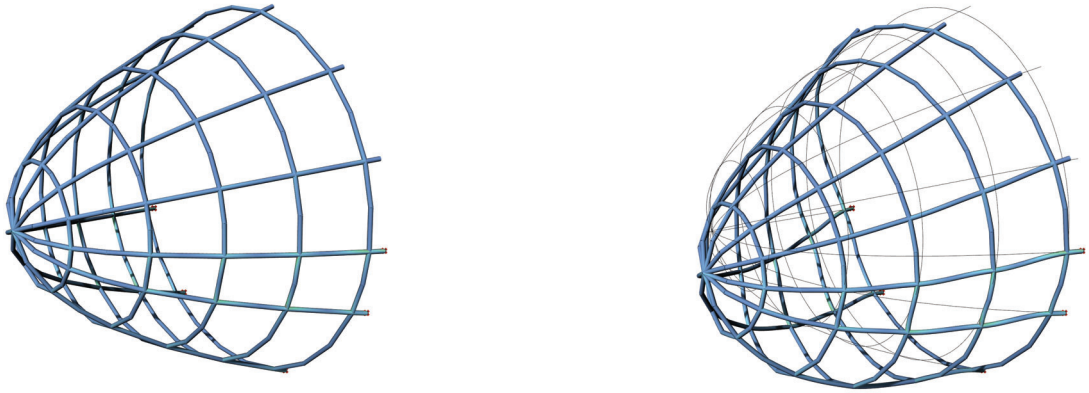

Figure 16. Frame element analysis. Author.

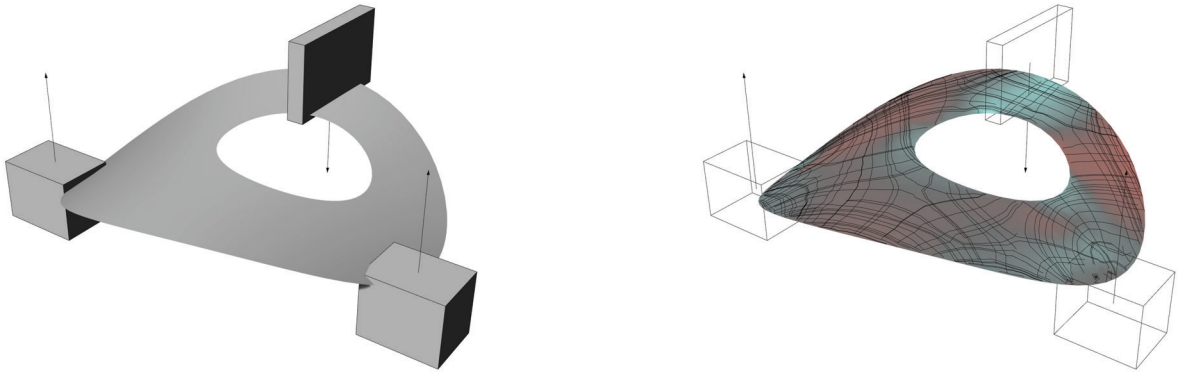

Figure 17. 2.5D shell structure analysis. Author.

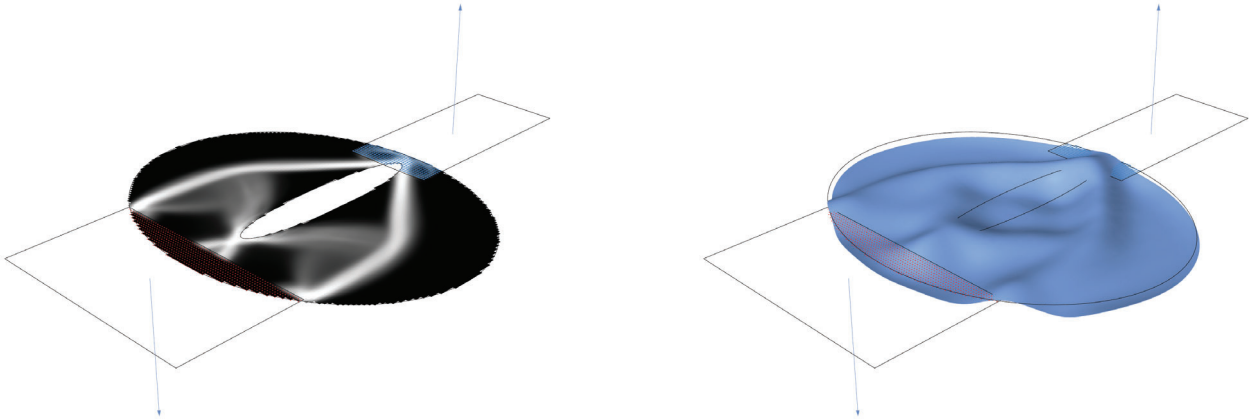

Figure 18. 2D topology optimised plate Structure. Author.

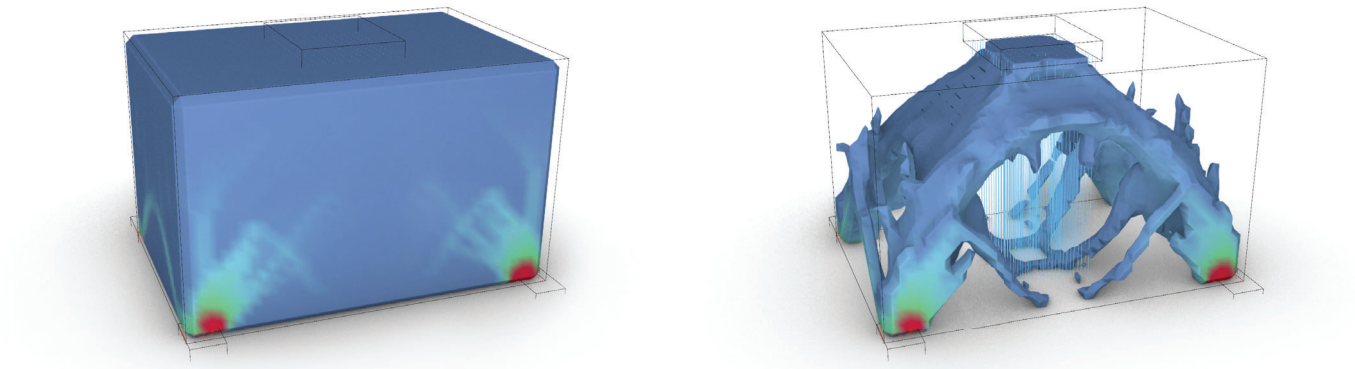

Figure 19. 3D topology optimised vault structure. Author.

Chapter - 3

Methodology

Research Scope and Limitations

How can 3D topology optimisation be used to inform the design of spatially printed structures?

This thesis aims to explore methods for using structural analysis tools in a creative, rather than evaluative, manner to generate novel structures and forms. The research will be approached from a design standpoint, focusing on the creative use of structural analysis tools, as opposed to the quality or validity of the analysis itself.

Any outputs in the form of structures or application based experiments are purely experimental, and should not be considered as a product. Furthermore, It should be noted that the design element of this thesis is not embodied in the individual structures or objects produced, these are only an output of the designed system, which is able to convert input data, in the form of virtual loads and support areas, into an optimised tangible output.

Sketches produced are also digital, they are sketches in the sense that they are quick and rough iterations of an idea, in most cases, they are sections of the script which have been tweaked and altered multiple times through a continous improvement process.

Research Methodology

While conducting the research-based thesis, I will adopt a design science methodology. This type of research model can be split into five phases (Vaishnavi, Kuechler, & Petter, 2011). Firstly the researcher must gain an "awareness of the problem" (Dresch, Lacerda, & Antunes Jr, 2015, p.74). Rodríguez Ramírez (2017) suggests performing background research, such as a systematic review of current literature, and design precedents, relating to the research topic. From this information, I will produce a set of criteria which will aid in my understanding of the problem, and help inform, and evaluate, the design of the systems and structures produced during the research. In the second stage, I will create a range of system concepts, which will address the problem to be solved (Dresch et al, 2015). The design of these concepts will be informed by the research and criteria from the first stage (Takeda et al. 1990; Vaishnavi et al, 2011). In the third stage a selection of design concepts are developed further and implemented (Takeda et al, 1990; Vaishnavi et al, 2011). The fourth stage involves the evaluation and critical analysis of the developed artefact/s against the criteria outlined during the first stage. The researcher may use a range of different tools in order to properly evaluate the artefact. Finally, the researcher draws a conclusion. If the artefacts do not meet the criteria developed during the first stage of the process, any number of stages may need to be repeated. Takeda et al (1990) emphasize that a single problem should be addressed per cycle, but if additional problems arise during the application of the method, these problems must be addressed with the application of additional cycles. This type of research may contribute knowledge to a field, in the form of "gaps in the theory" Dresch et al (2015), which can help to guide and create new areas of research. The aims and objectives detailed in Table 5 have been created to align the design science research model outlined by Takeda et al (1990), and Vaishnavi et al (2011), and summarised by Dresch et al (2015).

Aims	Objectives
1. Investigate the use of structural analysis and generative design tools in conjunction with spatial printing.	1a. Review literature and design precedents relating to spatial printing, structural analysis and generative design.
	1b. Analyse and trial a selection of generative design and optimisation software.
	1c. Identify opportunities to build upon existing research in the field of robotic spatial printing and utilise generative design and optimisation tools in an innovative manner.
2. Create a system for creating spatially printable structures	2a. Formulate optimal print settings and identify limitations of the printing process through experimentation.
	2b. Produce a range of conceptual systems and models which explore various structural optimisation techniques.
3. Create artefacts which exploit the qualities of physics simulation software and spatial robotic printing technologies. Case study	3a. Develop one, or a combination of systems from objective 2b, focusing on the production of outputs which emphasize structural optimisation qualities.
	3b. Produce a model Evaluate the developed artefacts against the criteria set in objective 1b.

Table 5. Aims, objectives, methods and criteria overview.

Methods	Criteria & Opportunities
A ***Review of Relevant Literature and Precedents*** is used to inform the design investigation and identify research oportunities (Martin & Hanington, 2012; Milton & Rodgers, 2013).	Objects produced by the structure generation algorithm should reflect the data created by the chosen analysis or optimisation system.
A ***Weighted Matrix*** is used to compare available CAD and optimisation software and select which programs will be used throughout the course of study (Martin & Hanington, 2012).	Prior Knowledge, Support & Documentation, Scripting Language, Pros & Cons, Paid, Number of analysis and optomisation methods supported.
See method for 1a.	
Experimental Research is used to evaluate the relationship between print settings and the quality of the structures produced (Capri & Egger, 2008).	Deflection, print quality, adhesion, failure height and modes.
Parallel Prototyping is used to explore a diverse range of design oportunities before choosing and refining one option (Martin & Hanington, 2012; Dow et al., 2010).	
Rapid Iterative design & Research through design methods are used to develop the most promising system from objective 2b (Martin & Hanington, 2012; Burdick, 2003).	
3b. Evaluate the developed spatial print system against the criteria set in objective 1a.	

Chapter - 4

Hardware Overview

Motion Platform

An ABB six-axis robotic arm acts as the motion platform of the spatial printing system. The robotic arm is capable of moving the tip of the end effector, the tool which is currently attached, to a point in space, and orientating the tool in almost any direction. This level of mobility enables the robotic arm to perform tasks and actions which cannot be performed with other CNC machines.

Robotic movements are defined by a toolpath, a series of points in space which the tip of the tool will pass through. In addition to x, y, and z coordinates, each point will have four angular units which define the orientation of the tool. The HAL Robotics plug-in for Grasshopper is used to generate Rapid code, which can be interpreted by the ABB controller unit and turned into robotic movements. In addition to the movements, a way of controlling the extruder through the Rapid Code was also devised. The commands to control the extruder are inserted into the HAL generated Rapid Code before it is exported from grasshopper. During initial tests, these commands were inserted manually, while later iterations of the Grasshopper script were configured to add them automatically.

Before a program is run, the Tool Centre Point (TCP) must be defined within Grasshopper, to ensure that the virtual geometry matches the real-world geometry. The TCP is defined by three dimensions, the x, y, and z distances from the tip of the tool, to where the tool attaches to the robot. The exact TCP of an end effector can be determined by manually controlling the robot and moving the tip of the end effector to touch a point in space four times from four different directions, the ABB robotic controller is then able to calculate the TCP values which are entered into Grasshopper.

Printing a structure involves exporting the Rapid code from Grasshopper and transferring it to the robot controller unit. Rapid programs must first be run in manual mode, slowly stepping through the program line by line, before the robot may be safely switched to automatic mode and move at its maximum speed.

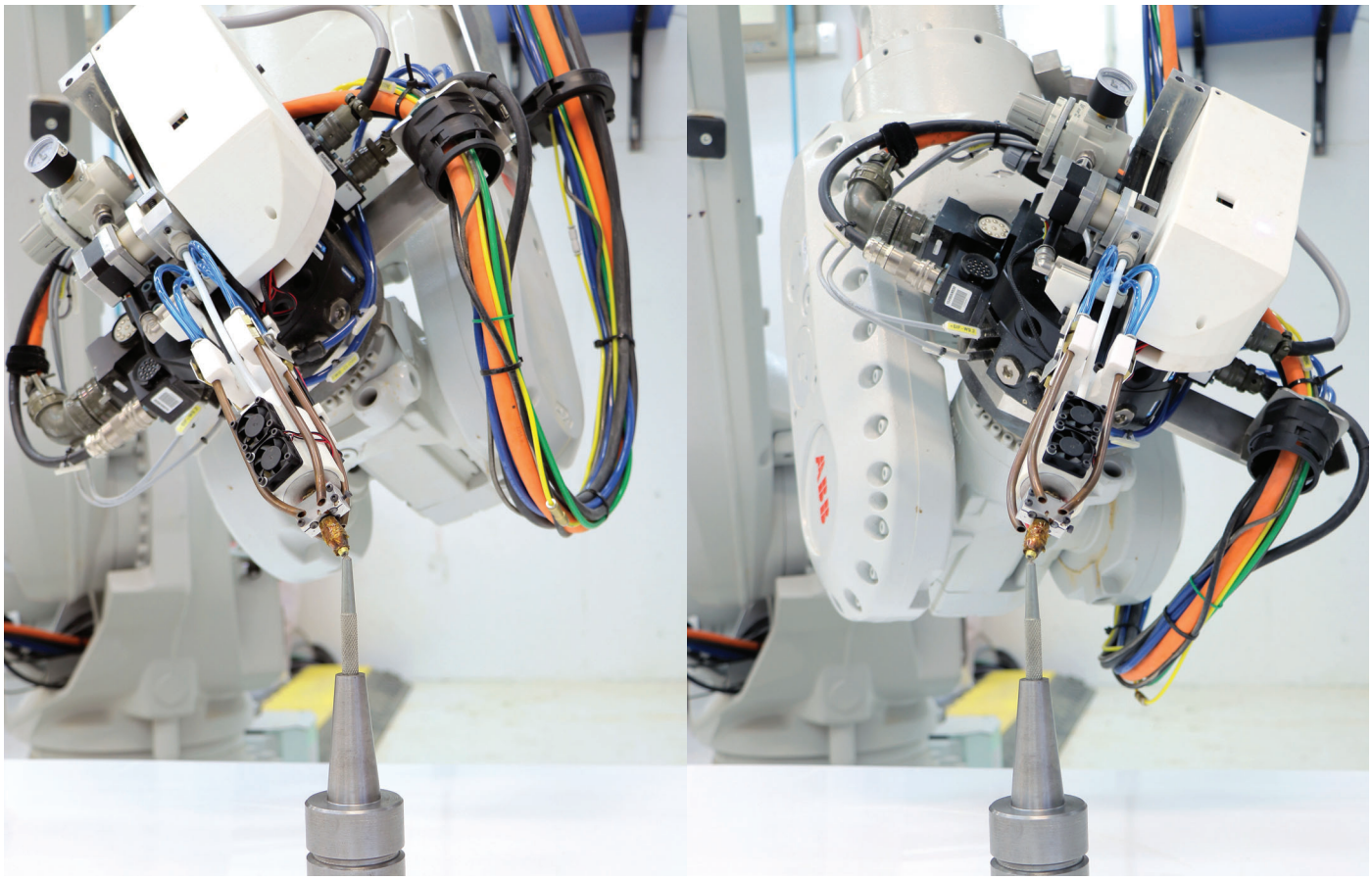

Figure 20. The TCP is determined through triangulation by approaching a point in space from multiple directions.

Extruder

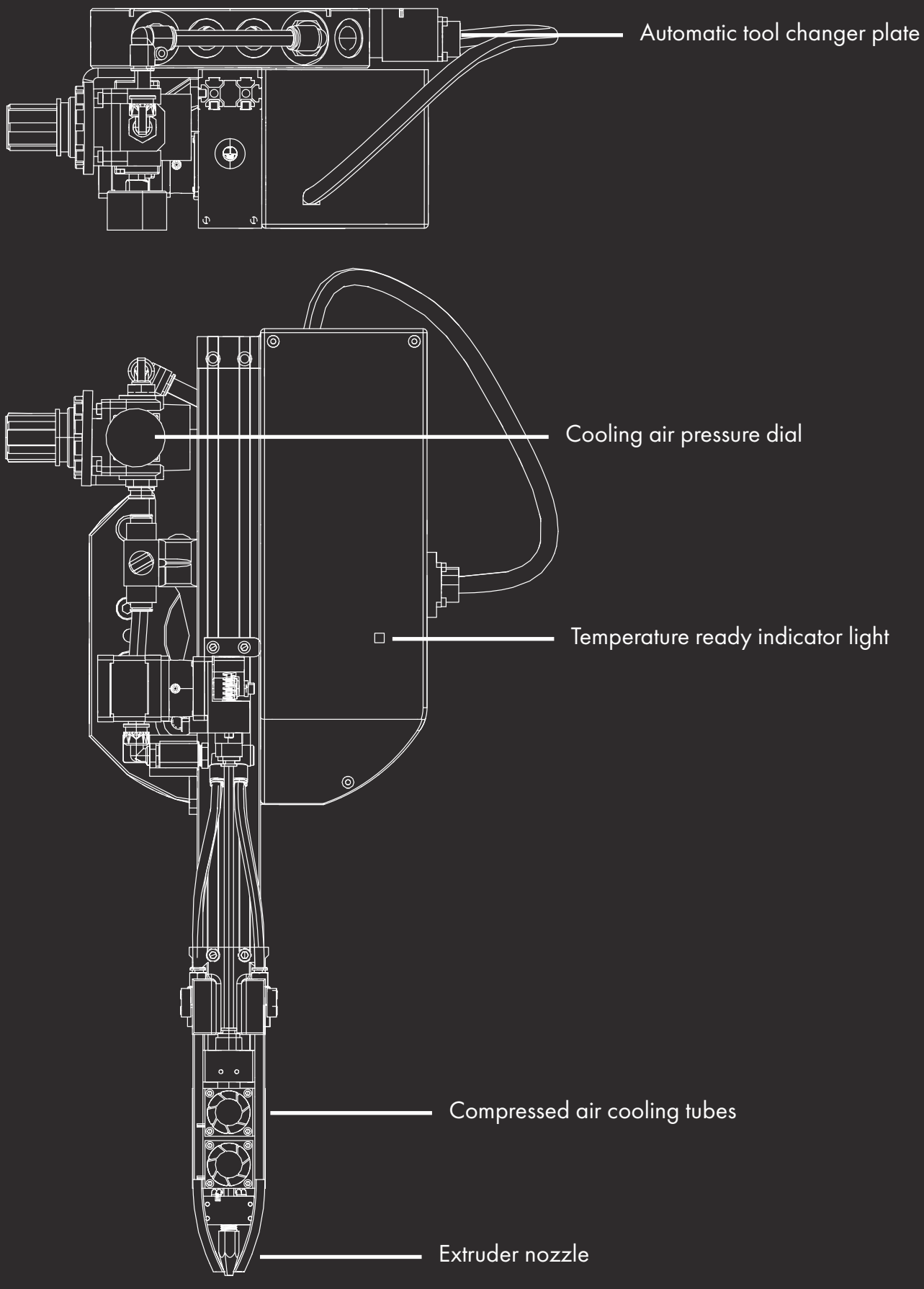

Figure 21. Spatial printing extruder.

Extruder

Extruder

A custom-built extruder, designed by Liam Gilbertson (2018), is used for spatial printing. However, this extruder remained untested in his research. As a result, the settings for optimal performance are established in this study. The extruder draws plastic filament through a heated chamber, where it becomes malleable, before being forced out through the nozzle. The extruder has an on-board Programmable Logic Controller (PLC) which receives and interprets electronic signals from the ABB robot control cabinet. Signals can be sent at any time during a print to alter the temperature of the extruder hot-end, the rate of extrudate flow, or activate/deactivate the compressed air cooling.

Material

PLA plastic has been selected as the material to be used throughout this research for a number of reasons. Firstly, PLA has higher flexural and tensile strength then most common FDM printed thermoplastics, including ABS, Polypropylene, Polyetherimide and Nylon12 (Beniak, Križan, Matúš, & Šajgalík, 2018; Song et al., 2017). Secondly, PLA has low shrinkage and is a biobased, renewable plastic which is Biodegradable (Kochesfahani, 2016). Lastly, the tools required to print PLA have been provided and I am able to build upon previous research conducted by Gilbertson (2018) and Papageorge (2018) at Victoria University of Wellington.

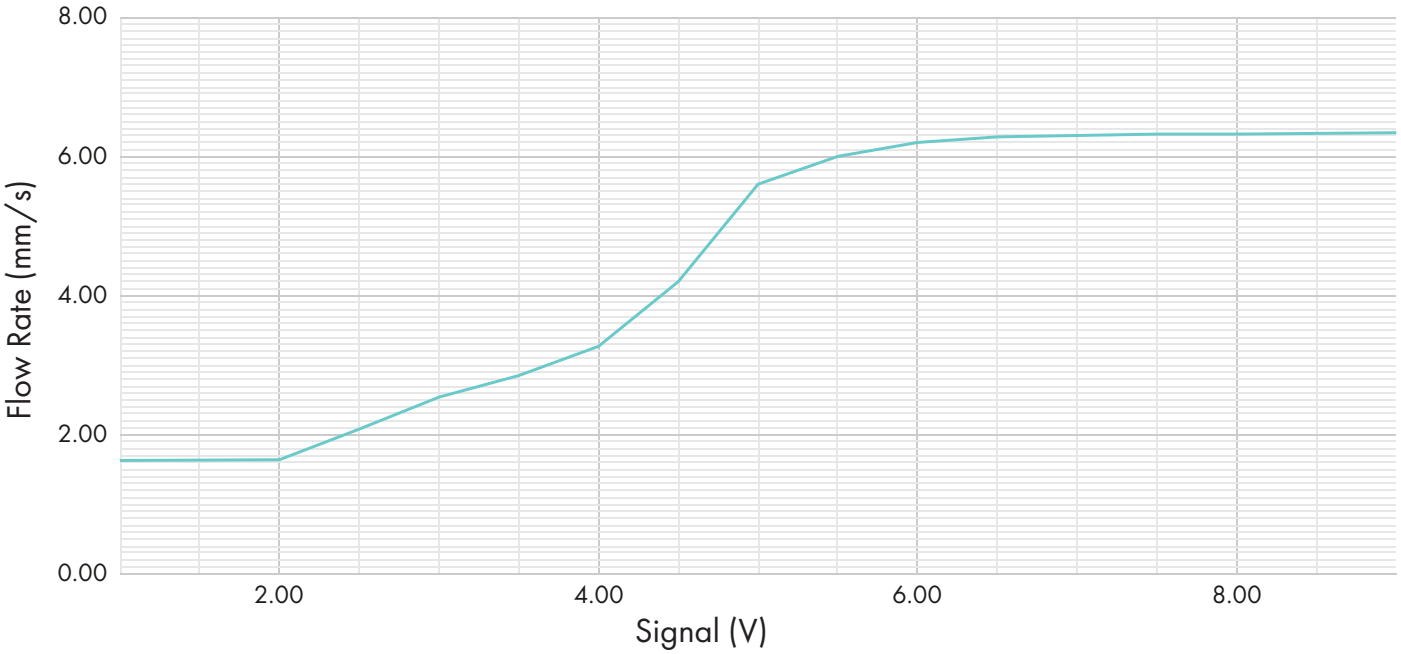

Figure 22. Flow Rate vs Signal Voltage graph.

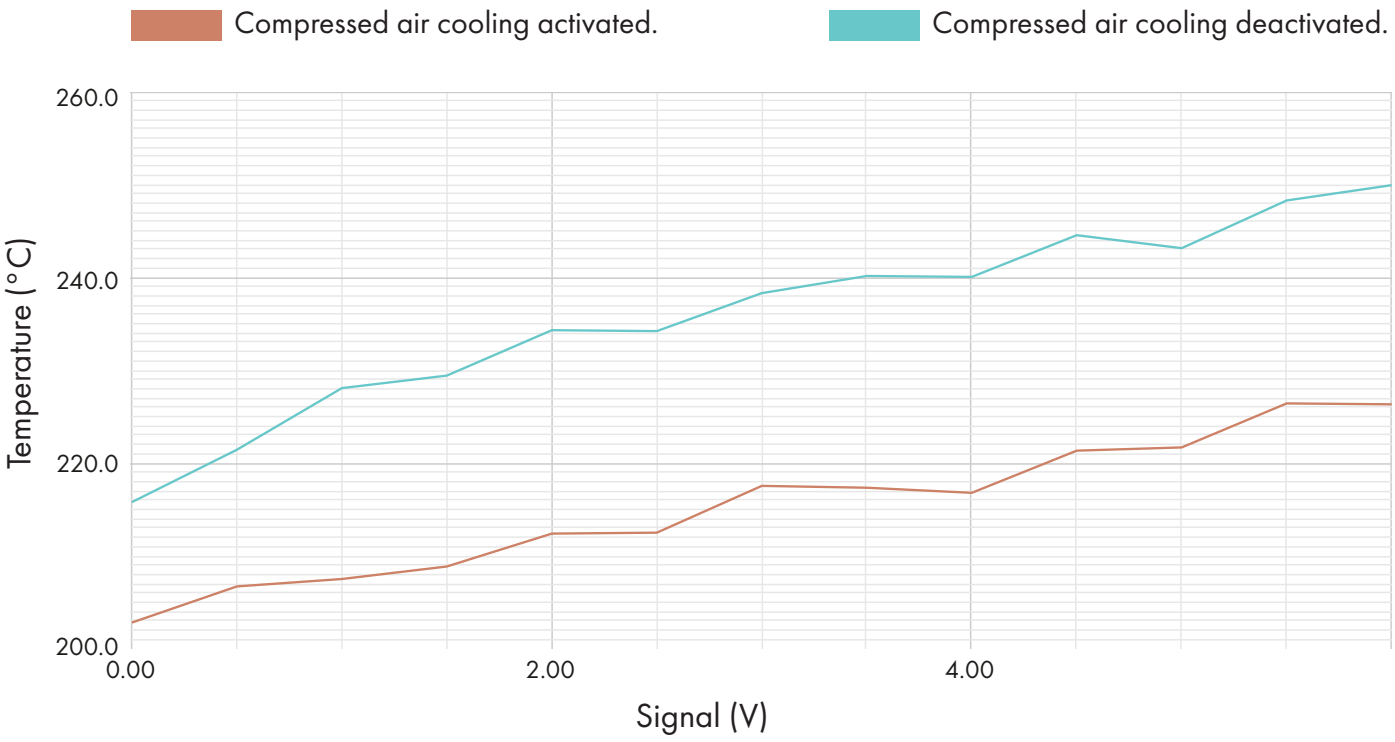

Figure 23. Extruder Temperature vs Signal Voltage graph.

Extruder Settings

Flow Rate

The flow rate in FDM printing is defined as how much material is extruded over time. Flow rate is an important factor to consider when spatial printing, as it has a large effect on the quality of the printed object. Over-extrusion is the result of a flow rate which is faster than the physical movement of the printer. It was found to produces elements which are bowed, kinked, or too thick. Under-extrusion, on the other hand, is encountered when too little material is being extruded. It resulted in weak elements and poor connections at nodes.

The code which has been uploaded to the extruder PLC (Programmable Logic Controller) determines the flow rate that corresponds to each signal voltage. However, forces, such as friction, often lead to inaccuracies between the programmed and real-world flow rates. To calculate the true flow rate in mm/s, I measured the time it takes for one metre of filament to be extruded in seconds, then 1000 is divided by the number measured. The test was repeated for a range of signal voltages, and the results were graphed, Figure 22. From this data the true flow rate for any signal voltage can be interpolated.

Extruder Temperature

Like flow rate, the temperature of the extruder can have a large influence over the quality of a spatial print. Extruder temperature dictates how soft the plastic is when exiting the extruder, how strong the joints between two extrusions are, and how long it takes for the plastic to cool and harden. The actual extruder temperature for each signal voltage was found to be different from the programmed value. Tests were performed to measure the actual temperature of the extruder at a range of signal voltages. The tests were completed with the compressed air cooling both activated, and deactivated, and this information was then graphed. It was found that turning the compressed air cooling on altered the temperature by approximately twenty degrees Celsius, as can be seen in Figure 23.

Chapter - 5

Print Based Calibration

Cube Test

The cube print order is such that extrusion is continous. First the base of the cube is printed, followed by the uprights and diagonals.

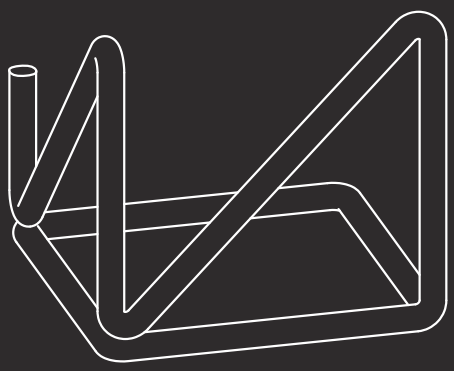

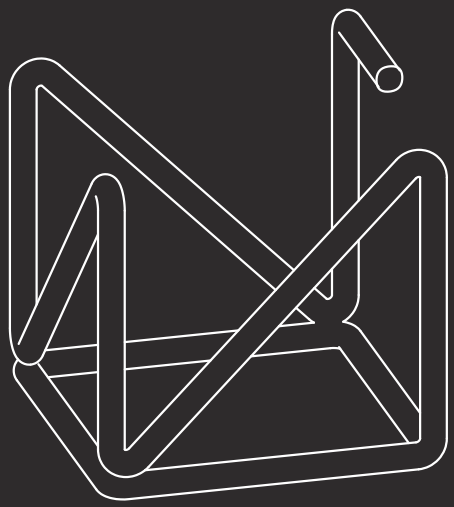

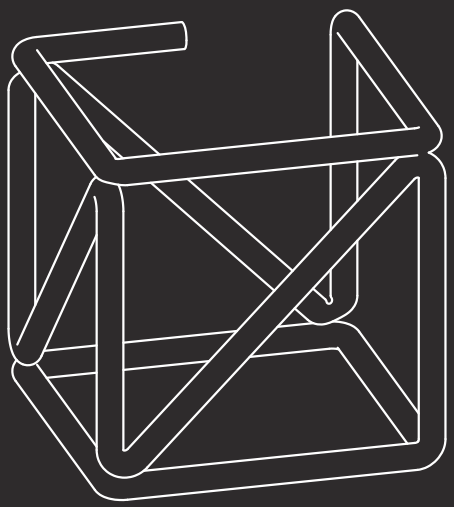

Bridging between the top corners forms the remaining four edges of the cube.

Figure 24. Cube test toolpath.

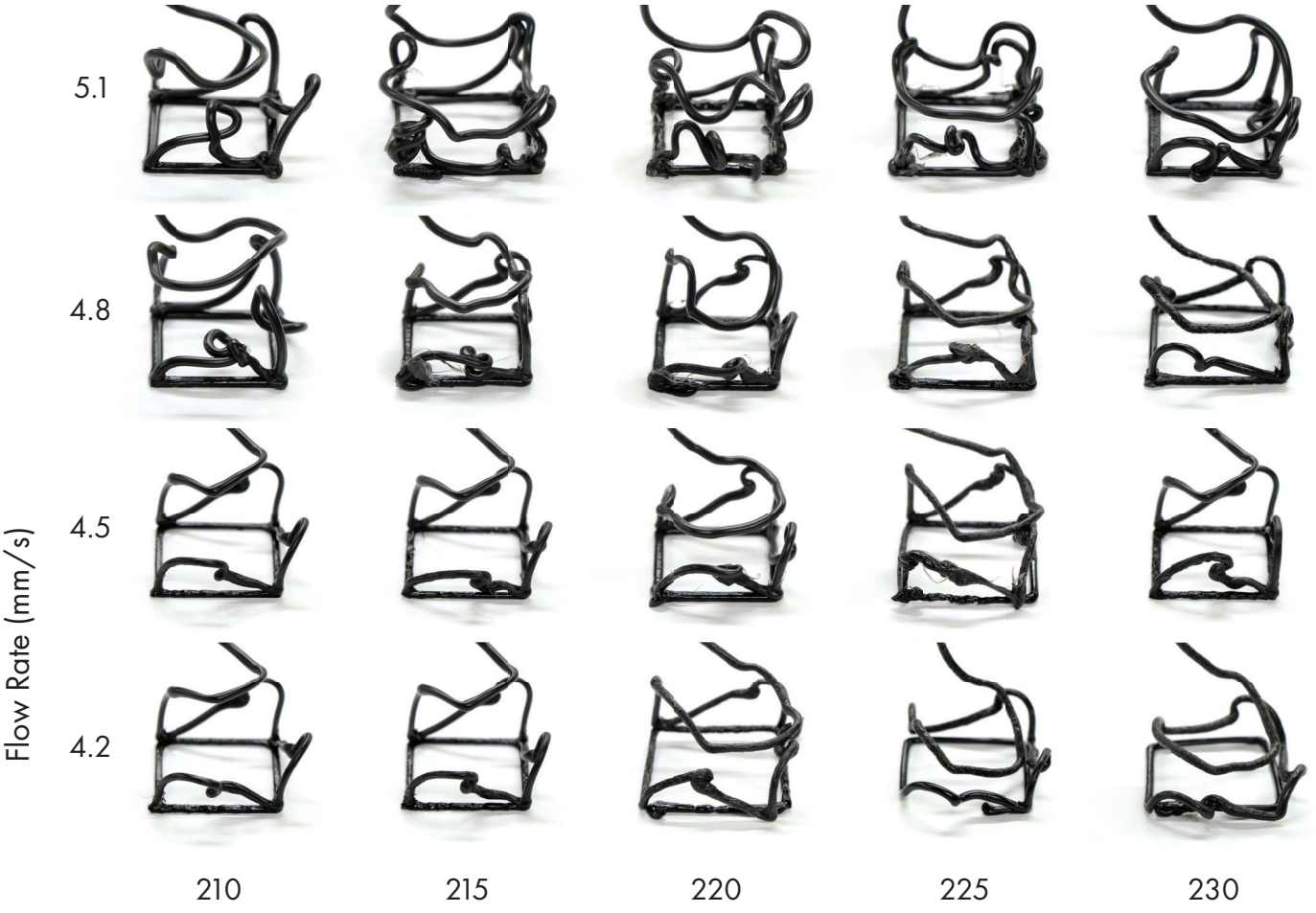

Figure 25. Matrix of cubes revealing the effect of different print parameters.

Three-Axis Cubes

Method

In order to find the optimum extrusion temperature, flow rate, and print speed, a series of 50mm cubes were printed. In the first series of tests, the print speed was set to 5mm/s, while the extruder temperature and flow rate were varied. Extruder temperatures between 210°C and 230°C were tested in 5°C increments. Flow rates of 4.2mm/s to 5.1mm/s were also tested in 0.3mm/s increments. When arranged in a matrix, Figure 25, the effects of different combinations of the three settings can be visually analysed.

Results

None of the tested combinations, of print speed, flow rate and extruder temperature, yielded successful results. It was noted that when printing the vertical members, the nozzle of the extruder would often become caught on the top of the member, as it began to move downwards to print the following diagonal element.

Initially, the compressed air cooling was set to be active throughout the entire print. However, it was found that when printing the base layer, close to the print bed, the compressed air would be reflected back at the nozzle and the extruder would often become to cool and stop extruding. I also encountered adherence issues between the first layer and the print bed. To overcome these problems, the cooling was deactivated while printing the first layer and was only activated once the first vertical member had begun printing.

Six-Axis Cubes

The most successful settings from the three-axis cube tests were carried over to the six-axis tests. In the three-axis tests, the extruder remained in the same orientation throughout the duration of the print, normal to the printing surface. In addition to moving in the x, y and z axes, robotic arms are also able to orientate a tool in almost any direction, in the tests shown opposite, Figure 27, this capability was utilised. It was found that reorienting the extruder, when printing diagonal members, produced more successful prints, as seen in Figure 26. For these initial tests, each reorientation was manually coded. However, this was a time-intensive process, if six-axis movements were to be used for printing more complex structures, a system for automatically generating reorientations would need to be implemented.

Additional experiments were performed which investigated the addition of pauses into the script. In conventional FDM printers, the size of the nozzle is typically around three times smaller than the diameter of the filament being used. In the spatial printing extruder, the diameter of the nozzle is only slightly smaller than that of the filament, as a result, the filament is able to pass through the hot-end with minimal heating. The time the filament spends in the hot-end dictates the amount it melts. While printing straight sections, the filament passes through the extruder quickly, softening only slightly. When a connection point is reached, there is a pause in the extrusion and robot movement, and the compressed air cooling is deactivated, to allow more heat to be transferred to the filament and allowing a stronger connection to be made at the nodes. The result of combining this method with the optimum settings from the previous experiments produced the cube pictured in Figure 27.

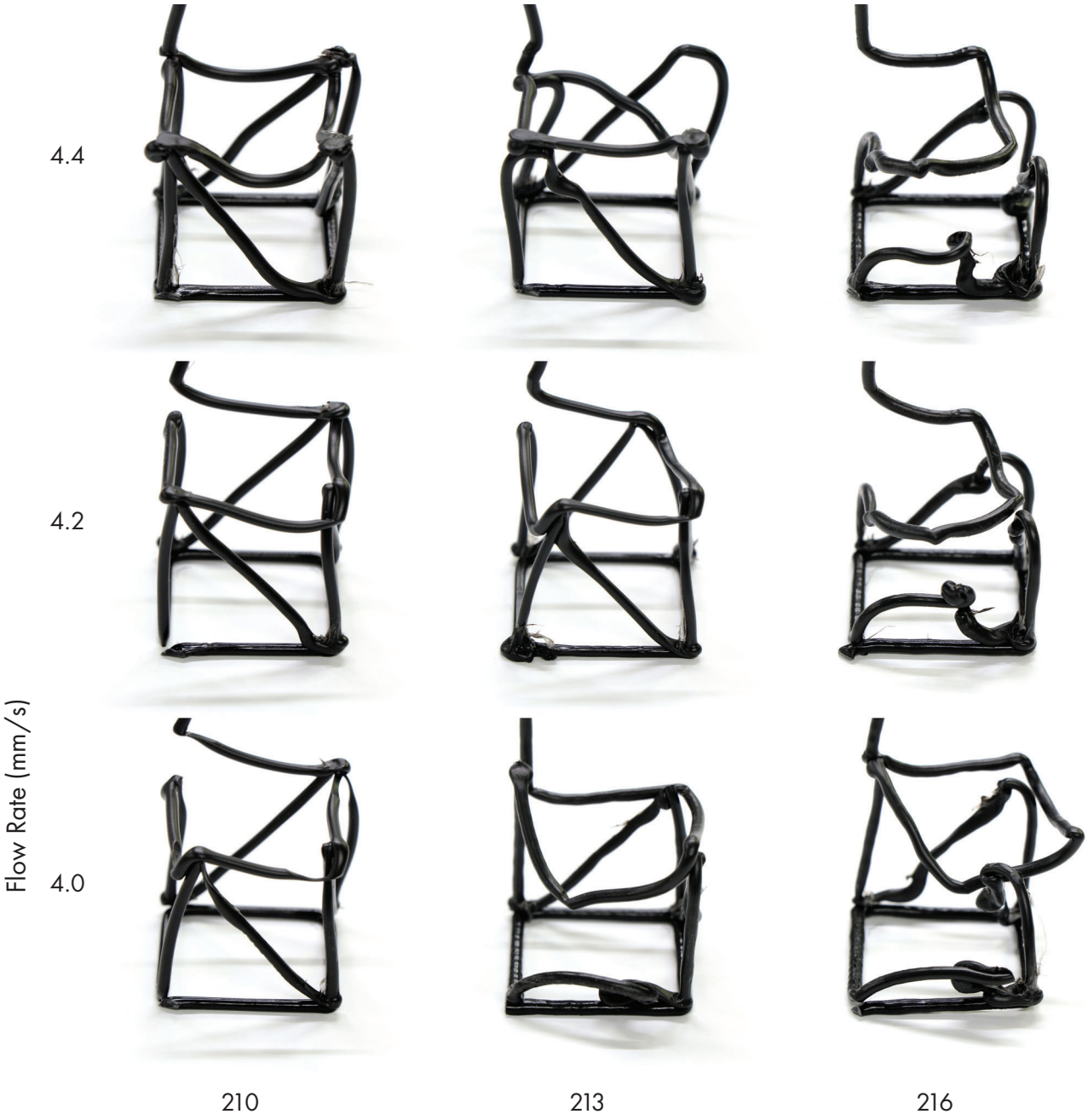

Figure 26. Matrix of six-axis printed cubes.

Figure 27. Six-axis printed cube with the addition of pauses.

Bridge Test

The footings are printed first. Dashed lines represent rapid movements, where extrusion is stopped, and the print head moves rapidly to the next footing.

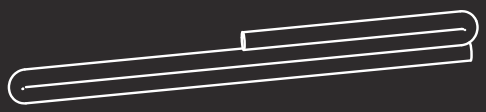

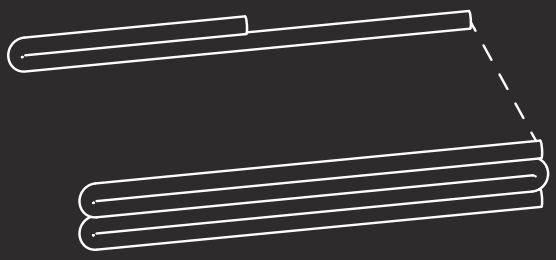

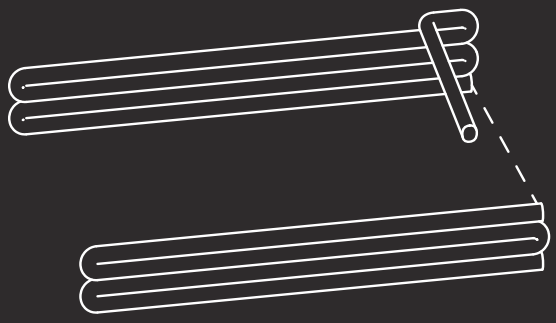

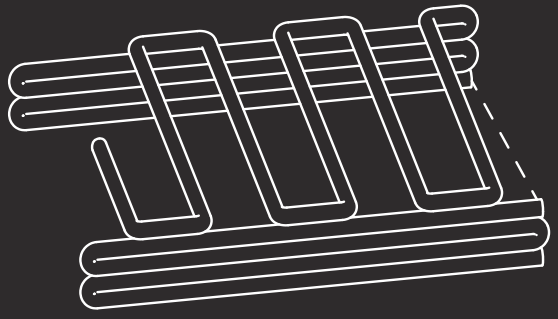

Spans are printed which bridge the space between each of the footings.

Figure 28. Bridge test toolpath.

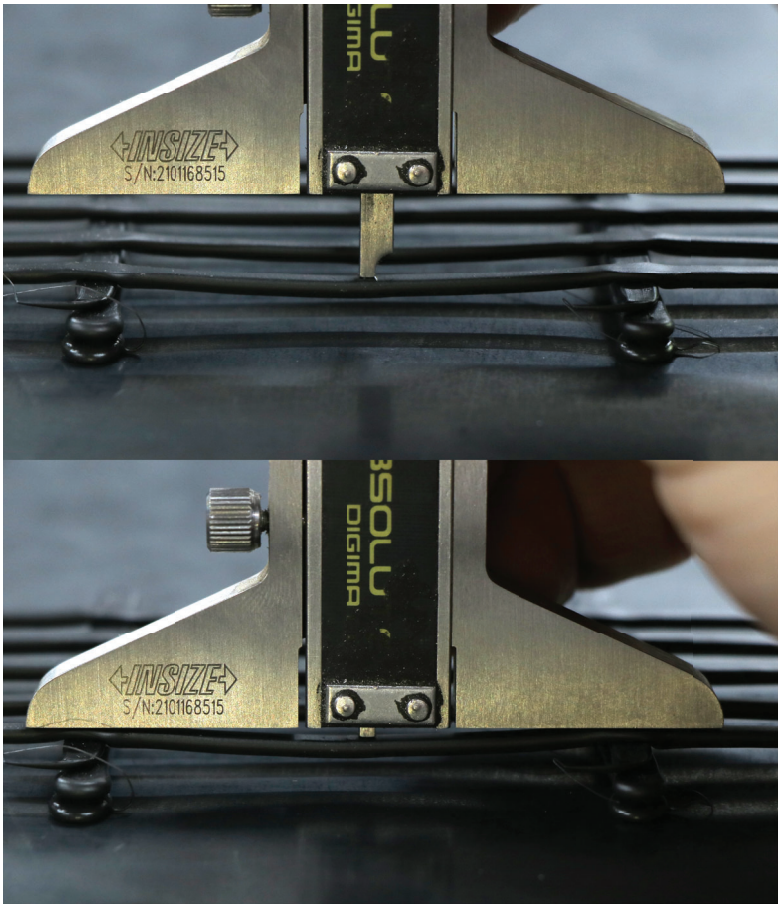

Figure 29. Digital calipers were used to measure how much each bridging element had bowed.

Bridge Test

Method

Bridging tests were performed in order to rigorously examine the effects of varying the flow rate at different print speeds. An extrusion temperature of 213°C was used for the bridge tests, as this was found to be the optimum temperature setting from the previous experiments. Flow rates between 3.5mm/s and 5.5mm/s were tested in 0.1 mm/s increments, for a total of twenty settings, tested at three different print speeds, 4mm/s, 5mm/s and 6mm/s. Each test was repeated five times, and the measurements averaged, to ensure the accuracy and validity of the results. The bowing of each bridging element was measured using the depth gauge of a pair of digital callipers, as seen in Figure 29. The callipers were zeroed on a surface plate before each measurement was taken. These tests provided quantifiable data, which was able to be graphed and analysed to find the optimal flow rate, and print speed, which produced bridging elements with minimum deflection.

Results

Every second span was found to have greater bowing than the span before it, producing the peaks and troughs seen in Figure 30, 31 and 32. It was concluded that this was a result of friction between the spool of filament and its mounting, and the direction each span was printed in. As the robotic arm printed from left to right additional filament was drawn off the spool, increasing friction. Printing in the opposite direction, from right to left, consumed the slack filament in the system, resulting in less friction and effectively increasing the flow rate, producing elements with greater bowing. However, it was found that higher print speeds, coupled with lower flow rates, helped to smooth inconsistencies and ultimately generated straighter spans.

An unexpected result of high print speeds coupled with low flow rates was decreased adhesion between the footings and bridging members. This is likely due to a reduction in the temperature of the extruded filament, as it passes through the extruder hot end more quickly, and/or a decrease in pressure when forming the joint, as a result of the thinner print bead. From the tests performed, and results analysed, the optimum print settings were determined to be a print speed of 5mm/s, a flow rate of 4.3mm/s, and an extruder temperature of 235°C without cooling activated, and 213°C with cooling activated. This combination of settings produced consistently straight bridging elements, with strong connections to the footings.

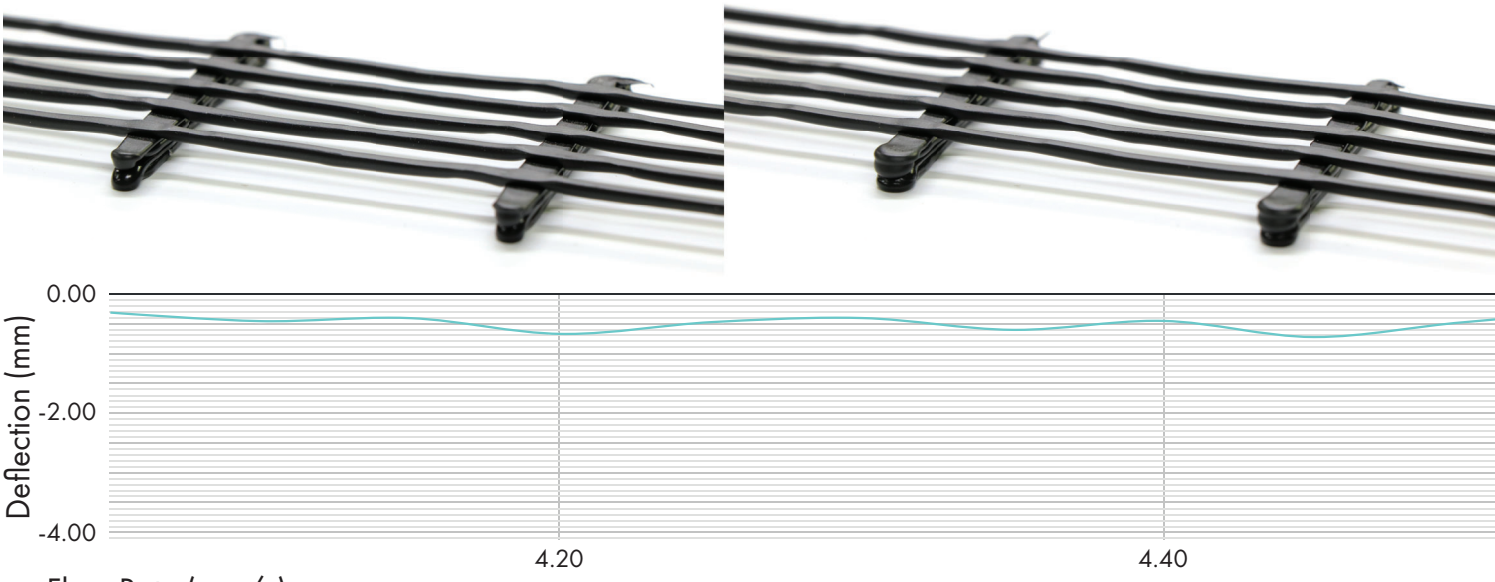
0.00
-2.00
-4.00
Deflection (mm)
4.20
4.40
Flow Rate (mm/s)

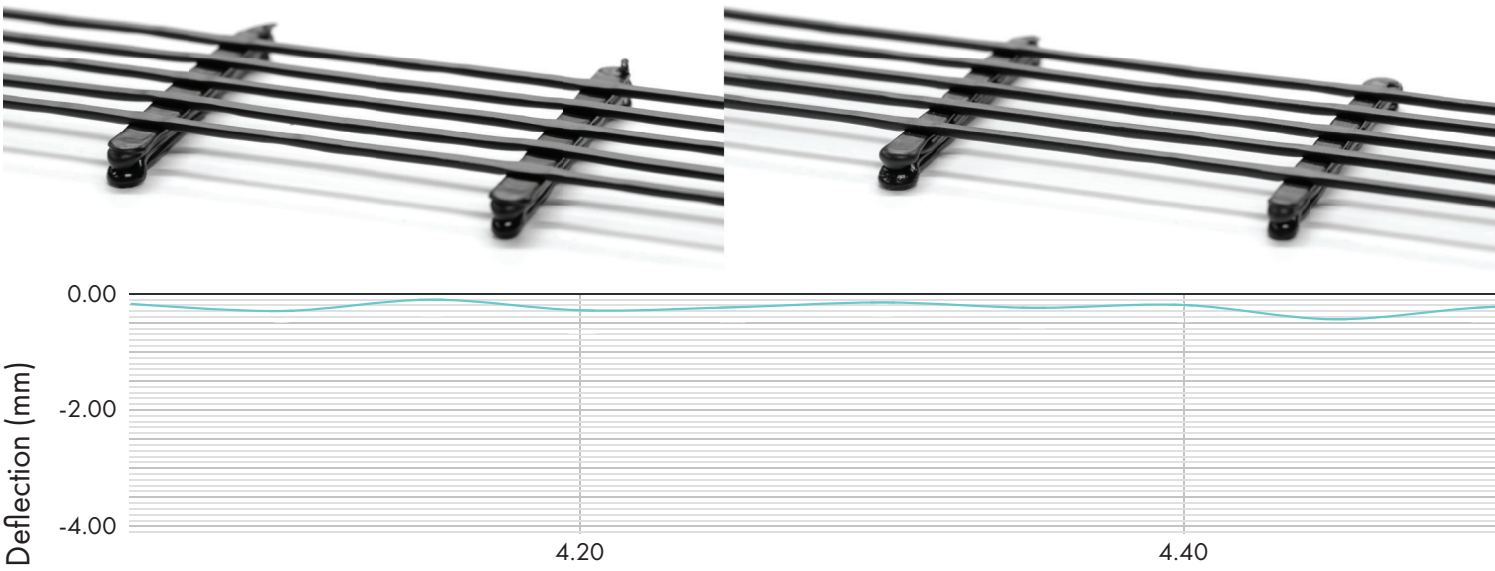
0.00
-2.00
-4.00
Deflection (mm)
4.20
4.40
Flow Rate (mm/s)

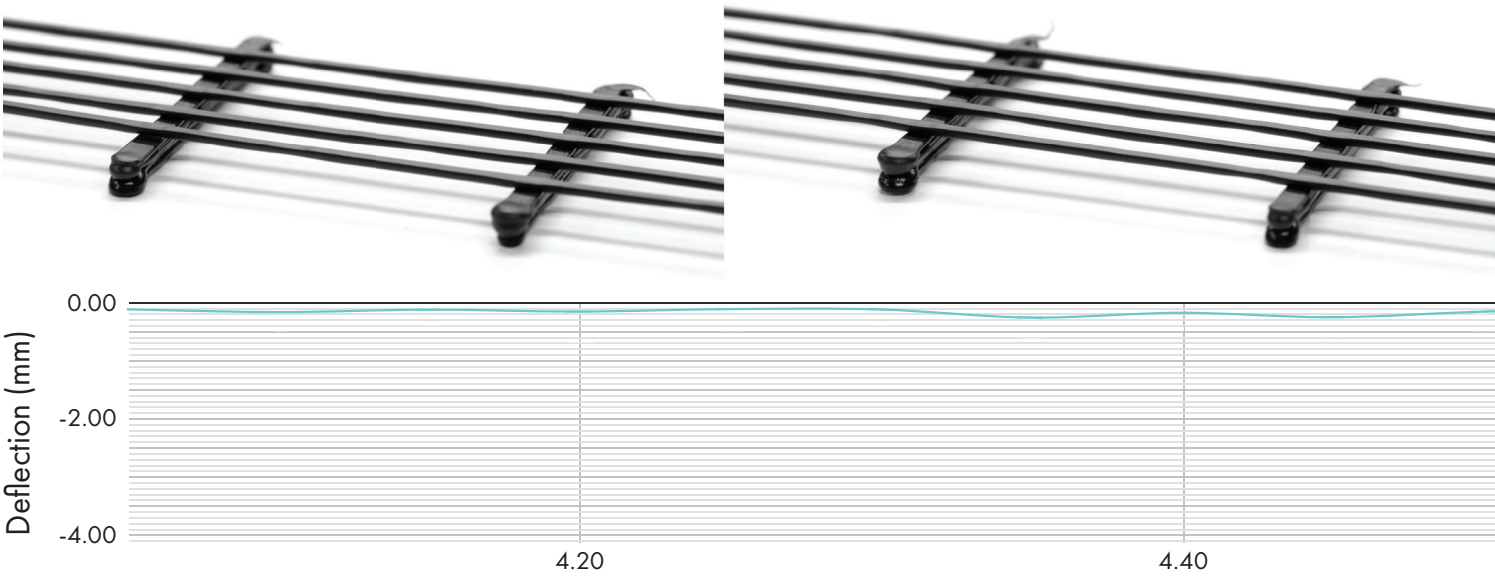
0.00
-2.00
-4.00
Deflection (mm)
4.20
4.40
Flow Rate (mm/s)

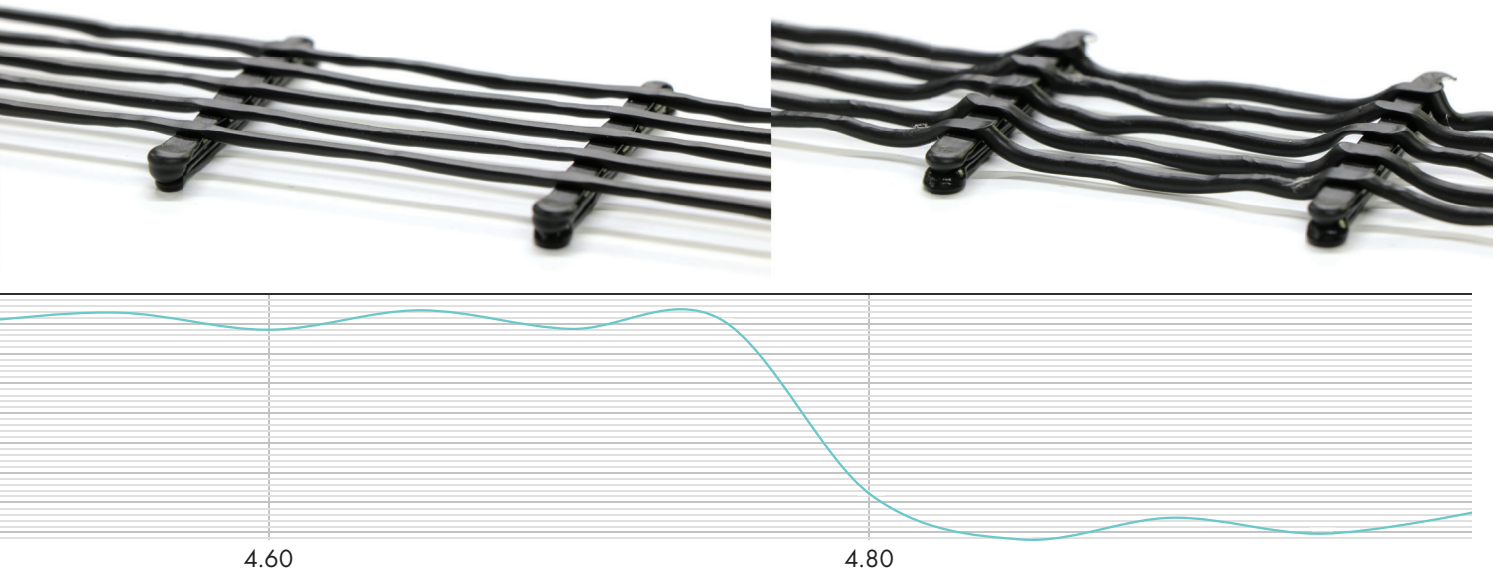

Figure 30. Results of the bridge test performed at 4mm/s print speed.

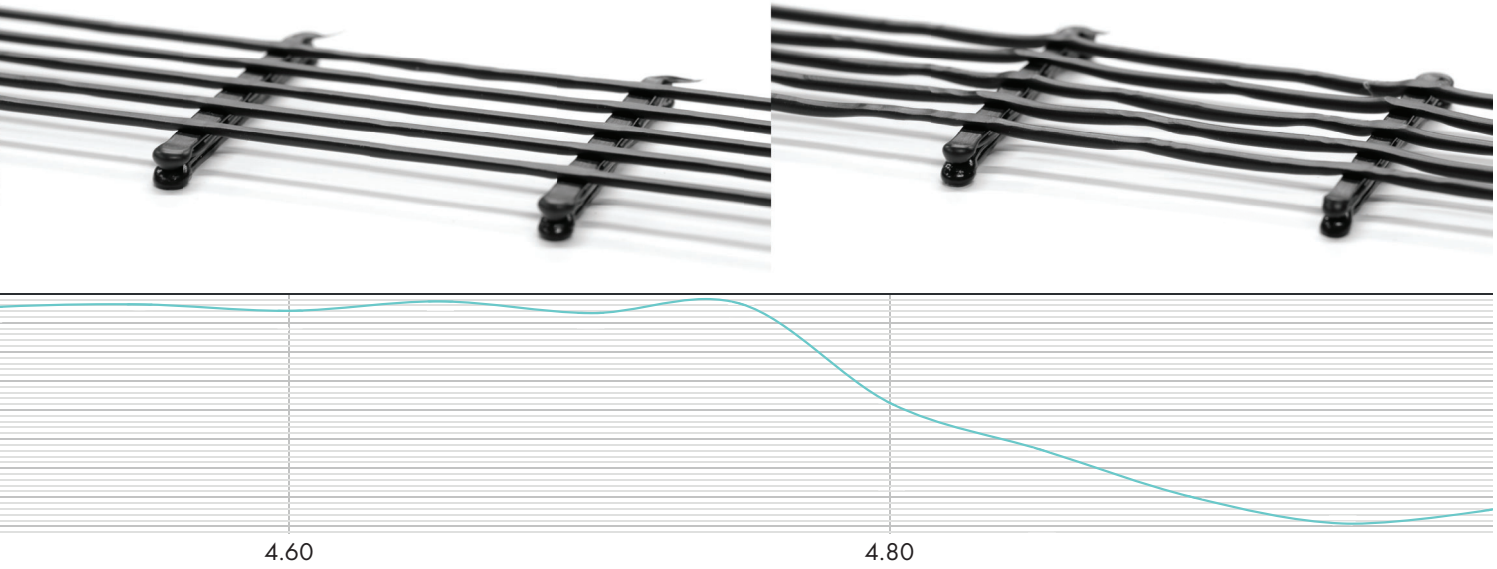

Figure 31. Results of the bridge test performed at 5mm/s print speed.

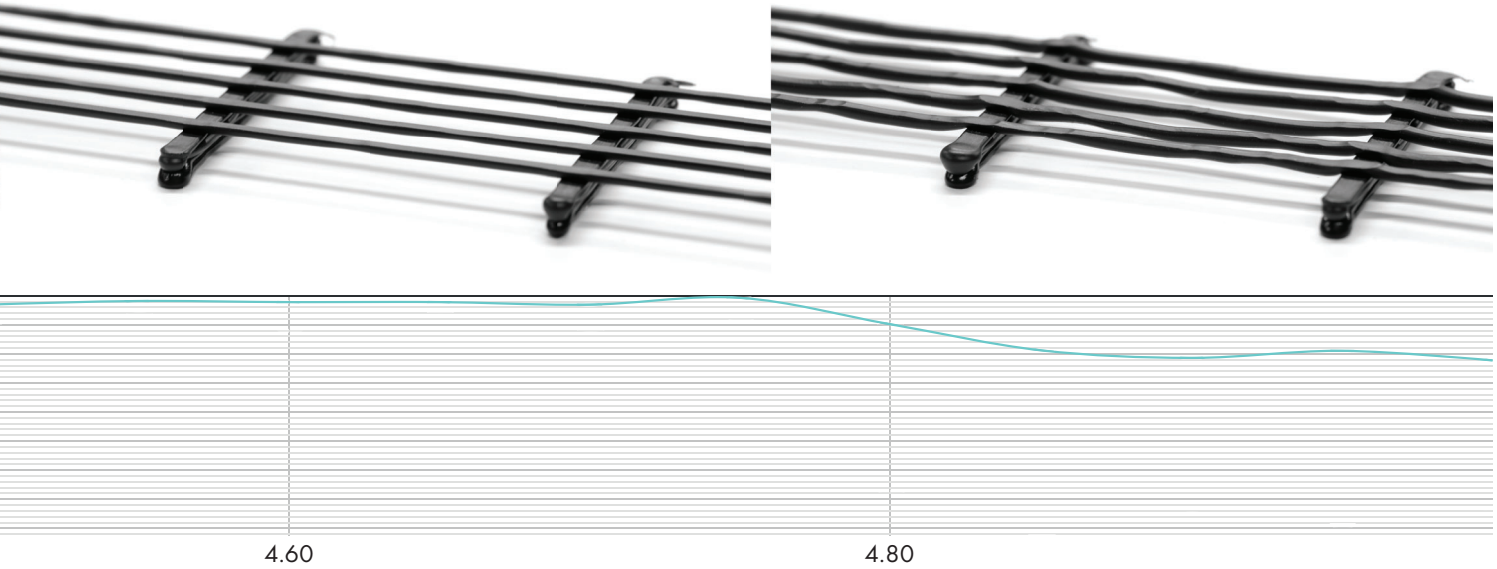

Figure 32. Results of the bridge test performed at 6mm/s print speed.

Helical Test

A Grasshopper component was created which generates a helical toolpath when given an input curve, section shape and radius.

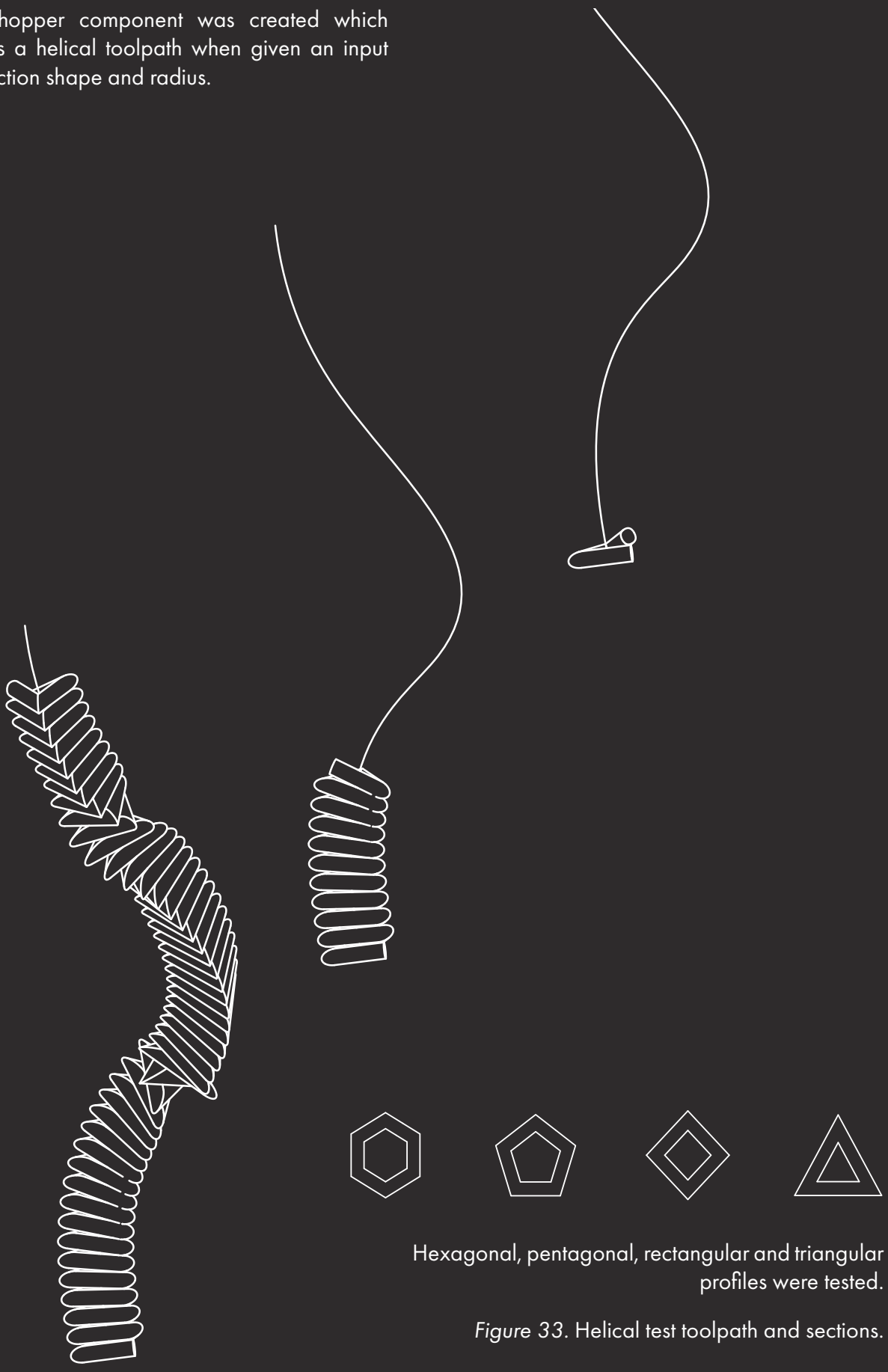

Hexagonal, pentagonal, rectangular and triangular profiles were tested.

Figure 33. Helical test toolpath and sections.

Figure 34. Helical test failure modes

Helical Test

Method

The helical tests investigated the production of thicker structural elements by spiralling upwards along a linear or curved toolpath. Hexagonal, pentagonal, rectangular and triangular profiles were tested at a range of different diameters.

Results

It was found that as the radius of the profile decreased, the definition of the profile edges was lost, with different profiles becoming indistinguishable below 6mm in diameter. Increasing the thickness of the helical columns increased the height at which the column failed. However, this relationship was not linear, as increasing the radius of the profile over 2 mm provided diminishing returns.

The point at which a column failed was difficult to determine. Often the profile of the column would become larger and more disorderly towards the top, resulting in a spring-like section, Figure 34 (left).

In other examples, after a certain height, the quality of the column decreased but the structure remained mostly intact, Figure 34 (centre). In one case, there were two anomalies situated partway through the print, but the structure managed to recover after these points, Figure 34 (right).

It was found that by printing helically, curved toolpaths, in addition to linear toolpaths, could be produced precisely. The larger elements produced are stronger in compression to the regularly printed elements, however, they are more susceptible to brittle fractures. The elements produced in the helical tests demonstrate a novel opportunity to create spatially printed structures consisting of elements of varying thicknesses. The thickness of elements in each section of a structure could be based upon the amount, and type of stress predicted in the analysis, with thicker helical members used in areas under compression, and standard members used in areas under tension.

Chapter - 6

Structure Generation

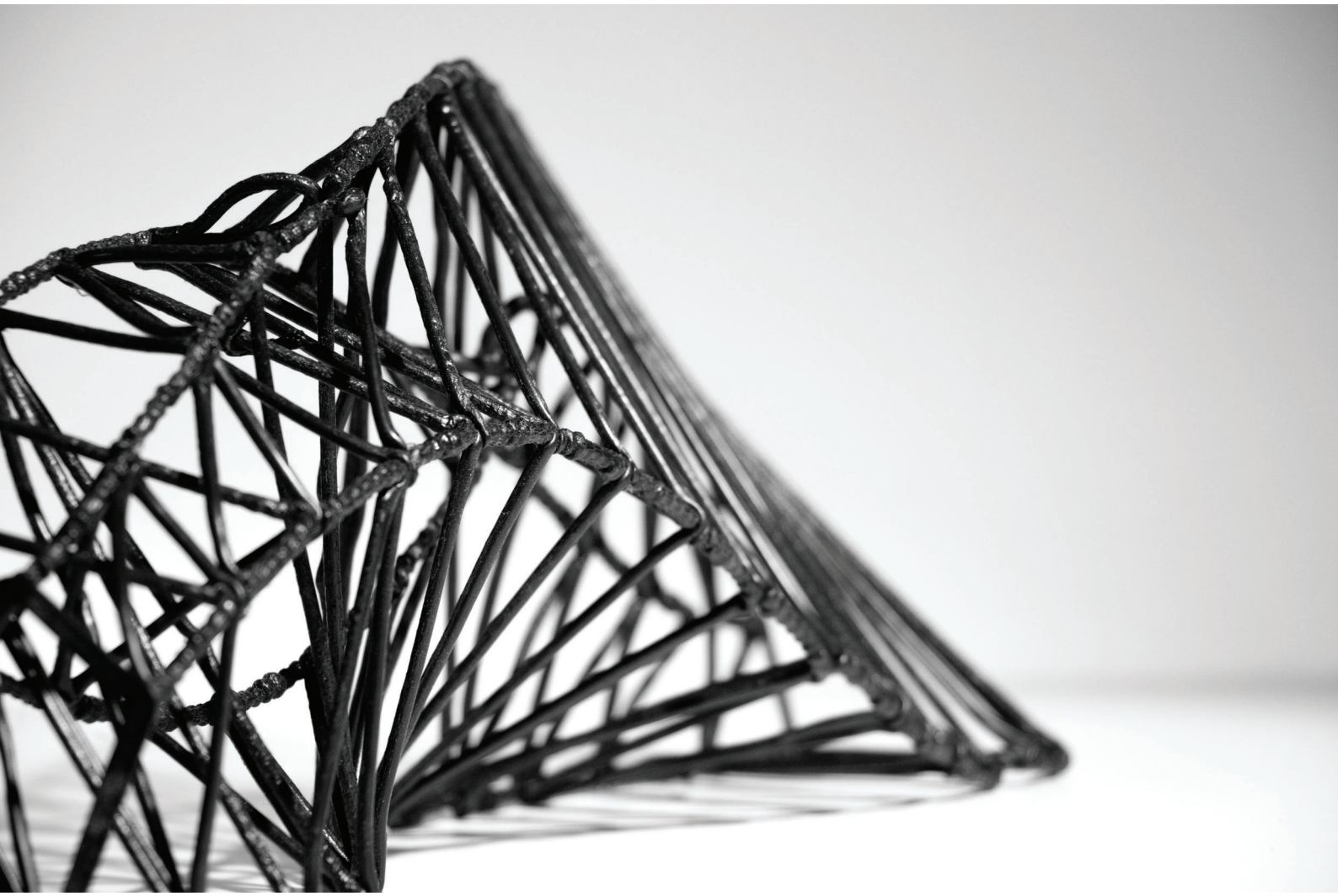

Figure 35. Example of a curve generated structure.

Curve Driven Structures

In this section parallel prototyping is used to explore four potential systems for generating optimised structures. The first two systems investigate what kind of structures can be generated using curves as input geometry, in order to simulate the use of data from a shell analysis.

The aim is to produce novel structures which are volumetric, rather than 2.5D, unlike the shell structures produced by Tam & Mueller (2016) and Battaglia, Miller & Zivkovic (2019). Both prototypes were produced using the CDA (Curve Driven Algorithm) to convert input curves into a complete, printable structure.

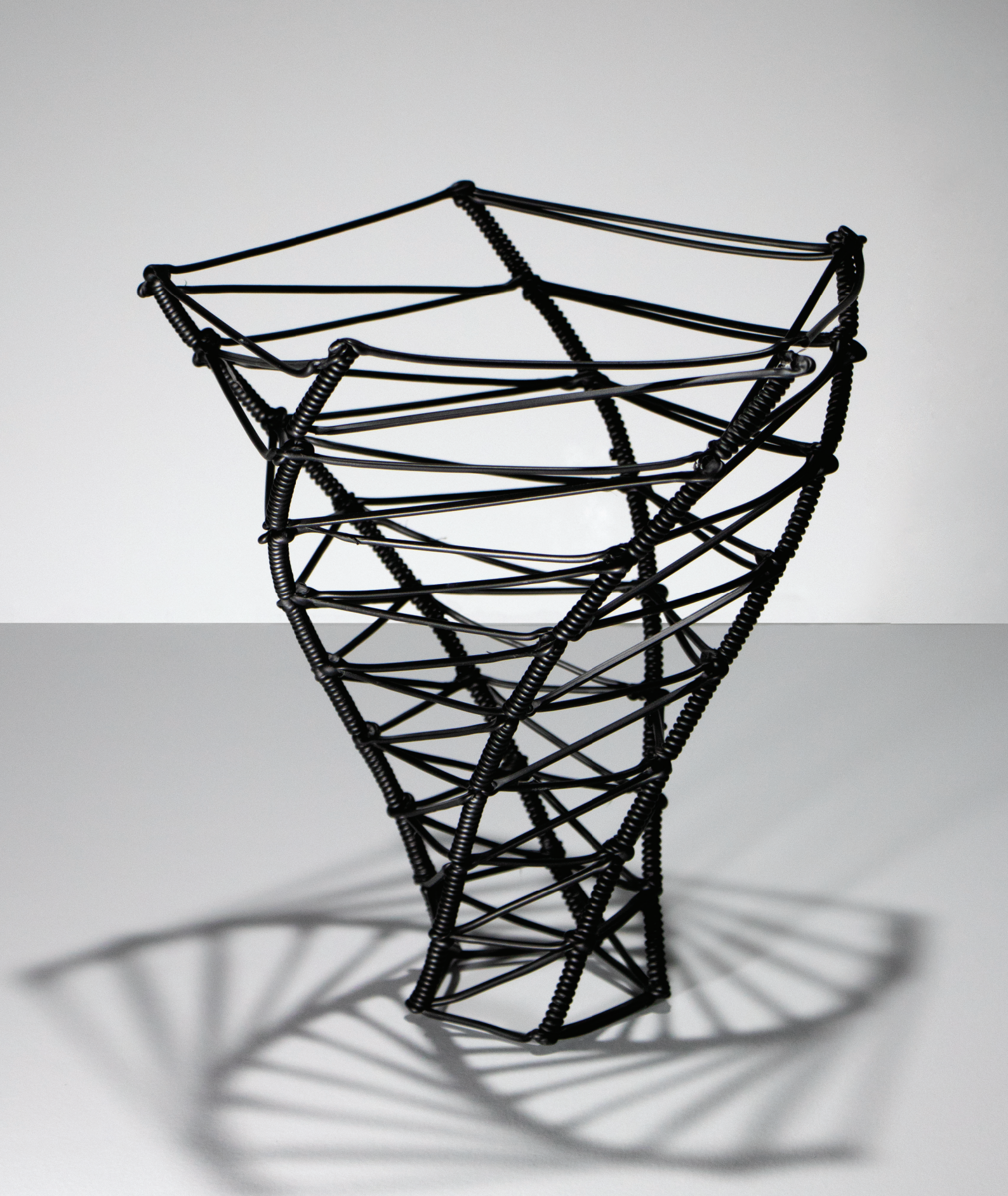

Figure 36. Non-Intersecting Input Curves Structure.

Non-Intersecting Input Curves

An array of five 3D curves were used as the input geometry to generate the first structure. This type of input geometry was used to test how the CDA dealt with non-intersecting spatial curves. To visually communicate the hierarchy of input geometry versus generated geometry, the input curves have been printed helically producing thicker geometry, while the generated parts of the structure, the diagonal and horizontal bracing, are thinner. In Figure 36 these input curves can be seen as the thicker, twisting vertical members.

The printed artefact had very little bowing in the horizontal members, even in the largest spans which measured up to 100mm, and strong connections at the nodes. There were no issues with print order or collisions between the extruder and printed geometry. However, issues with the height of the helically printed members, in relation to the horizontal bracing which is printed atop the members, were encountered. These height discrepancies caused the tip of the extruder to place a large force on the vertical members as it passed over them, resulting in print failures such as the vertical members shearing off at their lower connection points, or the structure coming loose from the print bed during printing.

At first, this was thought to be due to over-extrusion at the end of each of the helically printed members resulting from a programmed pause. But, upon closer inspection of the script, there was found to be no pause programmed at that point. Instead, the issue was found to be a result of the way the helical toolpath is generated from the input curve, with the toolpath extending above the endpoint of the input curve. The last points in each of the helical toolpaths were removed to compensate for this discrepancy, which resolved the issue.

Figure 37. Intersecting Input Curves Structure.

Intersecting Input Curves

Five procedurally generated curves were used as input geometry to generate the second structure. The generation and printing of this structure explored how the CDA dealt with more complex intersecting spatial curves, made to emulate the stress lines produced by finite element analysis plug-ins. Unlike the previous test, the input curves used to generate the second structure cross over one another multiple times within their bounding volume, producing an inconsistent print order. In the previous test, there was a consistent print order, meaning the order in which the vertical members were printed was exactly the same for each layer. In this test the input lines converge and diverge at different rates meaning the order the vertical members are printed in is inconsistent from layer to layer.

It was found that the algorithm used for the previous test was unable to generate a viable print order, as a result, there were multiple collisions between existing geometry and the extruder.

The print was able to complete but not without several defects caused by the collisions. This print was also attempted with helical paths used to represent input curves however the extra rigidity added by these members caused the print to become unstuck from the print bed any time there was a collision, rather than flexing as the first print did. Attempts were made to alter the script to remove collisions, however, a suitable method could not be found.

Furthermore, generating structures more complex than the early structures explored in these experiments would be difficult. The time required to develop this system of freeform printing is beyond the scope of this thesis. However, this system does present opportunities for future research. One option could be to offset the input curves inwards to produce a radial type grid structure.

Figure 38. Helical elements from the first Volume Defined Structure.

Volume Defined Structures

The following conceptual systems utilised volumes as input geometry. These Volume-Driven Algorithms (VDA) generate structure, and print order, simultaneously. The structures produced are based upon grid patterns and repeating print orders. While this method of structure generation is creatively limiting, it does produce dependable results, as once a single unit has been proven to print reliably, it can be patterned and reproduced without fear of collisions.

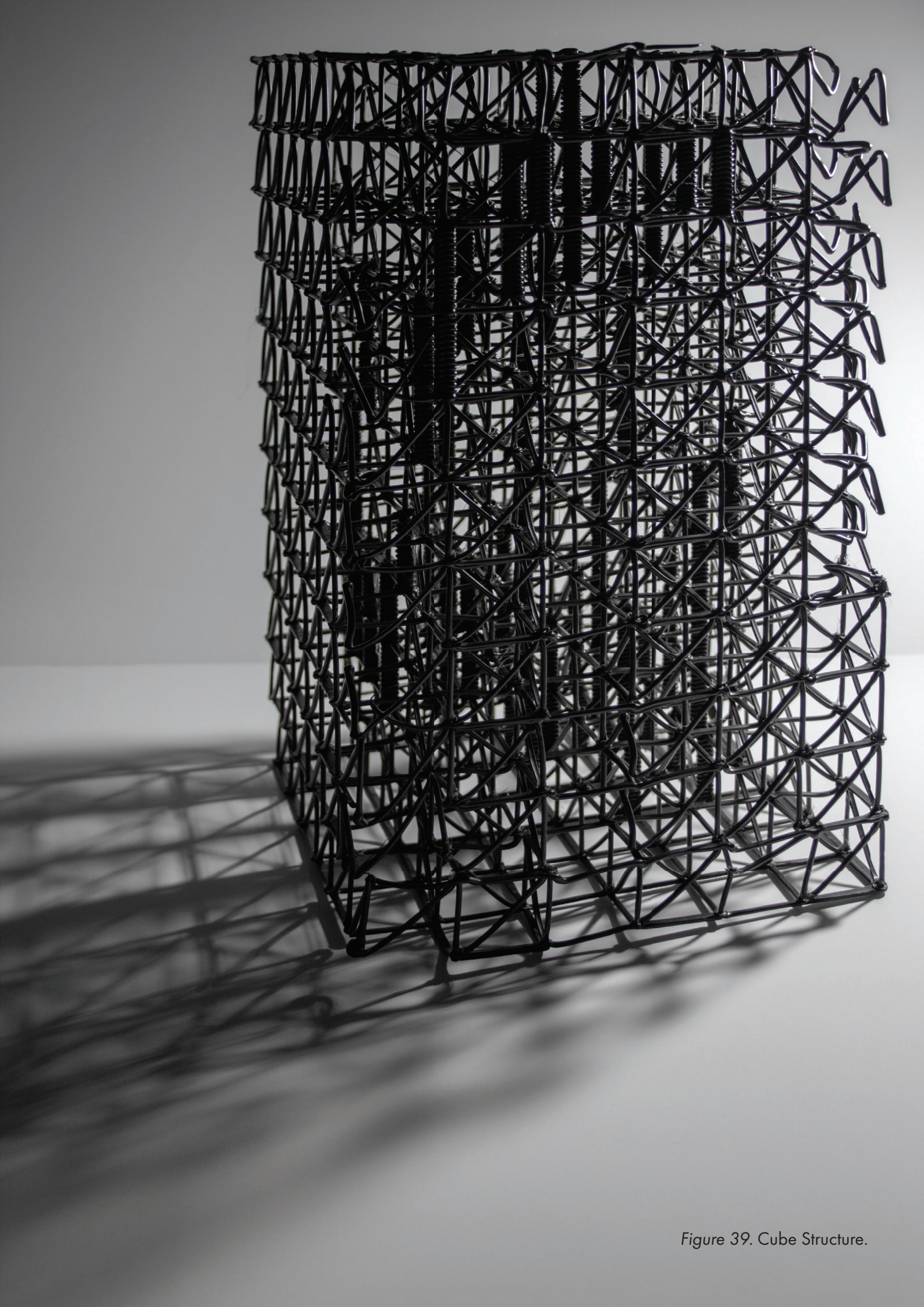

Figure 39. Cube Structure.

Cube Structure

This was the first structure produced with a standardised print order. It is essentially a rectangular volume which has been filled with a repeating print pattern. This print was a first step towards building a robust algorithm which is able to fill a volume defined by an input surface or mesh. Printing this structure ensured that the chosen print order was successful. Structural optimisation data was also integrated into the design of this model.

Vertical extrusions that fell within the mesh resulting from a topological optimisation of the volume were determined to be the optimum position for reinforced helically printed columns. The result of this is a concentration of material where the structural optimisation plug-in determined to be areas under high compressional load. Visually the columns create pockets of increased density.

Pairing 3D topology optimisation with helical elements, in this way, produced innovative results. However, producing a rectilinear form did not take full advantage of the geometry produced by the optimisation system.

Overall the print quality is good, however, the four corner edges of the cuboid show signs of failure. During printing, it was observed that if one layer of the corner elements failed it produced a domino effect, where the print could not regain a controlled structure, as seen in Figure 39. However, if a member in the centre of the cube failed to connect, the printer was able to bridge this gap on the next horizontal layer and regain control.

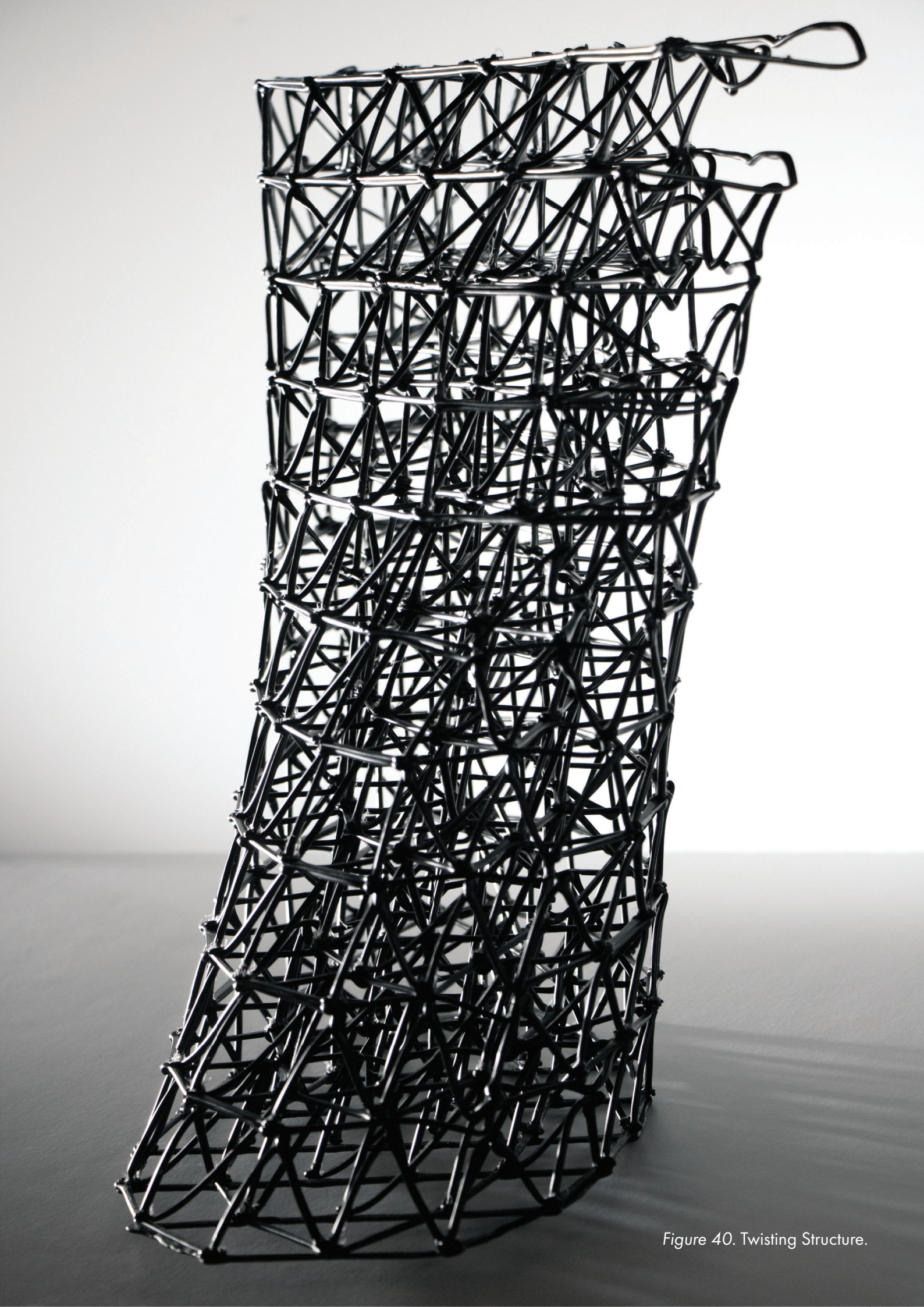

Figure 40. Twisting Structure.

Twisting Structure

The twisting structure was generated by a similar system to the cube structure. However, unlike the cube structure, this system is able to produce more organic, twisting forms, by culling areas from the initial square grid which do not lie within the input volume. This is a simple method which has been explored by groups such as García et al. (2015) and Huang et al. (2018). In their research García et al. (2015) refer to this method as voxelisation, where a voxel is the equivalent of a three-dimensional pixel. Voxelisation of a volume produces a less accurate representation of the input-form unless individual voxels are very small. Voxelisation also produces structures with interrupted and sharp jagged surfaces which reduces the number of applications for this technique.

However, the structures generated by the VDA are slightly more form responsive than those produced by García et al. (2015) and Huang et al. (2018), as the VDA scales and twists planes to more closely reproduce the input form.

Chapter - 7

System Development

Development Overview

After producing four conceptual algorithms and structures, I found that the VDA held the most opportunity for development into a novel design system. Development of the VDA was a continuous improvement process, meaning that refinement was a result of both small incremental improvements and breakthrough improvements (American Society for Quality, 2019).

Incremental improvements included streamlining and minimising the number of components in the algorithm wherever possible, adding lower-level functionality to the algorithm, and checking and repairing existing parts of the algorithm after changes were made. These improvements were difficult to document concisely, therefore this section focuses on the development of the VDA through the breakthrough improvements.

There were four breakthrough improvements made throughout VDA development. Each breakthrough improvement enabled the VDA to successfully manipulate more complex input geometry. The ultimate goal was to produce an algorithm that could convert the intricate branching forms, generated with 3D topological optimisation software, into a spatially printable structure and toolpath. The most computationally demanding aspect of the forms produced by these programs was the way in which they morphed and branched; often with sections splitting off into multiple branches, then those branches recombining in an alternate order. If the spatial printing system under development is to fully utilise 3D topological optimisation, it will need to be able to deal with these complex branching forms. The iterations of the VDA resulting from the breakthrough advancements are discussed below.

Note: For enlarged images of each of the Grasshopper algorithms shown below, see Appendix One

Figure 41. Structure produced by the fourth iteration of the VDA.

VDA version 1

Script function

The first iteration of the VDA generated structures by creating a number of evenly spaced grids through the centre of the input volume. Each grid had the same number of cells, but these cells were scaled, according to the dimensions of the volume at the height of the grid, Figure 44 (1-2) .

Next, lines were created which connected the grids at each intersection point. Any lines which fell outside of the input volume were removed, Figure 44 (3-4).

Lastly, the toolpath was determined by arranging each of the lines in a predetermined order, depending on their position in the grid. Diagonal and horizontal lines were then added between each of the vertical lines, to complete the structure, Figure 44 (5-6).

Evaluation

VDA version 1 is missing a lot of the functionality necessary to deal with more complex forms. It is able to deal with simple lofted forms but is unable to deal with twisting or branching geometry. Furthermore, the technique of using a rectangular grid to determine the structure, then removing cells in order to create form, produces a voxelised effect, as seen in Figure 42 which is not desired.

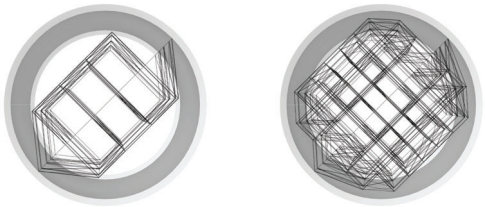

Figure 42. Voxelisation of the generated structure.

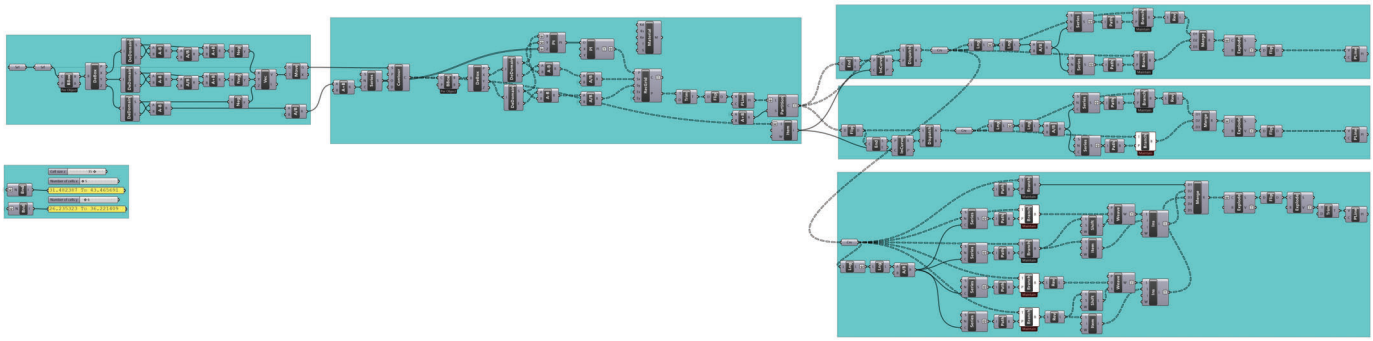

Figure 43. The first iteration of the VDA Grasshopper script.

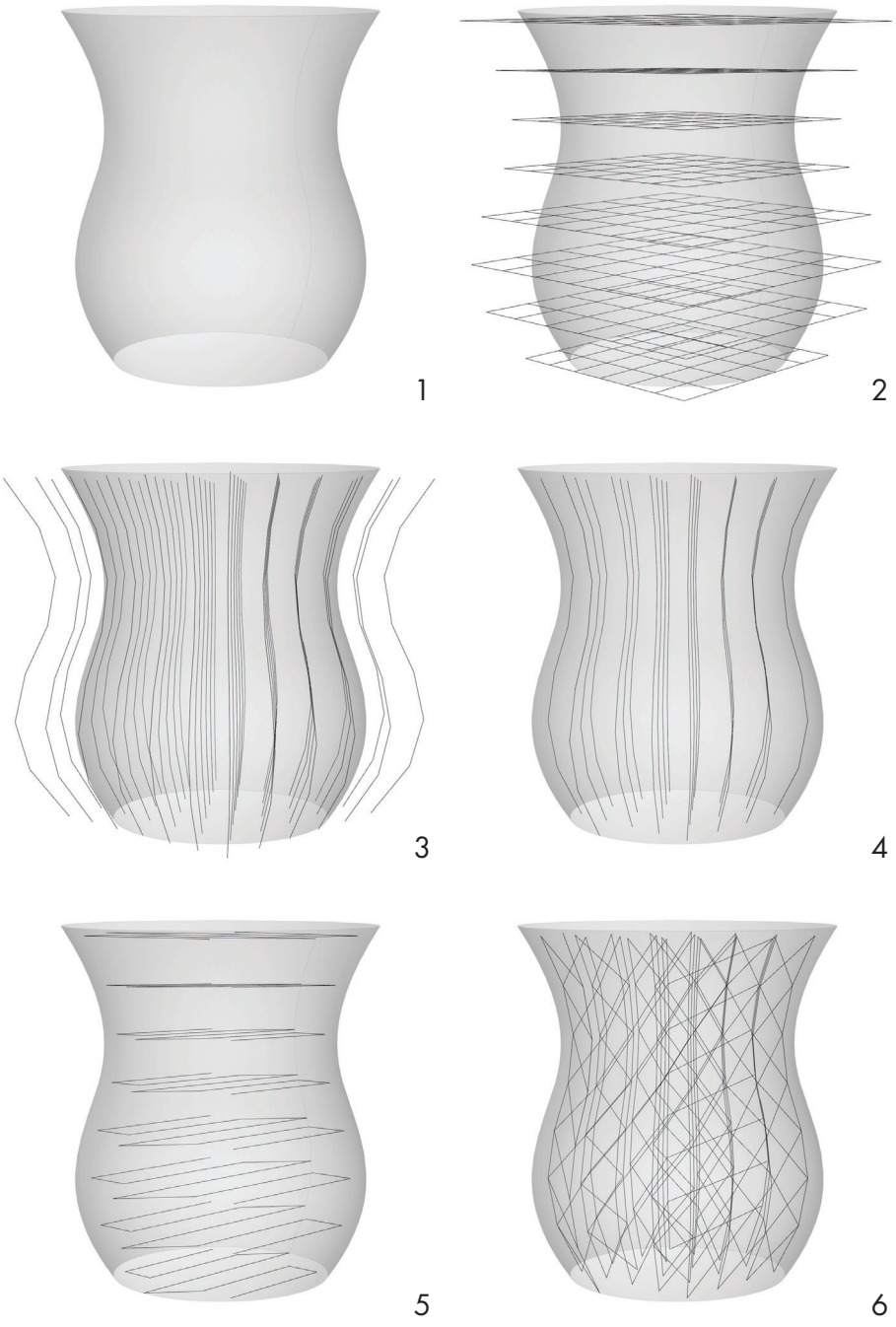

Figure 44. VDA version 1 - Structure generation process.

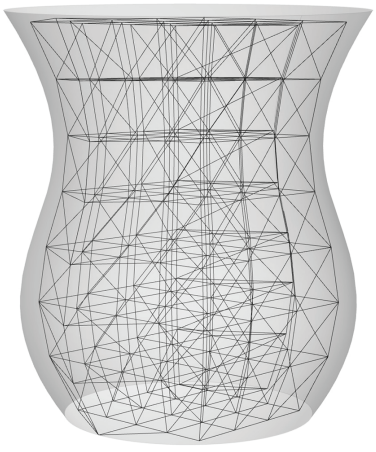

Figure 45. VDA version 1 - Final output.

VDA version 2

Structure Generation Process

The second iteration of the VDA generated spatial structures by first splitting the input form vertically, into a number of evenly sized sections. An array of lines was then created for each of these sections. By measuring the length of each line the angle at which each section is widest was found, Figure 47(1-3).

Next, grids were created at each of the sections and were aligned to the lines generated in Figure 47 (3). Lines were created which connected the grids at each intersection point. Any lines which fell outside of the input volume were removed, Figure 47 (4-6).

Lastly, the toolpath was determined by arranging each of the lines in a predetermined order, depending on their position in the grid. Diagonal and horizontal lines were then added between each of the vertical lines, to complete the structure, Figure 47 (7-9).

Evaluation

VDA version 2 is able to better deal with twisting and asymmetrical input forms. However, like VDA version 1 when there are a low number of cells the input form is not faithfully reproduced due to voxelisation. Version 2 is also unable to deal with branching, all input forms must be simple, column-like volumes.

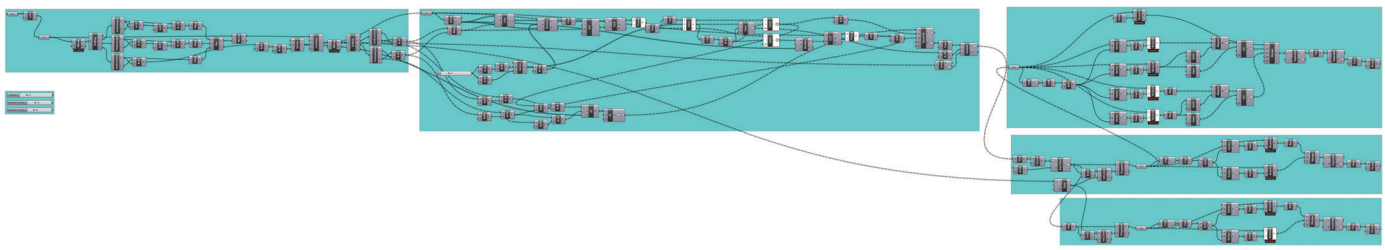

Figure 46. The second iteration of the VDA Grasshopper script.

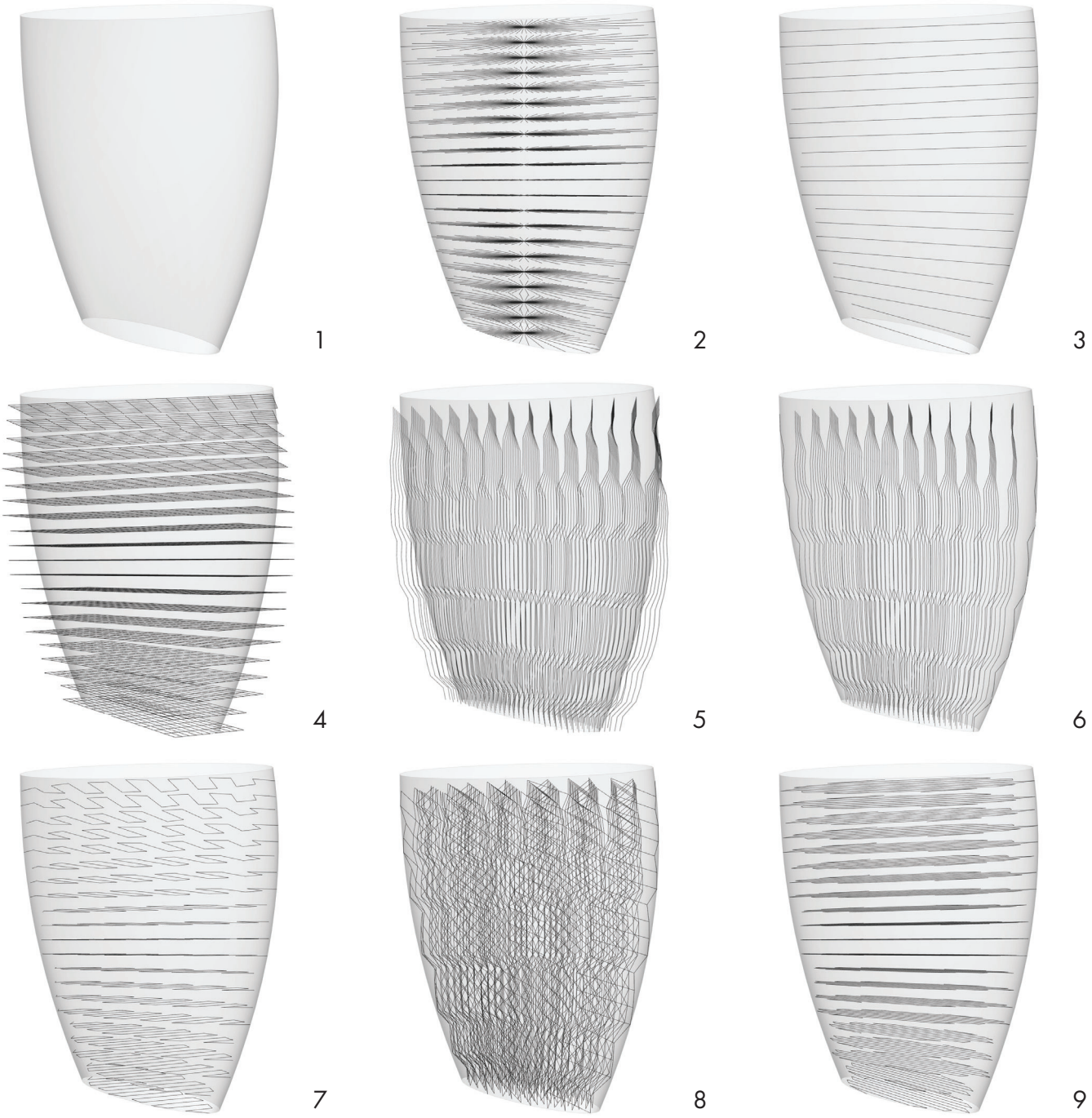

Figure 47. VDA version 2 - Structure generation process.

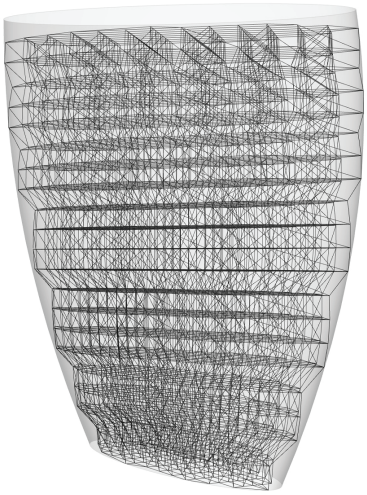

Figure 48. VDA version 2 - Final output.

VDA version 3

Structure Generation Process

The third iteration of the VDA generated spatial structures by first splitting the input form vertically, into a number of evenly sized sections. An array of lines was then created for each of these sections. By measuring the length of each line the angle at which each section is widest was found, Figure 50 (1-3).

Next, a number of evenly spaced lines are created which are perpendicular to the lines generated in Figure 50 (3). These lines are then split into equally sized segments. Vertical lines are then created which connect the endpoints of each segment, Figure 50 (4-6).

Lastly, the toolpath was determined by arranging each of the lines in a predetermined order, depending on their position in the form. Diagonal and horizontal lines were then added between each of the vertical lines, to complete the structure, Figure 50 (7-9).

Evaluation

VDA version 3 is able to generate a custom grid, where the outermost points are always positioned on the surface of the input form. This means the structure generated more closely resembles the input form as no voxelisation occurs. Version 3 is also able to deal with forms that split into two branches and recombine, however, it is still unable to deal with more complicated forms than this.

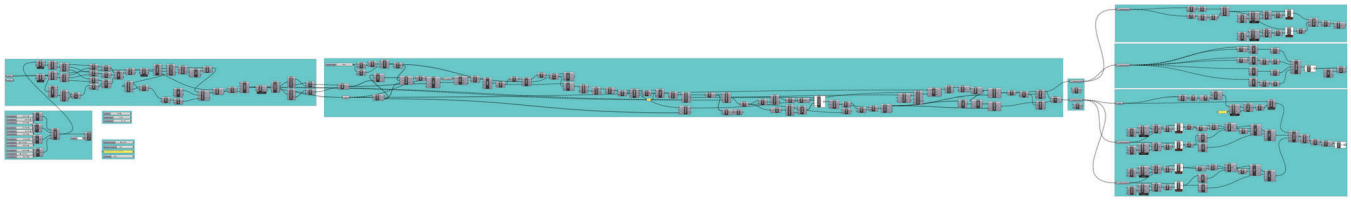

Figure 49. The third iteration of the VDA Grasshopper script.

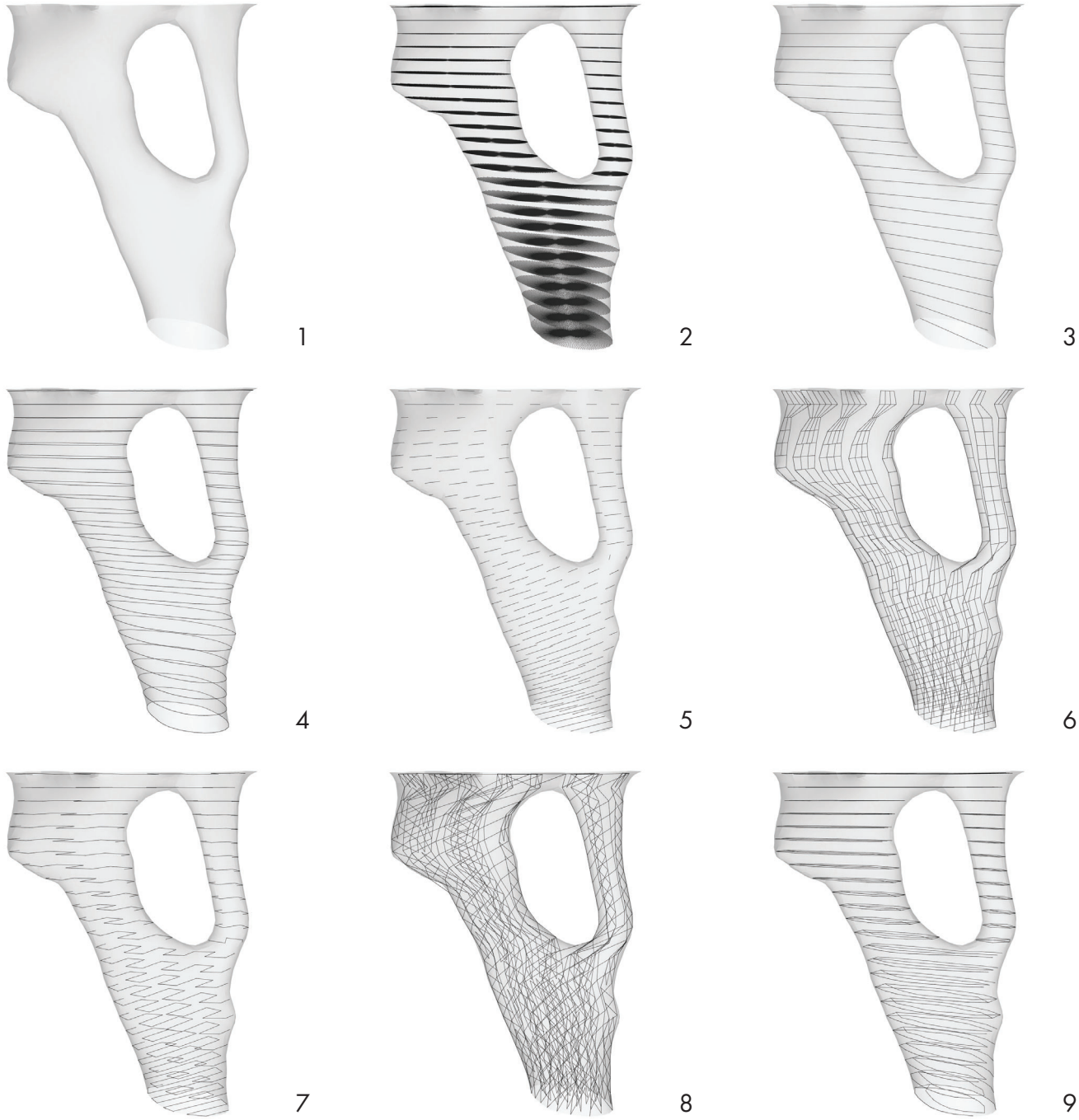

Figure 50. VDA version 3 - Structure generation process.

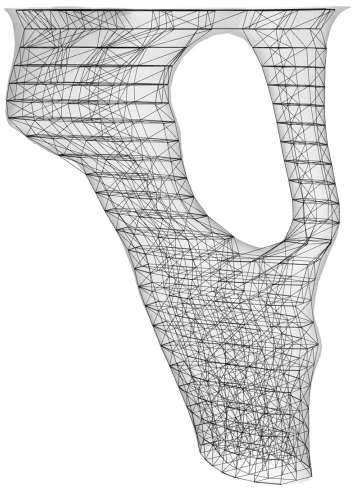

Figure 51. VDA version 3 - Final output.

VDA version 4

Structure Generation Process

The fourth iteration of the VDA generated spatial structures by first splitting the input form vertically, into a number of evenly sized sections. Each section was broken up into a number of points. A custom script then calculated the most distant points and created a line through them, Figure 53 (1-3).

Next, a number of evenly spaced lines are created which are perpendicular to the lines generated in Figure 53 (3). These lines are then split into equally sized segments. Vertical lines are then created between the closest endpoints of each segment, Figure 53 (4-6).

Lastly, the toolpath was determined by arranging each of the lines in a predetermined order, depending on their position in the form. Vertical elements are replaced with Helical elements were required. Diagonal and horizontal lines were then added between each of the vertical lines, to complete the structure, Figure 53 (7-9).

Evaluation

VDA version 4 retains the same system for generating structures as version 3. However, custom scripted components have been added, which calculate the number of elements to split into each branch of a divided form. This allows VDA version 4 to deal with almost any geometry generated by 3D topology optimisation software. Another custom component has also been added which is able to generate helical toolpaths.

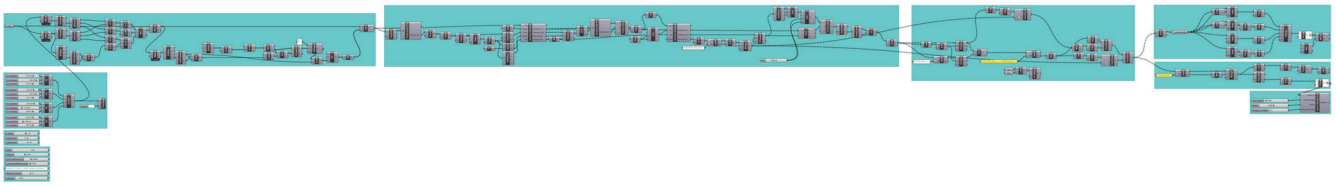

Figure 52. Structure produced by the third iteration of the VDA.

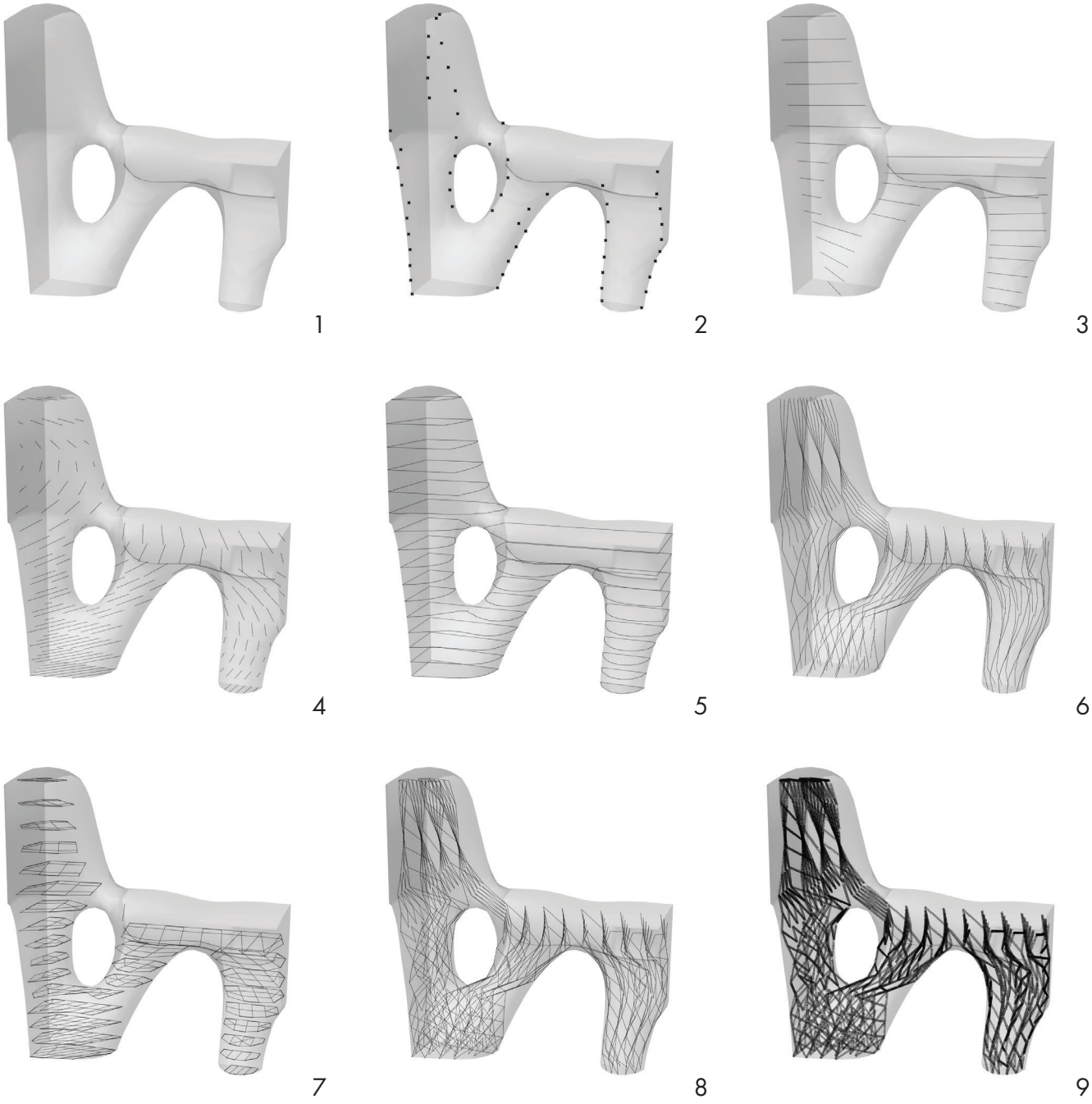

Figure 53. VDA version 4 - Structure generation process.

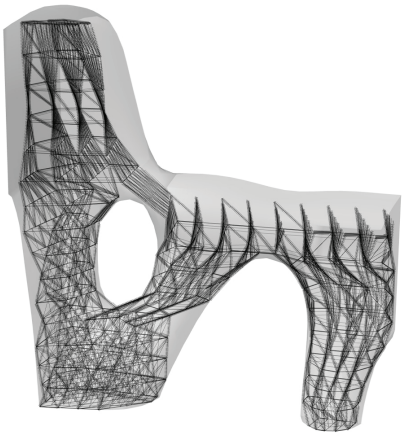

Figure 54. VDA version 4 - Final output

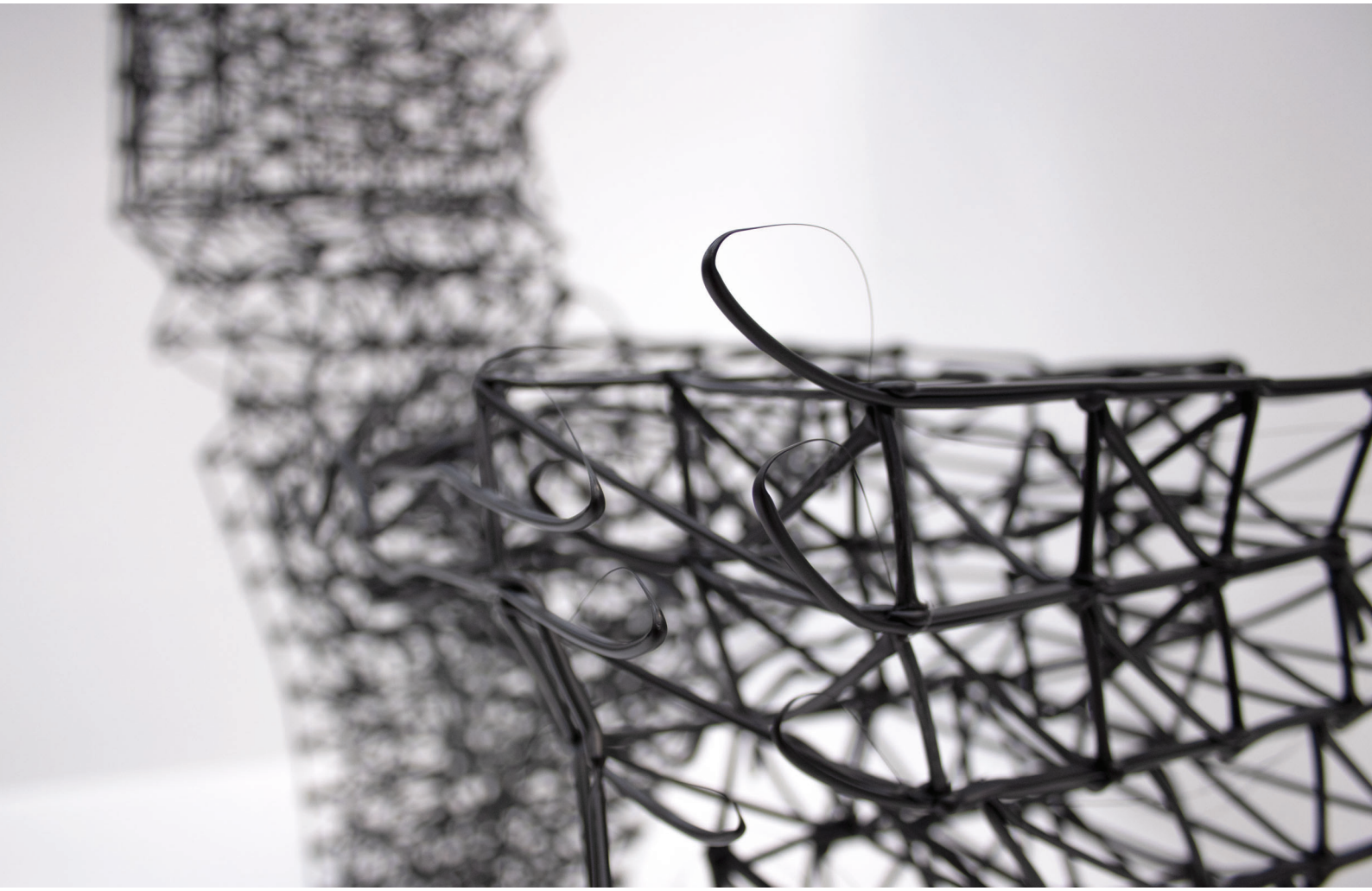

Figure 55. Rapid movement related print issues.

Print System Development

Throughout the development of the VDA, alterations were also being made to the print system, to enable higher levels of automation and more refined prints.

One of the first areas to be developed was a component that autonomously calculated six-axis robotic movements from the lines produced by the VDA. The component calculates the direction in which the nozzle of the printer will be moving and, depending on a series of preset values, will orient the tool to the optimum position for extruding each member.

Another custom component was developed to control the master print settings. This component receives a number of inputs from sliders that define print settings such as temperature, flow rate, pause time and pre-extrusion time. This component also receives data from the automatic orientation component, allowing it to perform special actions when printing specific geometry, for example adjusting the flow rate when printing vertically. Pauses are also automatically programmed into the rapid code. These pauses were found to aid in the adhesion between strands of plastic at the node points where they meet. Additionally, pauses have been added at specific points to allow the extrusion to solidify before the next movement begins helping to produce more accurate geometry. Other actions controlled by this component are extrusion and cooling activation/deactivation.

Rapid movements are performed when the extruder must move from one point to another and no extrusion is desired. There are several issues which have arisen from rapid movements. Firstly, in all cases, there is a fine bead of plastic drawn out of the nozzle as the extruder moves. This problem is also common in layer-based FDM printing, where it is referred to as stringing. While this could be exploited to achieve a variety of different effects, for the majority of printing it is not desirable. The second issue is a lack of connection between the endpoint of the last printed path and the corresponding vertical member. This is a result of the nozzle not reaching the final node before commencing the rapid movement. Because it has not properly connected, when the rapid movement is performed, the end of the horizontal member is pulled upwards, as seen in Figure 55. To remedy these issues, longer pause times were placed before rapid movements, to allow the geometry to cool before the extruder began to move.

Application Based Experiments

Optimised Chair Structure

A chair has been chosen as an application based experiment to evaluate and demonstrate how the developed printing system functions. A chair was selected because it offers interesting load vectors and a variety of load cases to optimise for.

The first chair was designed solely to test the functionality of the workflow, from optimisation plug-in through to structural generation and printing. The forces which were set in Millipede for this initial test were estimates of the real-world forces. A load of 800 newtons was applied to the geometry representing the seat, and a load of 200 newtons was applied to the backrest. Four support volumes were set to represent the feet of the chair. The last geometry to be set as inputs were a large cuboid that indicated the area which could be built within, and a second cuboid, located above the seat, which represented an exclusion zone.

Because the bounding volume set was not much larger than the seat and backrest geometry, Millipede produced a form which is flat on the outer surfaces. However, on the underside, it is evident where unnecessary material has been removed.

This juxtaposition of rectilinear geometry, where material has been built right up to the bounding volume, versus curvilinear geometry, on the underside of the chair, is striking and reflects the way in which the chair was designed.

Helical toolpaths have been generated on the outer surface of the chair. These thicker elements serve two purposes. Firstly, they are tougher and more rigid in compression then single extrusions, helping to add strength to the outermost surface which receives the most interaction. Secondly, they aid in the print process by providing a more rigid perimeter then if only single extrusions are used.

Test Rig and Second Chair

A second chair was intended to be produced, based on empirical load data, collected with a test rig. The test rig was built, pictured in Figure 56, with three force sensors under the seat and three force sensors in the backrest, however, due to limited time, this data was not collected. Producing a second chair, generated from data collected with this test rig would have helped to further substantiate the research produced in this thesis. However, the first chair produced also provides compelling evidence of the functionality of the system.

Figure 56. Test rig.

Figure 57. Optimised chair structure.

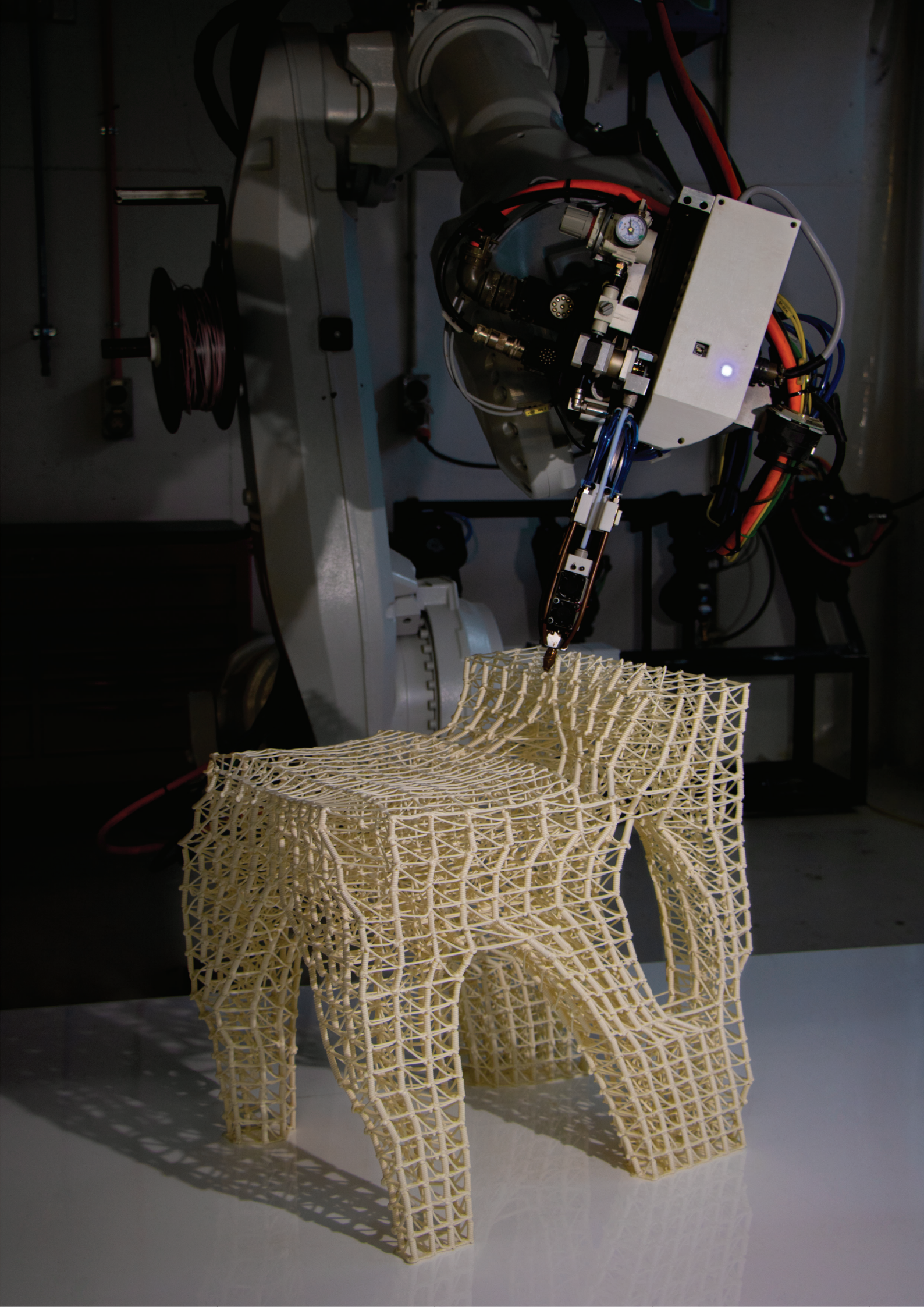

Discussion

The final iteration of the volume-driven algorithm is able to sympathetically respond to the branching organic forms produced by topological optimisation software such as Millipede. Unlike the voxelisation method, explored by García et al. (2015) and Huang et al. (2018), the VDA created in this research attempts to reproduce the form of the input volume as faithfully as possible. In doing so, fidelity is not lost between the input form and the structure generated. The result is an innovative method for producing spatially printed structures.

The use case presented in the previous section demonstrates the production of an optimised tangible output. This output is the result of two load forces, four support forces, one bounding volume and one exclusion volume being set as input data for the VDA. This use case demonstrates the functionality of the system, from input forces to fabrication. Due to restrictions in time, the system has not been able to be tested with empirical evidence. Which would have further validated the performance of the system.

Limitations

This research encountered a number of limitations related to materials, technology and time. Many of the skills required to produce a spatial printing system are broad and cross-disciplinary. A large number of the precedents reviewed were the result of teams of designers, architects, engineers, material scientists and computer scientists. The time required to learn any one of these skills, individually, is beyond the scope of this thesis. In order to advance this research further, cross-collaboration is necessary, to enable expertise from each of these fields to be drawn on. The result of each of these limitations is discussed further below.

Further advancements in spatially printable materials and material systems are one of the major limiting factors in this field of research. Material properties dictate the feasibility of spatial printing for manufacturing, as the speed of production, and the strength and reliability of parts produced, are all reliant on the materials that are available. However, many of the techniques and methods for developing a spatial printing system demonstrated in this thesis are transferable to alternative material systems, reducing the impact of this limitation on the value of this research.

Limited experience and knowledge in the fields of computer science and engineering have also impacted the scope of this research. The time taken to develop a working volume-driven algorithm could have been decreased dramatically with the aid of a computer scientist, enabling more time to be spent testing the system on a range of different use cases.

Furthermore, input from an engineer familiar with a range of different analysis and optimisation methods and software would have been extremely valuable and may have helped validate the forms produced by Millipedes 3D topology optimisation solver. However, one of the benefits of using a volume as the input for the VDA is that any topological optimisation could be used to produce an optimised form, which could then be imported into Grasshopper, reducing the importance of the selected analysis software.

Future Research

The limitations previously discussed impacted the scope of the research, often forcing a single opportunity to be pursued when multiple arose. Future research could address any number of the opportunities suggested below.

Helical elements were used in a number of experiments throughout this study, however, this novel deposition technique was not explored to its full potential. The intention was to inform the placement and size of these elements through an analysis of the stresses present in the second iteration of the optimised chair. Unfortunately, time did not permit this further exploration.

Future research could analyse structures produced by the VDA, and use this data to refine the system, updating the way in which spatially printable geometry is generated. Artificial Intelligence could also be implemented as a method of generating optimised structures, or structures with specific aesthetic qualities.

Non-linear banding is a further way in which this research could be built upon. Splitting forms with curved surfaces or planes which are oriented to the flow of the geometry could produce structures which are more sympathetic to the input forms and are visually unique.

Figure 58. Optimised chair during printing.

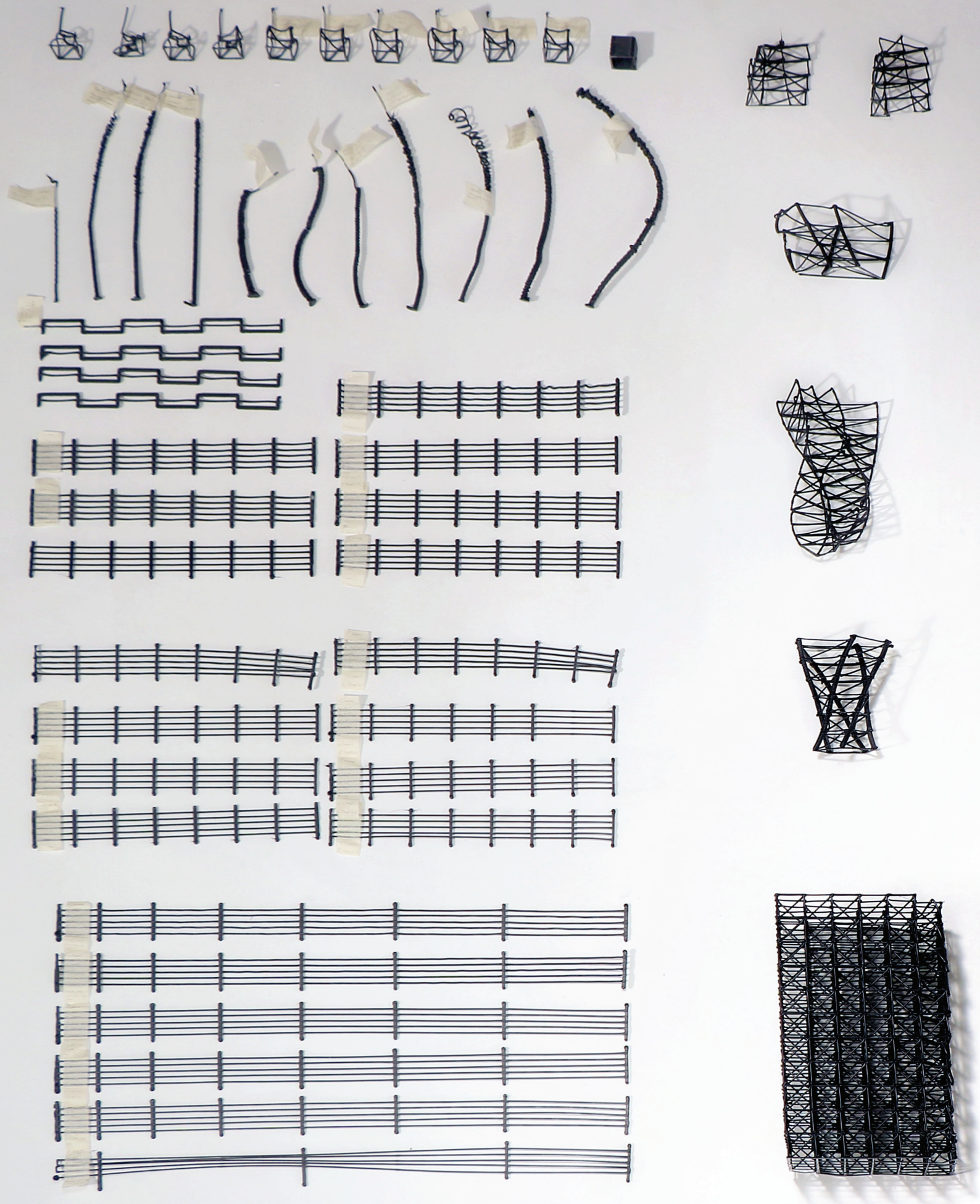

Figure 59. An overview of the different structures produced in this thesis.

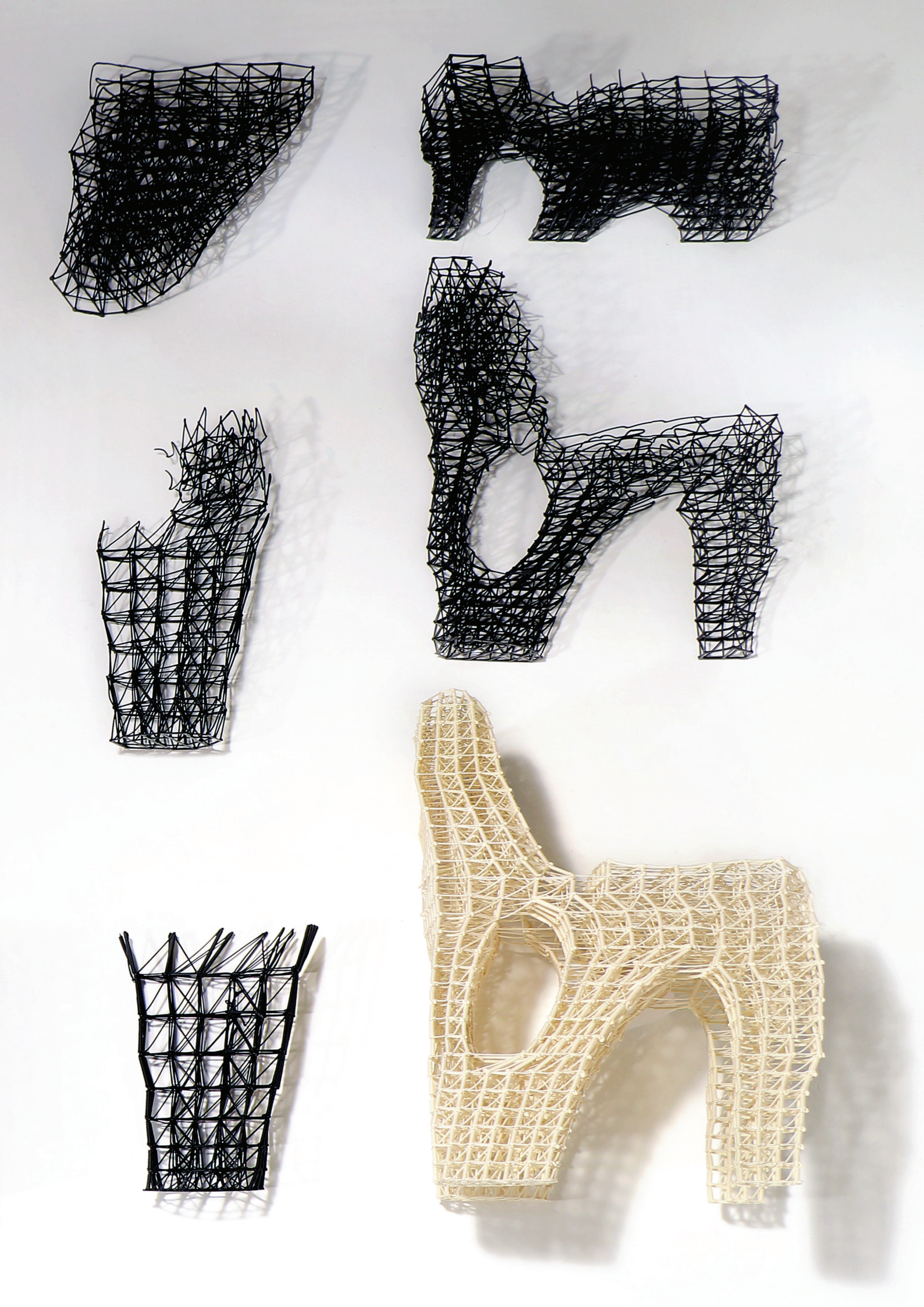

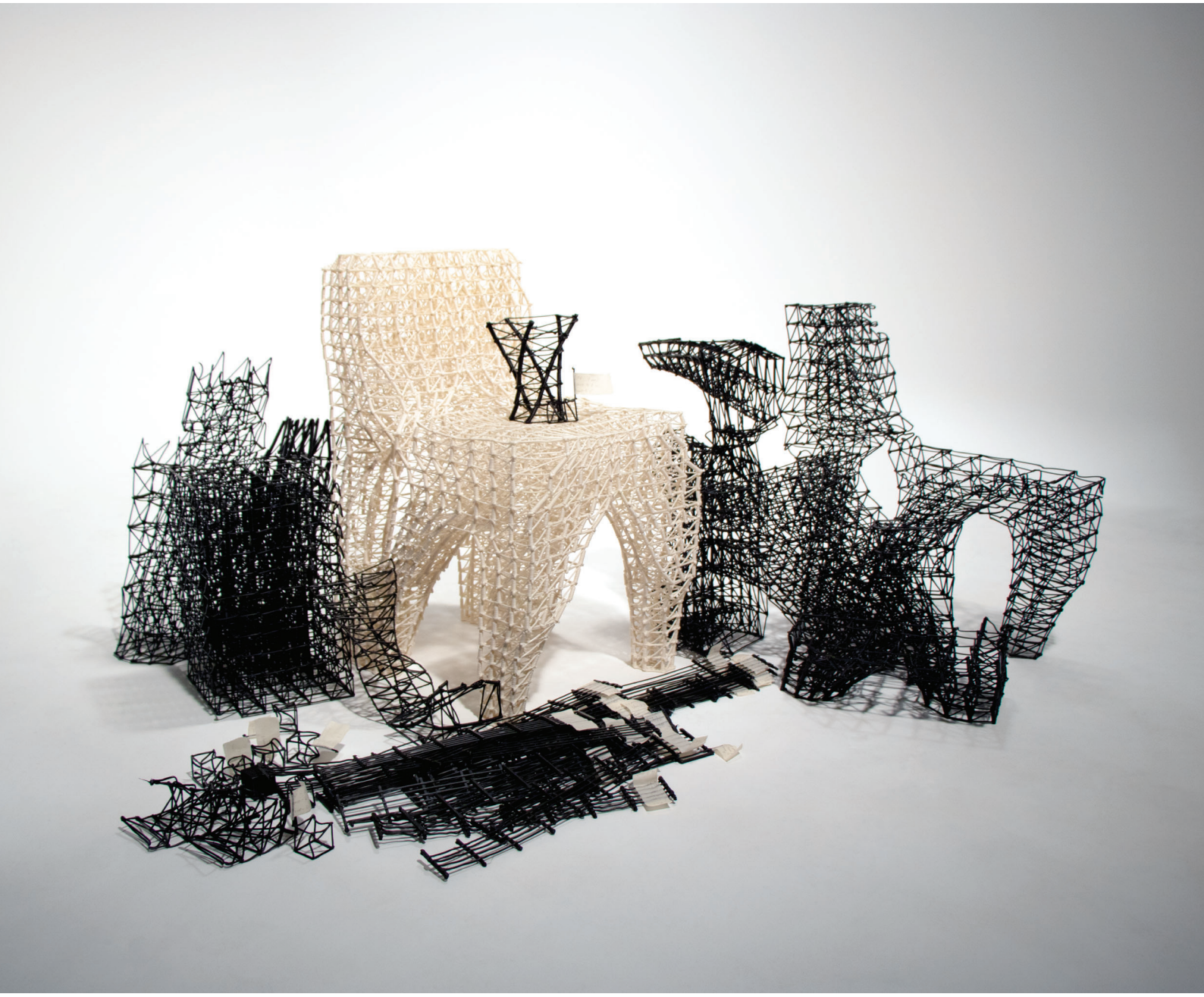

Figure 60. Experimental structures produced throughout the thesis.

Conclusion

In traditional subtractive manufacturing, material is cheap in comparison to the time required to produce complex forms. In additive manufacturing, the opposite is true, cost is based on the amount of material deposited and not on the intricacy of a part's form. Within this thesis, I have demonstrated a systematic approach to building a spatial printing system, which harnesses the potential of 3D topology optimisation software, to generate optimised structures.

None of the structures produced in this thesis have been designed in the traditional sense of the word. The experimental structure that could be considered the final design of the study, the chair produced in the use case section, took less than one afternoon to develop. However, without optimisation software and the spatial printing system produced in this research, it would most likely take months to reproduce such a complex structure. What I do consider to be the designed element of this thesis, is the development and configuration of the spatial printing algorithm.

During initial experiments, I adjusted the system for each structure, in an attempt to steer it towards producing a particular outcome. However, upon reflection, I feel that the most successful method has been to leave the design of the structures up to the optimisation system and the volume-driven algorithm. I now believe my role, as the designer, has been to ask two questions. What are the qualities of the forms produced by the optimisation system? And how can I produce an algorithm which capitalises on these qualities?

After a review of different analysis and optimisation methods and a number of conceptual experiments, 3D topology optimisation was selected as the method of optimisation on which to focus. The forms generated by 3D topology optimisation offered unique challenges and opportunities in terms of spatial printing, due to their complex, organic, branching nature. A custom algorithm was developed specifically to deal with these volumes, ensuring that the resulting structures fully exploit the curvilinear forms generated by the optimisation software. The result of this research is a robust spatial printing system that is able to produce novel optimised structures with minimal designer input.

Bibliography

American Society for Quality.(2019). *Continuous Improvement* [Web log message]. Retrieved from https://asq.org/quality-resources/continuous-improvement

Anthony Carpi, & Anne Egger. (2008). *Experimentation in Scientific Research* [Web log message]. Retrieved from https://www.visionlearning.com/en/library/Process-of-Science/49/Experimentation-in-Scientific-Research/150

Beniak, J., Križan, P., Matúš, M., & Šajgalík, M. (2018). Experimental testing of PLA biodegradable thermoplastic in the frame of 3D printing FDM technology. *MATEC Web of Conferences, 157*, 1-7. https://doi.org/10.1051/matecconf/201815706001

Dawoud, M., Taha, I., & Ebeid. S. J. (2016). Mechanical behaviour of ABS: An experimental study using FDM and injection moulding techniques. *Journal of Manufacturing Processes, 21*, 39-45. https://doi.org/10.1016/j.jmapro.2015.11.002

Doerstelmann, M., Knippers, J., Koslowski, V., Menges, A., Prado, M., Schieber, G., & Vasey, L. (2015). Fibre Placement on a Pneumatic Body Based on a Water Spider Web. *Architectural Design, 85*(5), 60–65. https://doi.org/10.1002/ad.1955

Doerstelmann, M., Knippers, J., Menges, A., Parascho, S., Prado, M., & Schwinn, T. (2015). Modular Coreless Filament Winding Based on Beetle Elytra. *Architectural Design, 85*(5), 54–59. https://doi.org/10.1002/ad.1954

Dow, S., Glassco, A., Kass, J., Schwarz, M., Schwartz, D., & Klemmer, S. (2010). Parallel prototyping leads to better design results, more divergence, and increased self-efficacy. *ACM Transactions on Computer-Human Interaction (TOCHI), 17*(4), 1–24. https://doi.org/10.1145/1879831.1879836

Gilbertson, L. (2018). *Robotic Spatial Printing For Designers* (Master's thesis, Victoria University of Wellington, Wellington, New Zealand). Retrieved from http://researcharchive.vuw.ac.nz

Gordeev, E., Galushko, A., & Ananikov, V. (2018). Improvement of quality of 3D printed objects by elimination of microscopic structural defects in fused deposition modeling. *PLoS ONE, 13*(6), e0198370. https://doi.org/10.1371/journal.pone.0198370

Hack, N., Lauer, W., Gramazio, F., & Kohler, M. (2014). Mesh-Mould: Robotically Fabricated Spatial Meshes as Reinforced Concrete Formwork. *Architectural Design, 84*(3), 44-53.

Hajash, K., Sparrman, B., Guberan, C., Laucks, J., & Tibbits, S. (2017). Large-scale rapid liquid printing. *3D Printing and Additive Manufacturing, 4*(3), 123-121. http://doi.org/10.1089/3dp.2017.0037

Hanington, B., & Martin, B. (2012). *Universal Methods of Design* (1st edition). Rockport Publishers.
https://www.academia.edu/11353656/Autonomous_Tectonics_II?auto=download

Huang, Y., Carstensen, J. V., & Mueller, C. T. (2018). 3D truss topology optimization for automated robotic spatial extrusion. In C. Mueller, & S. Adriaenssens (Eds.), *Creativity in structural design* (pp. 1-8). Massachusetts, USA: Massachusetts Institute of Technology.

Huang, Y., Zhang, J., Hu, X., Song, G., Liu, Z., Yu, L., & Liu, L. (2016). FrameFab: Robotic fabrication of frame shapes. *ACM Transactions on Graphics (TOG), 35*(6), 1-11. https://doi.org/10.1145/2980179.2982401

Jiang, N., Wang, Y., Chen, Y., & Ahmed, Z. (2014). *Spacewires-Filamentrics* (Design portfolio, Bartlett School of Architecture). Retrieved from https://issuu.com/nanjiang_filamentrics/docs/spacewires

Khan, S., & Awan, M. (2018). A generative design technique for exploring shape variations. *Advanced Engineering Informatics, 38*, 712–724. https://doi.org/10.1016/j.aei.2018.10.005

Knippers, J., La Magna, R., Menges, A., Reichert, S., Schwinn, T., & Waimer, F. (2015). Coreless Filament Winding Based on the Morphological Principles of an Arthropod Exoskeleton. *Architectural Design, 85*(5), 48–53. https://doi.org/10.1002/ad.1953

Kochesfahani, S. (2016). Improving PLA-based material for 3-D printers using fused deposition modeling. *Plastics Engineering, 72*(5), 36–43. https://doi.org/10.1002/j.1941-9635.2016.tb01538.x

Lovegrove, R. (2016). 'Super-natural': parametricism in product design. *Architectural Design, 86*(2), 100-107. https://doi.org/10.1002/ad.2030

Milton, A., & Rodgers, P. (2013). *Research methods for product design*. London: Laurence King Pub.

Molloy, I. (2018). *Designed deposition: freeform 3d printing for digitally crafted artefacts* (Master's thesis, Victoria University of Wellington, Wellington, New Zealand). Retrieved from http://researcharchive.vuw.ac.nz

Mueller, S., Im, S., Gurevich, S., Teibrich, A., Pfisterer, L., Guimbretiere, F., & Baudisch, P. (2014, October). *WirePrint: 3D Printed Previews for Fast Prototyping*. Paper presented at UIST'14, Honolulu, USA. Retrieved from https://www.researchgate.net/publication/266938293_WirePrint_3D_Printed_Previews_for_Fast_Prototyping

Oxman, N., Laucks, J., Kayser, M.A., Tsai, E.Y., & Firstenberg, M. (2013). *Freeform 3D printing: towards a sustainable approach to additive manufacturing*. Advanced online publication. https://www.semanticscholar.org/paper/Freeform-3-D-Printing-%3A-Towards-a-Sustainable-to-Oxman-Laucks/7642980a2881a16883ac1c43ace73d5167259902

Papageorge, A. D., (2018). *Freeform 3D Printing: A Sustainable, Efficient Construction Alternative* (Master's thesis, Victoria University of Wellington, Wellington, New Zealand). Retrieved from http://researcharchive.vuw.ac.nz

Péter Máté. (2019, July 23). *NURBS and Polygon Mesh—why both models are needed* [Web log message]. Retrieved from https://www.bimobject.com/en/news/articles/nurbs-and-polygon-meshwhy-both-models-are-needed

Peter Zelinski. (1999, July 1). *Understanding NURBS interpolation* [Web log message]. Retrieved from https://www.mmsonline.com/articles/understanding-nurbs-interpolation

Retsin, G. & Garcia, M.J. (2016). *Discrete computational methods for robotic additive manufacturing: combinatorial toolpaths*. Paper presented at the 36th Annual Conference of the Association for Computer Aided Design in Architecture, Michigan, USA. Retrieved from http://papers.cumincad.org/cgi-bin/works/Show?acadia16_332

Rocha, C. R., Torrado Perez, A. A., Roberson, D. M., Shemelya, C. B., MacDonald, E., & Wicker, R. (2014). Novel ABS-based binary and ternary polymer blends for material extrusion 3D printing. *Journal of Materials Research, 29*(17), 1859-1866. https://doi.org/10.1557/jmr.2014.158

Sean Rohringer. (2019, July 15). *3D Printer Filament Buyer's Guide* [Web log message]. Retrieved from https://all3dp.com/1/3d-printer-filament-types-3d-printing-3d-filament/

Shelton, T. (2017). Cellular Fabrication. *Technology|Architecture + Design, 1*(2), 251-253. https://doi.org/10.1080/24751448.2017.1354636

Song, Y., Li, Y., Song, W., Yee, K., Lee, K., & Tagarielli, V. (2017). Measurements of the mechanical response of unidirectional 3D-printed PLA. *Materials & Design, 123*, 154–164. https://doi.org/10.1016/j.matdes.2017.03.051

Tam, K. M., & Mueller, C. (2015). *Stress line generation for structurally performative architectural design*. Paper presented at the 35th Annual Conference of the Association for Computer Aided Design in Architecture, Cincinnati, USA. Retrieved from https://www.researchgate.net/publication/310645017_Stress_Line_Generation_for_Structurally_Performative_Architectural_Design

Tedeschi, A. (2014). *AAD: Algorithms-aided design*. Napoli, Italy: Le Penseur.

Vincent, J., & Garcia, M. (2009). Biomimetic Patterns in Architectural Design. Architectural Design, *79*(6), *74*-81. https://doi.org/10.1002/ad.982

Weng, Z., Wang, J., Senthil, T., & Wu. L. (2016). Mechanical and thermal properties of ABS/montmorillonite nanocomposites for fused deposition modeling 3D printing. *Materials & Design, 102*, 276-283. https://doi.org/10.1016/j.matdes.2016.04.045

Yuan, P. F., Meng, H., Yu, L., & Zhang, L. (2016). Robotic multi-dimensional printing based on structural performance. In D. Reinhardt, R. Saunders, & J. Burry (Eds.), *Robotic Fabrication in Architecture, Art and Design 2016* (pp. 92-105). Switzerland: Springer International Publishing.

Zohdi, T. (2018). Dynamic thermomechanical modeling and simulation of the design of rapid free-form 3D printing processes with evolutionary machine learning. *Computer Methods in Applied Mechanics and Engineering, 331*, 343. https://doi.org/10.1016/j.cma.2017.11.030

Figures

Figure	Title	Source
1	Early Spatial Print Models.	From Freeform 3D printing : towards a sustainable approach to additive manufacturing, by Oxman, N., Laucks, J., Kayser, M.A., Tsai, E.Y., & Firstenberg, M, 2013. Copyright [2013] by Taylor Francis.
2	Design Miami Pavillions.	From Branch Technology. Retrieved from https://www.branch.technology/projects-1/2017/6/9/shop. Copyright [2019] by Branch Technology.
3	Dragon Bench. From Joris Laarman Lab.	Retrieved from https://www.jorislaarman.com/work/mx3d-metal/. Copyright [2019] by Joris Laarman Lab.
4	RLP Bag.	From Dezeen. Retrieved from https://www.dezeen.com/2017/12/14/mit-self-assembly-lab-rapid-liquid-printed-bags-lamps-design-miami/. Copyright [2019] by Dezeen.
5	2014-2015 ICD/ITKE Pavillion.	From University of Stuttgart ICD. Retrieved from https://icd.uni-stuttgart.de/?p=12965. Copyright [2019] by ICD/ITKE University of Stuttgart.
6	Bone Chair.	From Joris Laarman Lab. Retrieved from https://www.jorislaarman.com/work/bone-chair/. Copyright [2019] by Joris Laarman Lab.
7	Multi-nozzle extruder.	From "Robotic multi-dimensional printing based on structural performance," by P. F. Yuan, H. Meng, L. Yu, & L. Zhang, 2016. In Robotic Fabrication in Architecture, Art and Design 2016, p. 101. Copyright [2016] by Springer International Publishing.
8	Concrete structure.	From "Sub-Additive 3D Printing of Optimized Double
9	Curved Concrete Lattice Structures,"	By C. A. Battaglia, M. F. Miller, & S. Zivkovic, 2018, Robotic Fabrication in Architecture, Art and Design, 2019, p. 252. Copyright [2019] by the Springer Nature Switzerland AG.
10	Voxel Panton chair.	From "CurVoxels," by M. J. García et al., 2015.
11	Volumetric Optimisation.	From "3D truss topology optimization for automated robotic spatial extrusion," by Y. Huang, J. V. Carstensen, & C. T. Mueller, 2018, Proceedings of the IASS Symposium 2018, p. 6. Copyright [2018] by Yijiang Huang, Josephine V. Carstensen, Caitlin T. Mueller.
12	Spatial print with generated fabriction sequence.	From "FrameFab: Robotic fabrication of frame shapes," by Y. Huang et al., 2016, ACM Transactions on Graphics (TOG), 35(6), p. 8. Copyright [2019] by ACM, Inc.
13	Whisk, Seive and Measuring Cup.	From "Designed Deposition," by I. Molloy, 2017.
14	Mesh Mould.	From "Mesh-Mould: Robotically Fabricated Spatial Meshes as Reinforced Concrete Formwork," by N. Hack, W. Lauer, F. Gramazio, & M. Kohler, (2014), Architectural Design, 84(3), p. 53. Copyright [2014] by Gramazio & Kohler, Architecture and Digital Fabrication, ETH Zurich.
15-60	Various	Author

Appendix One - Optimised Spatial Printing System Development

VDA version 1

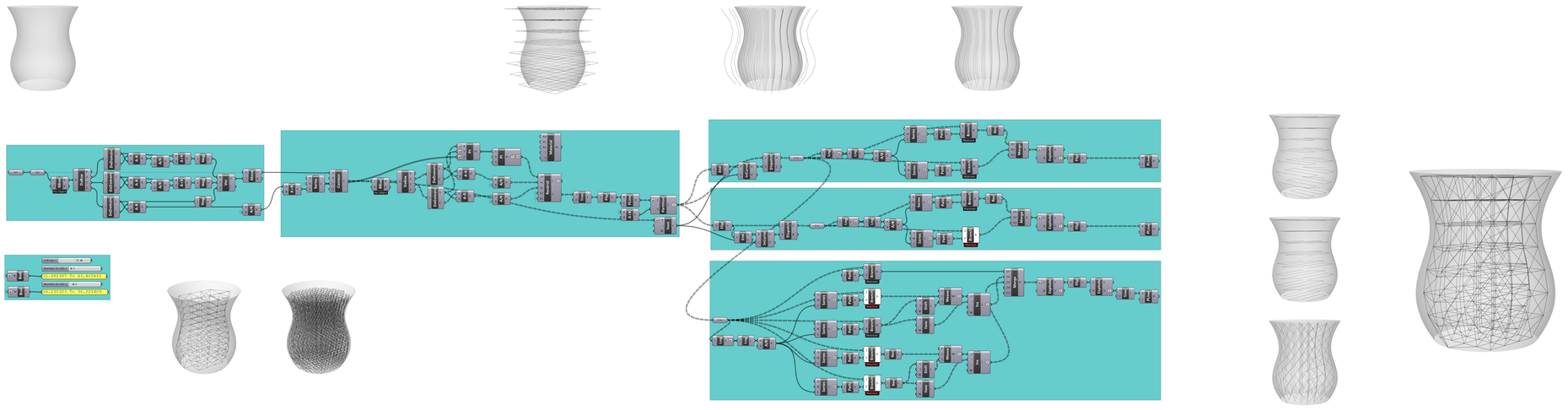

VDA version 2

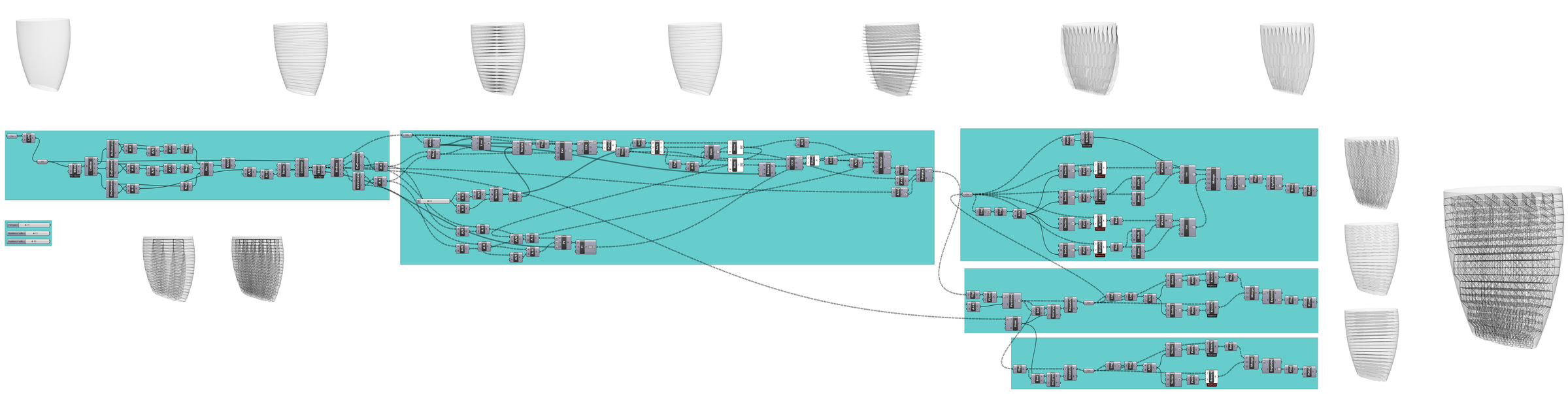

VDA version 3

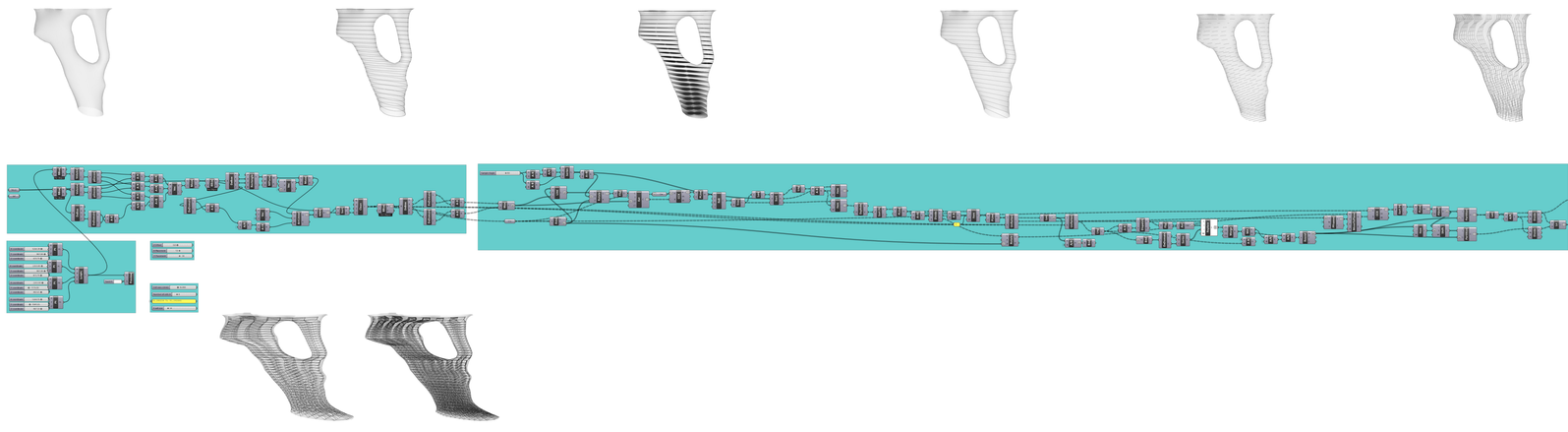

VDA version 4

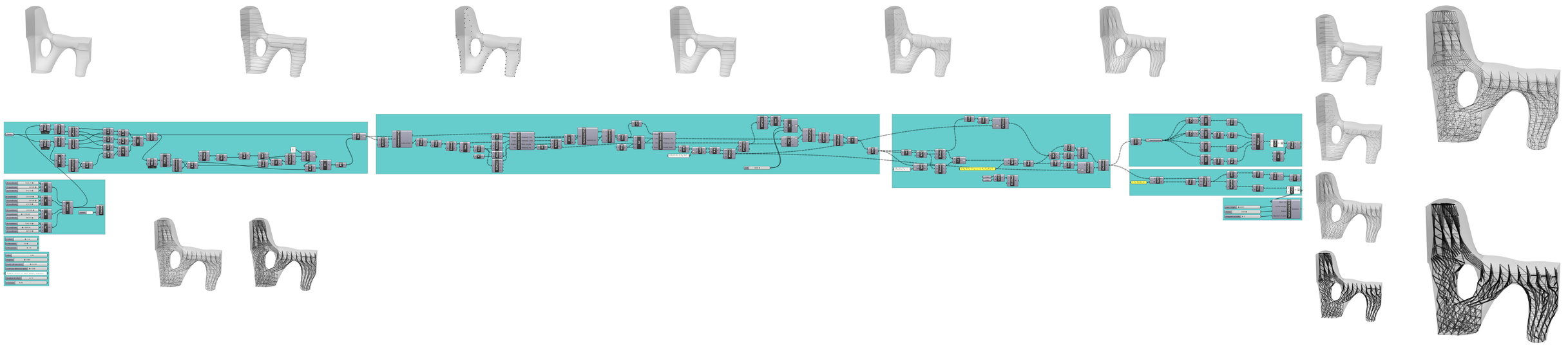

Robotic control and Reorientation

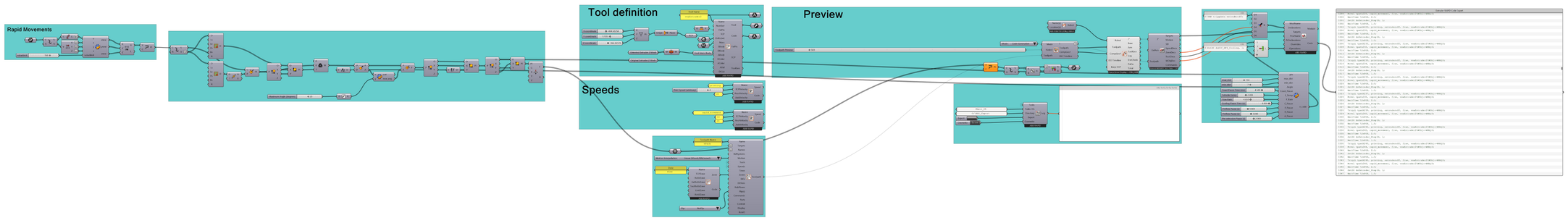

Topological Optimisation System